Ref.TH.3810-CERN

CALT-68-1075
DOE RESEARCH AND
DEVELOPMENT REPORT

Hadronization and Fragmentation*

Thomas D. Gottschalk

California Institute of Technology†
Pasadena, CA 91125
and
CERN
CH-1211 Geneva 23
Switzerland

ABSTRACT

Models for hadron production in e^+e^- annihilation are examined. Topics discussed include conventional models (the Feynman-Field and LUND approaches) and the newer QCD-Cluster description of hard processes. Elements of perturbative QCD which enter into these models are reviewed.

Lectures at the 19th Int. School of Elementary Particle Physics, Kupari-Dubrovnik, Yugoslavia, 1983.

*Work supported in part by U.S. Department of Energy under Contract No. DE-AC03-81-ER40050.

†Permanent Address

Ref.TH.3810-CERN
January 1984

1. Introduction
2. Some Aspects of Perturbative QCD
   2.1 Elementary Cross Section
   2.2 Virtual Corrections and "Dressed Jets"
   2.3 Gauges and "All Orders" Summations
   2.4 The QCD-Improved Parton Model
   2.5 Parton Shower Monte Carlo Models
   2.6 Shape Variables for e^+e^- Annihilation
   2.7 Some Lessons from Higher Orders
3. Conventional Hadronization Models
   3.1 The Feynman-Field Quark Jet Model
   3.2 Applications of the (Extended) FF Model
   3.3 Problems with the FF Model
   3.4 The LUND Model for String Fragmentation
   3.5 The LUND Model for Gluon Fragmentation
   3.6 Independent Fragmentation versus LUND
4. QCD-Cluster Models
   4.1 Some General Considerations
   4.2 The Field-Wolfram Model
   4.3 Soft Gluons and the Webber Model
   4.4 An Improved Description of Low Mass Hadronization
   4.5 Limited-p_T Jets Without the Feynman-Field Mechanism
   4.6 Adding Bremsstrahlung--and an Assessment

1. Introduction

According to the posters announcing this summer school, these lectures deal with "Clarifying the Hadronic Mess". This is quite a tall order, and there are at least two important general areas that could be covered under such a title: (1) hadronic initial states, hadron-hadron collisions and the dramatic jet results now seen at the CERN $p\bar{p}$ collider [1-3]; (2) hadron production after hard scatterings--e.g., details of hadron production in e^+e^- annihilation. Both experimental arenas have produced results in general agreement with expectations based on our present understanding of QCD. Neither area, however, can as yet be precisely understood, given our present lack of understanding as to how physical hadrons arise in QCD. In these notes we deal with the simpler final state problem of hadronization after a hard QCD scattering, using e^+e^- annihilation as the primary example.

Since we seek to understand hadron production in terms of Quantum Chromodynamics (QCD), we might first ask what QCD is [4-10]. This question does have a well-defined answer.

QCD is a local, gauge invariant field theory specified by the Lagrangian (ignoring masses for quarks)

$$L_{QCD} = -\tfrac{1}{4}\sum_{A=1}^{8} F^A_{\mu\nu}F^{A\mu\nu} + i\sum_{k=1}^{N_f}\bar{\psi}_i^A\gamma^\mu D_\mu^{AB}\psi_i^B \tag{1.1}$$

where

$$D_\mu^{AB} = \delta^{AB}\partial_\mu - ig\,\lambda_C^{AB}G_\mu^C \tag{1.2}$$

and the matrices λ_C in Eq. (1.2) satisfy

$$[\lambda_a,\lambda_b] = if_{abc}\lambda_c \tag{1.3}$$

for fundamental structure constants f_{abc}. The interactions of QCD are described in terms of elementary fields ψ (quarks) and G_μ (gluons). The tensor $F^A_{\mu\nu}$ in Eq. (1.1) is given by

$$F^A_{\mu\nu} = \partial_\mu G^A_\nu - \partial_\nu G^A_\mu + gf^{ABC}G^B_\mu G^C_\nu \tag{1.4}$$

The theory has a single coupling constant g in Eqs. (1.2, 1.4).

The next question, clearly, is "What do Eqs. (1.1-1.4) mean?". The only completely honest answer to this question is

"Nobody really knows--at least not yet"

We are in the rather peculiar situation of having a widely accepted candidate for the fundamental theory of strong interactions and yet having few--if any--uncontroversial results or predictions of this theory on which to base our confidence.

To understand our "lack of understanding" a bit further, it is helpful to compare L_{QCD} in Eq. (1.1) to the other local, gauge-invariant field theory of particle physics, Quantum Electrodynamics (QED)

$$L_{QED} = -\tfrac{1}{4}F_{\mu\nu}F^{\mu\nu} + i\bar{\psi}(\gamma^{\mu}D_{\mu} + im_{e})\psi \tag{1.5}$$

which describes the interactions of electrons (ψ) and photons (A_{μ}). In Eq. (1.5),

$$D_{\mu} = \partial_{\mu} - ieA_{\mu} \tag{1.6}$$

$$F_{\mu\nu} = \partial_{\mu}A_{\nu} - \partial_{\nu}A_{\mu} \tag{1.7}$$

Eqs. (1.5-1.7) are very similar to Eqs. (1.1-1.4). Yet, QED is one of the most precise theories in all of physics, while QCD has, to date, essentially predicted nothing quantitative. What are the differences?

There are at least two important (and presumably related) differences between L_{QED} and L_{QCD}. The interaction charge (e) for QED is simple (abelian "color" structure). There are no non-trivial structure constants in QED (no Eq. (1.3)), and the photon does not interact with itself (no $A{\cdot}A$ term in Eq. (1.7)). In QCD, due to the non-trivial (non-abelian) structure of the SU(3) color group, the gauge boson is itself colored, allowing gluons to interact. Perturbation theory rules obtained from Eq. (1.1) are shown in Fig. (1). Eq. (1.1) gives rise to a number of elementary vertices, including the very important gluon self couplings.

The second, more important, difference between QED and QCD lies in the physical states which are described by the theories. With suitable redefinitions (renormalizations), the basic fields ψ and A_{μ} in Eqs. (1.5-1.7) correspond to physically observable particles--electrons (and muons and taus) and photons. In contrast, the elementary fields of QCD are <u>not</u> observed in nature. Color is presumably confined in QCD, so that the physical, asymptotic states of Eqs. (1.1-1.4) are not the quarks and gluons described by ψ and G, but rather, colorless bound states of these constituents.

QCD FEYNMAN RULES

PROPAGATORS

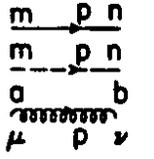

$$i\,\delta_{mn}/[\not{p} - m + i\epsilon]$$

$$i\,\delta_{mn}/[p^2 + i\epsilon]$$

$$-i\,\delta_{ab}\left[g_{\mu\nu} - (1-\alpha)\frac{p_{\mu}p_{\nu}}{p^2+i\epsilon}\right]\Big/[p^2+i\epsilon]$$

VERTICES

$$-ig\gamma^{\alpha}T^{a}_{ij}$$

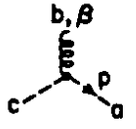

$$gf^{abc}\,p^{\beta}$$

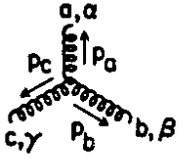

$$-gf^{abc}\{g^{\alpha\beta}(p_a^{\gamma}-p_b^{\gamma})$$
$$+g^{\beta\gamma}(p_b^{\alpha}-p_c^{\alpha})+g^{\gamma\alpha}(p_c^{\beta}-p_a^{\beta})\}$$

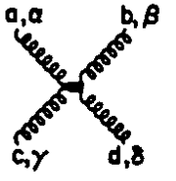

$$-ig^2 f^{xab}\,f^{xcd}\,K(\alpha\beta,\gamma\delta)$$
$$-ig^2 f^{xac}\,f^{xdb}\,K(\alpha\gamma,\delta\beta)$$
$$-ig^2 f^{xad}\,f^{xbc}\,K(\alpha\delta,\beta\gamma)$$
$$K(\alpha\beta,\gamma\delta) \equiv g^{\alpha\gamma}g^{\beta\delta} - g^{\alpha\delta}g^{\beta\gamma}$$

Fig. 1. Feynman rules for perturbative quantum chromodynamics.

Bound state problems in relativistic field theories are notoriously difficult, and it has been very hard to derive properties of hadronic final states from the quark-gluon interactions in Eq. (1.1). At present, analysis of QCD tends to follow one of two paths.

Lattice gauge theory methods [11] attempt to directly compute properties derivable from the field theory Lagrangian in Eq. (1.1). This is a powerful technique which will be described in other lectures at this school [12]. Calculations on a lattice are difficult, requiring a great deal of computer time with present techniques. Present results generally deal with "static" issues, such as the spectrum of hadronic masses. Dynamical questions, such as hadron production in hard scattering experiments, are well beyond the realm of present lattice techniques.

The second approach is to use perturbation theory of quarks and gluons and hope that, in some sense, the ultimate transition from colored quanta to physical, colorless hadrons is sufficiently "soft" that results of the perturbative calculations should have some connection to experiment. This hope is motivated, in part, by the historical successes of a parton model description of hard scattering processes [13-17]. The parton model describes hard scatterings as a convolution of underlying constituent subprocesses with basic probability functions describing the distributions of these constituents inside physical hadrons. Parton model descriptions of various physical processes are illustrated in Fig. (2). The function $G_{d/N}(x)$, for example, gives the probability of finding a down quark in a nucleon, carrying a fraction x of the (high energy) nucleon's momentum.

Perturbative QCD predicts several modifications of the basic parton model. The constituents are identified (partons are quarks and/or gluons) and their interactions are specified in Fig. (1). More elaborate constituent subprocesses are allowed, such as $e^+e^- \to q\bar{q}G$, which give rise to distinctive multijet topologies in hadronic final states. The (singular) behavior of QCD perturbation theory for nearly collinear parton configurations leads to an important generalization of the parton model in the form of a mild (logarithmic) scale dependence for the distribution and fragmentation functions $G(x)$ and $D(z)$ in Fig. (2).

Nearly all analyses of high energy data are done in the framework of the QCD-improved parton model. It is hoped that a careful study of certain properties of the hadronic final state can be used to study basic features of QCD, as well as to a determination of the QCD coupling

PARTON MODEL EXPANSIONS

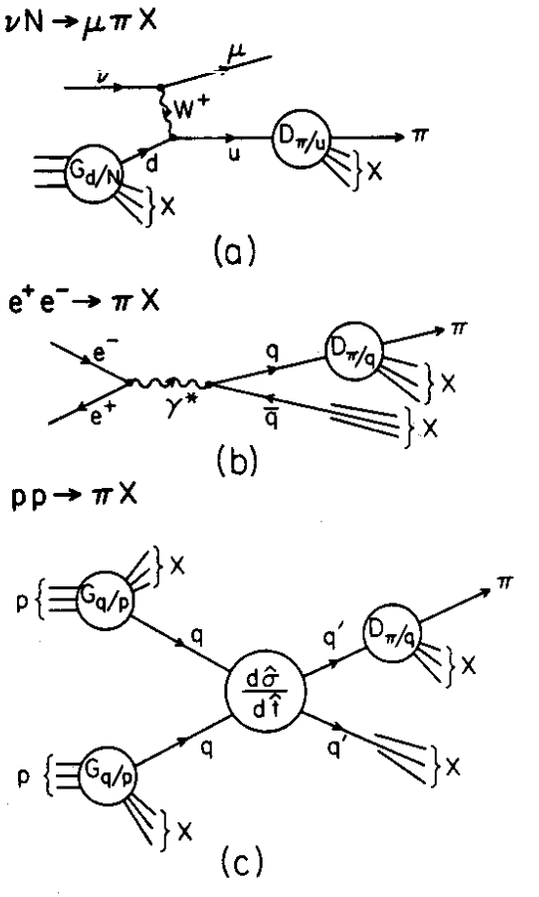

Fig. 2. Parton model expansions for various hard scattering processes.

$$\alpha_s \equiv \frac{g^2}{4\pi} \tag{1.8}$$

associated with the elementary vertices in Fig. (1). By and large, this conventional QCD-phenomenology approach is qualitatively quite successful. However, difficulties and ambiguities arise when we try to make truly detailed studies. Careful analyses of experimental data require very specific assumptions on how the (unknown) hadronization process actually occurs in nature. The results of these analyses (e.g., measurements of α_s) do depend on details of the hadronization models. The separation between perturbative hard scatterings and non-perturbative hadronization in nature is not as "clean" as the simple picture of the QCD-Improved parton model might imply.

As is noted by Politzer (one of the fathers of the QCD-Improved parton model) in his introduction to a recent reprint volume on perturbative QCD [18], the division of present QCD calculations into "perturbative" and "non-perturbative" methods is artificial--reflecting primarily our inability to determine what Eq. (1.1) really means. As better and higher energy data for e^+e^- annihilation and $\bar{p}p$ scattering become available, it is clearly important to analyze them not only with the hope of "testing" perturbative QCD, but also, with the goal of learning how hadronization itself actually works.

The next two sections of these lectures deal with what might be called "traditional dogma": the QCD-Improved parton model and conventional hadronization schemes. We adopt a rather cautious (negative?) point of view, however, trying to point out places where either perturbation theory approximations or model-dependent fragmentation assumptions might fall out of line with the warning from the preceding paragraph. The final section deals with a basically new picture of hadronization which has been developing over the last two years. This "QCD-Cluster" description provides a promising framework for investigating hadronization without the unnecessary, model-dependent fragmentation function formalism of more conventional models.

2. Some Aspects of Perturbative QCD

Monte Carlo models for e^+e^- annihilation [19-26,] all begin with the generation of a quark-gluon final state according to perturbative QCD. This is usually done either exactly to some low order in the perturbative coupling, or through an "all orders" approximate summation of a particular subset of perturbative graphs. In this section we examine a number of aspects of perturbative

QCD which are used in current e^+e^- annihilation models. This section is not intended to be any sort of comprehensive review of QCD--for that, the reader is referred to any of a number of good review articles [4-10]. Instead, we intend of illustrate (primarily through simple examples) a number of key features of perturbative QCD, such as the idea of "dressed jets" and the manner in which quark-gluon perturbation theory is (hopefully) consistent with a parton model picture of hadron production. We also examine a number of approximations and ambiguities which arise is associating parton final states with "physical" jets, and we try to point out some of the ways in which these ambiguities can affect the interpretations of experimental results.

2.1 Elementary Cross Sections

The lowest order parton subprocess for $e^+e^- \to$ hadrons is the one-photon

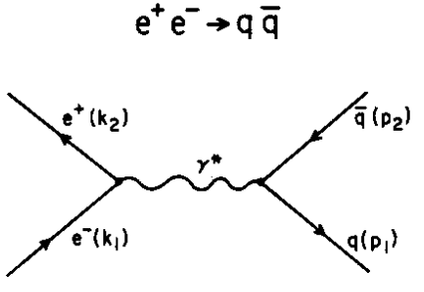

Fig. 3. Lowest order parton model contribution to $e^+e^- \to$ hadrons.

annihilation shown in Fig. (3). The amplitude for this graph can be written as

$$\mathbf{M} \simeq \frac{ie^2}{Q^2} j_\mu J_\mu \tag{2.1}$$

where the lepton and quark currents are

$$j_\mu = \bar{u}(k_1)\gamma_\mu v(k_2) \tag{2.2}$$

$$J_\mu = \bar{u}(p_1)\gamma_\mu v(p_2) \tag{2.3}$$

The Born cross section resulting from Eq. (2.1) is

$$d\sigma_0 = 3\left[\frac{4\pi\alpha_{EM}^2}{2Q^2}\right]\frac{3\beta}{8}[1+\beta^2\cos^2\vartheta]d(\cos\vartheta) \tag{2.4}$$

ϑ is the CM scattering angle between the incident electron $e^-(k_1)$ and the outgoing quark $q(p_1)$, and

$$\beta \equiv \left[1-\frac{4M^2}{Q^2}\right]^{1/2} \tag{2.5}$$

where M is the quark mass. What is probably the lowest energy evidence for the $e^+e^- \to q\bar{q}$ subprocess comes from the observations of the Mark I group at SPEAR that leading hadrons produced at $E_{CM} \simeq 4$-5 GeV tend to follow the $1+\cos^2\vartheta$ distribution predicted in Eq. (2.4) [27].

Integrating over the scattering angle, the total cross section is

$$\sigma_0[e^+e^- \to q\bar{q}] = 2\sigma_{\mu\mu}\left(\frac{e_q}{e}\right)^2\frac{3\beta}{4}\left[1+\frac{\beta^2}{3}\right] \tag{2.6}$$

$$\underset{(\beta\to 0)}{\to} 2\sigma_{\mu\mu}\left(\frac{e_q}{e}\right)^2 \tag{2.7}$$

where e_q, e are the quark and electron charges and

$$\sigma_{\mu\mu} \equiv \sigma[e^+e^- \to \mu\bar{\mu}] = \frac{4\pi\alpha_{EM}^2}{3Q^2} \tag{2.8}$$

The factor of 3 in Eq. (2.6) comes from the three possible quark colors. The threshold behavior for small β in Eq. (2.6) is characteristic of the spin-½ nature of quarks. Fits of $\sigma(e^+e^- \to \tau\bar{\tau})$ to the energy dependence of Eq. (2.6) are used to provide an accurate determination of the τ mass [28].

The lowest order parton model estimate to

$$R \equiv \frac{\sigma(e^+e^- \to \text{hadrons})}{\sigma(e^+e^- \to \mu^+\mu^-)} \tag{2.9}$$

is given by summing Eq. (2.8) over quark flavors

$$R = \sum_f 3\left(\frac{e_f}{e}\right)^2\beta_f(3+\beta_f^2)/4 \tag{2.10}$$

$$\underset{\beta_f\to 1}{\to} 3\sum_f(e_f/e)^2 \tag{2.11}$$

For simplicity, we set all quark masses to zero in subsequent discussions.

$e^+e^- \to q\bar{q}G$

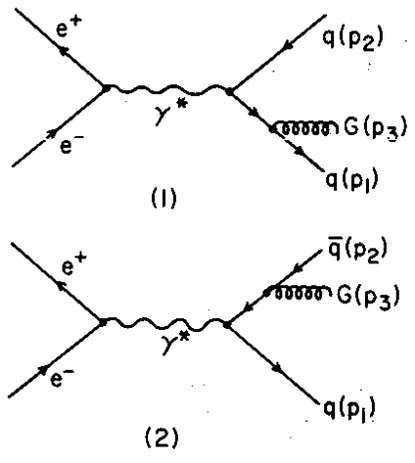

Fig. 4. $O(\alpha_s)$ QCD graphs for $e^+e^- \to q\bar{q}G$.

QCD corrections to $e^+e^- \to$ hadrons first arise from the subprocess

$$e^-(k_1) + e^+(k_2) \to q(p_1) + \bar{q}(p_2) + G(p_3) \tag{2.12}$$

The corresponding Feynman graphs are shown in Fig. (4). The matrix elements for these two graphs can be written as

$$\mathbf{M} = \mathbf{M}_1 + \mathbf{M}_2 \tag{2.13}$$

$$\mathbf{M}_j = j^\mu \mathbf{M}_j^{\mu\alpha}\varepsilon^\alpha \tag{2.14}$$

where ε^α is the gluon polarization vector and

$$\mathbf{M}_1^{\mu\alpha} \sim \frac{q}{t}T_{ij}^a\bar{u}(p_1)\gamma^\alpha(\not{p}_1+\not{p}_3)\gamma^\mu v(p_2) \tag{2.15}$$

$$\mathbf{M}_2^{\mu\alpha} \sim \frac{-q}{u}T_{ij}^a\bar{u}(p_1)\gamma^\mu(\not{p}_2+\not{p}_3)\gamma^\alpha v(p_2) \tag{2.16}$$

The factor T_{ij}^a is a color matrix, and we have introduced the kinematic variables

$$s \equiv (p_1+p_2)^2 \tag{2.17}$$

$$t \equiv (p_1 + p_3)^2 \tag{2.18}$$

$$u \equiv (p_2 + p_3)^2 \tag{2.19}$$

Integrating over the angular orientations of the $q\bar{q}G$ production plane, the differential cross section for (2.12) is given by

$$\frac{1}{\sigma_0}\frac{d\sigma}{dudt} = \left[\frac{2\alpha_s}{3\pi}\right]\left[\frac{t^2 + u^2 + 2sQ^2}{utQ^4}\right] \tag{2.20}$$

Defining new variables

$$x_j \equiv 2E_j/Q = (p_i + p_k)^2/Q^2 \quad (i,j,k \text{ distinct}) \tag{2.21}$$

with

$$x_1 + x_2 + x_3 = 2 \tag{2.22}$$

the result in Eq. (2.20) takes the more familiar form [29]

$$\frac{1}{\sigma_0}\frac{d\sigma}{dx_1 dx_2} = \left[\frac{2\alpha_s}{3\pi}\right]\left[\frac{x_1^2 + x_1^2}{(1-x_1)(1-x_2)}\right] \tag{2.23}$$

The physical regions are

$$0 \le t \le Q^2 \tag{2.24}$$

$$0 \le u \le Q^2 - t \tag{2.25}$$

for Eq. (2.20) and

$$0 \le x_1 \le 1 \tag{2.26}$$

$$1 - x_1 \le x_2 \le 1 \tag{2.27}$$

for Eq. (2.23)

We note that the results in Eqs. (2.20, 2.23) are divergent along the borders of phase space. These singularities are important characteristics of perturbative QCD, so we will investigate them further.

Consider the $t \to 0$ limit of Eq. (2.20). In this limit, the quark $q(p_1)$ and the gluon $G(p_3)$ in Eq. (2.12) become parallel, and the pair becomes *indistinguishable* from a single quark of 4-momentum

$$\tilde{p} \equiv p_1 + p_3 \tag{2.28}$$

Define momentum sharing in this composite system by the scaling variable z:

$$p_1 = z\tilde{p} \tag{2.29}$$

$$p_3 = (1-z)\tilde{p} \tag{2.30}$$

Then, $du = (Q^2 - t)dz$, and Eq. (2.20) can be rewritten as

$$d\sigma \underset{(t\to 0)}{\to} \sigma_0 \times \left\{\frac{\alpha_s}{2\pi}\frac{dt}{t}dz\left[\frac{4}{3}\right]\left[\frac{1+z^2}{1-z}\right]\right\} \tag{2.31}$$

In the singular limit, the 3 jet cross section is proportional to the lowest order cross section times a "correction" piece which depends only on the mass ($\sqrt{t}$) and the momentum sharing (z) in the composite $g + G$ system.

The expression in Eq. (2.31) is a specific example of an important general feature of perturbative QCD: the factorization of mass singularities [30-33]. If σ_N is the cross section for producing N-partons, and if σ_{N+1} is the cross section obtained from σ_N by allowing one of the partons to split into a parallel pair, then

$$d\sigma_{N+1} \underset{(t\to 0)}{\to} \sigma_N\left\{\frac{\alpha_s}{2\pi}\frac{dt}{t}dz P_{A/B}(z)\right\} \tag{2.32}$$

The coefficients $P_{A/B}(z)$ of these perturbative poles are universal functions (Altarelli-Parisi kernels [34]), which depend only on the type of parton splitting:

$$q \to q + G: \quad P_{q/q}(z) = C_F\left[\frac{1+z^2}{1-z}\right] \tag{2.33}$$

$$G \to G + G: \quad P_{G/G}(z) = \frac{2C_G(1 - z + z^2)^2}{z(1-z)} \tag{2.34}$$

$$G \to q + \bar{q}: \quad P_{G/q}(z) = T_R[z^2 + (1-z)^2] \tag{2.35}$$

In the general case, C_F, C_G and T_R are simple numbers related to the underlying group structure of the theory. For SU(3) color, $C_F = 4/3$, $C_G = 3$, and $T_R = N_f/2$, where N_f is the number of quark flavors. Simple, instructive derivations of Eq. (2.32) can be found in Refs. [33,35] for $q \to q + G$ splittings.

The result in Eq. (2.32) is the first step in demonstrating the factorization of perturbative QCD. This is a very important result in that it shows that the parton model is not inconsistent with QCD perturbation theory. Specifically, it can be shown that all the mass singularities in perturbative QCD can be uniquely

associated with individual final state "partons": The major modifications to the simple parton model results come from a slow (logarithmic) Q-dependence of the quark distribution functions and fragmentation functions.

To help make the claims in the preceding paragraph at least plausible (though not proved in these notes), we discuss in the next two sections two slightly technical topics: "virtual corrections" and "gauges".

2.2 Virtual Corrections and "Dressed Jets"

Before examining the virtual corrections to $e^+e^- \to q\bar{q}$, it is useful to rewrite the cross section for $e^+e^- \to q\bar{q}G$ in a form in which the singularities are uniquely associated with the individual transitions $q \to q + G$ and $\bar{q} \to \bar{q} + G$. For the easy case of $e^+e^- \to q\bar{q}G$, this can be done by a simple partial fraction expansion of the denominator in Eq. (2.20)

$$d\sigma = \sigma^0\left\{\frac{2\alpha_s}{3\pi}\right\}\frac{1}{Q^4}\frac{dt}{t}du\left\{u + \frac{2sQ^2}{u+t}\right\} \qquad (2.36)$$

$$+ (t \leftrightarrow u)$$

Using the integration region in Eqs. (2.24-2.25), the total cross section for $e^+e^- \to q\bar{q}G$ is seen to be infinite

$$\sigma(e^+e^- \to q\bar{q}G) \overset{?}{\sim} \ln^2(\hat{t} \to 0) \qquad (2.37)$$

The divergence in Eq. (2.37) is canceled by a similar term coming from the interference of the Born diagram in Fig. (3) with the $O(\alpha_s^2)$ virtual corrections shown in Fig. (5). In order to subtract divergences, however, it is first necessary to use some sort of technique to make the individual terms "temporarily finite". This procedure is known as regularization.

For our simple example, one possible regularization scheme is to give the gluon in Fig. (4) a mass. The real and virtual contributions are then calculated and added together, and the gluon mass is set to zero after the individual divergences have been canceled.

Let M be a (temporary) gluon mass. The mass-dependent form of the symmetrized $q\bar{q}G$ cross section in Eq. (2.36) becomes [36]

$$\frac{1}{\sigma^0}\frac{d\sigma^R}{dtdu} = \left\{\frac{2\alpha_s}{3\pi}\right\}\frac{1}{Q^4}\frac{1}{t}\left\{u + \frac{2(Q^2+M^2)(s+M^2)}{u+t} - \frac{M^4}{t}\right\} \qquad (2.38)$$

$e^+e^- \to q\bar{q}$ $\{O(\alpha_s^2)\}$

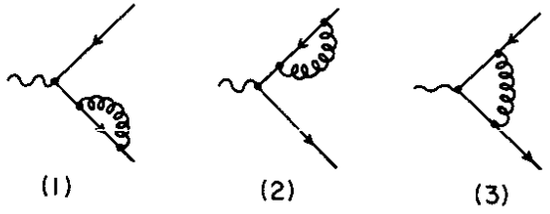

Fig. 5. QCD corrections to $e^+e^- \to q\bar{q}$.

$$+ (u \leftrightarrow t)$$

{The superscript "R" stands for Real gluon emissions.} The physical region is now

$$M^2 \le t \le Q^2 \qquad (2.39)$$

$$M^2/t \le u \le Q^2 + M^2 - t \qquad (2.40)$$

Integrating Eq. (2.38) over this physical region, the total 3-parton cross section contribution is

$$\sigma^R = 2\sigma_0\left\{\frac{2\alpha_s}{3\pi}\right\}\left\{\tfrac{1}{2}\ln^2\beta + \frac{3}{2}\ln\beta + \frac{5}{2} - \frac{\pi^2}{6} + h_R(\beta)\right\} \qquad (2.41)$$

where

$$\beta \equiv M^2/Q^2 \qquad (2.42)$$

and $h_R(\beta)$ is a sum of terms like $\beta\ln(\beta)$ which vanish for $\beta \to 0$. The divergences in σ^R are now well defined, and, in addition, we find some specific constant pieces.

The divergences in σ^R all come from the soft or "infrared" region $\beta \to 0$. In contrast, the virtual corrections in Fig. (5) have two kinds of divergences--infrared and "ultraviolet" divergences. The latter are associated with the flow of very high energy virtual gluons in the various closed loops of Fig. (5).

The ultraviolet divergences of perturbation theory are interpreted through a procedure known as renormalization -- which amounts to a redefinition of what

the external particles and coupling constants in the theory really are. Renormalization is an intricate, sometimes subtle topic [7,37,38]. However, at a "zeroth order", the physical ideas involved are fairly simple.

QUARK SELF-ENERGY

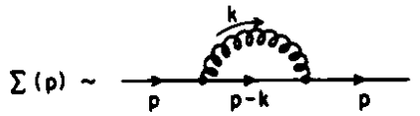

Fig. 6. $O(\alpha_s^2)$ perturbative quark self-energy term.

Consider the simple graph shown in Fig. (6). This process, in which a quark emits a virtual gluon then reabsorbs it without interacting with anything else, is interpreted as an $O(\alpha_s)$ correction in the definition of a final state quark. Note that the first two graphs in Fig. (5) are simply the Born graph in Fig. (3) multiplied by the "correction" factor in Fig. (6).

The effect of adding the graph in Fig. (6) to the lowest order quark propagator can be summarized as a multiplication of the inverse quark propagator

$$\not{p}(\text{Lowest Order}) \to Z\not{p} \tag{2.43}$$

where

$$Z \sim 1 + i\alpha_s \sum(p^2) \tag{2.44}$$

In perturbative expansions, $\sum(p^2)$ is a divergent expression. For example, using a gluon mass M and an ultraviolet momentum cutoff Λ as regulators, $\sum(p^2)$ is of the form

$$\sum \sim A \ln\left[\frac{\Lambda^2}{M^2}\right] + B \tag{2.45}$$

We can absorb these divergences into the definition of a renormalized external quark by writing

$$\psi_R \simeq \psi_U Z_\psi^{-\frac{1}{2}} \tag{2.46}$$

The unrenormalized quark field ψ_U corresponds to the "straight lines" in the

Feynman rules in Fig. (1), while the renormalized field ψ_R describes a quark dressed by all possible self interactions, as illustrated schematically in Fig. (7).

QUARK RENORMALIZATION

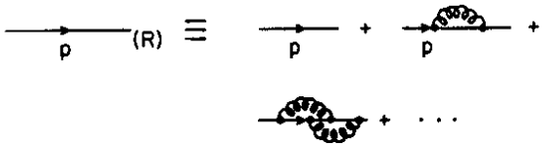

Fig. 7. Schematic illustration of quark wave function renormalization.

Note that the redefinition in Eq. (2.46) would be conceptually necessary even if Z_ψ were finite. That is, the interactions shown in Fig. (7) are associated with the definition of what an external quark ("real quark") really is, and not with the description of the interactions of a quark with other external quanta.

After renormalization of the external quark lines in Fig. (5), the $O(\alpha_s^2)$ virtual corrections to e^+e^- annihilation have only infrared divergences and can be written as [36]

$$\sigma^V = 2 \times \left[\frac{2\alpha_s}{3\pi}\right] \sigma_0 \left\{-\tfrac{1}{2}\ln^2\beta - \frac{3}{2}\ln\beta - \frac{7}{4} + \frac{\pi^2}{6} + h_V(\beta)\right\} \tag{2.47}$$

where $h_V(\beta)$ vanishes for $\beta \to 0$. Adding the virtual and real contributions from Eqs. (2.41, 2.47), the $O(\alpha_s^2)$ correction to the total cross section is

$$\Delta\sigma = \sigma^R + \sigma^V = \sigma_0 \left[\frac{\alpha_s}{\pi}\right] \tag{2.48}$$

The $O(\alpha_s^2)$ expression for R is thus

$$R = R_0 \left[1 + \frac{\alpha_s}{\pi}\right] \tag{2.49}$$

where R_0 is the parton model result in Eq. (2.11)

We note that, after integrating over the phase space for real gluon emissions and adding virtual corrections, the lowest order QCD correction to σ is rather small. How then are we to interpret the differential 3-jet cross section in

Eq. (2.20), which becomes arbitrarily large for u or $t \to 0$?

An important clue on how to proceed comes from investigating the space-time evolution of $q \to qG$ splittings. Consider the

$$q^*(p_1 + p_3) \to q(p_1) + G(p_3) \tag{2.50}$$

transition associated with the first diagram in Fig. (4) (q^* indicates a virtual quark-off mass shell). From the uncertainty principle

$$\Delta E \Delta\tau \simeq \hbar \tag{2.51}$$

we can estimate the lifetime $\Delta\tau$ of the virtual quark to be

$$\Delta\tau(q^*) \simeq \frac{\hbar}{\Delta E} \tag{2.52}$$

$$\simeq \frac{\hbar}{E - |\vec{p}|} \simeq \frac{\hbar Q}{t} \tag{2.53}$$

Thus, the largest contributions to the 3-jet cross section in Eq. (2.20) come from the production and decay of long-lived, low mass q^* intermediate states.

However, because quarks and gluons are presumably confined in QCD, we cannot expect perturbative QCD to provide a reasonable description of physics on long time scales. In the $q^* \to q + G$ splitting example, the oppositely colored virtual q^* and the $\bar{q}$ from the original $\gamma^* \to q^*\bar{q}$ vertex have separated by a distance

$$\Delta x \simeq c\,\Delta\tau \tag{2.54}$$

$$\simeq \frac{\hbar c Q}{\tau} \simeq \left(\frac{Q}{t}\right) (0.2\ \text{GeV–fm}) \tag{2.55}$$

If t is too small (say $t \sim 1\ \text{GeV}^2$), this corresponds to a rather large Color separation ($\Delta x \simeq 6 fm$ at PETRA/PEP energies). But "non-perturbative" color confinement is expected to dominate QCD physics at distances $\Delta x \gtrsim 0(1\ fm)$. The use of Eq. (2.20) to describe real gluon emissions at small t extends perturbative QCD into a domain where it most likely is inapplicable!

To use the perturbative cross section in Eq. (2.20) for calculations of $e^+e^- \to$ hadrons, we must first cut out the small-mass (long-time) components. This can be done consistently by introducing the idea of a " Dressed Perturbative Jet ".

We begin by introducing a resolution criterion for resolvable perturbative radiations, e.g.:

The quark and gluon in the $e^+e^- \to q\bar{q}G$ final state are treated as (distinct) resolvable jets only if

$$t > t_c \tag{2.56}$$

where t_c is some fixed cutoff parameter.

Configurations which do not satisfy the resolution criterion are to be integrated out. The integrated small-mass real contributions are added to the virtual corrections, giving a finite correction to the 2-jet cross section.

The sum of the Born cross section in Eq. (2.7), the virtual corrections in Eq. (2.47) and the integrated real emissions defines the cross section for dressed 2-jet production to $O(\alpha_s)$. The term "dressing" refers to the integration over small mass 3 parton configurations, which allows the cancellation of real and virtual singularities at the level of the 2-jet and 3-jet cross section, not just in the total cross section in Eq. (2.48). Note that the dressing of the perturbative 3-jet cross section does not occur until $O(\alpha_s^2)$ terms are calculated.

A subtle but important point is that the integrated 3-parton cross sections are all "assigned" to the kinematic configuration of two massless jets. Thus, the $e^+e^- \to q\bar{q}G$ cross section for $t < t_c$ is treated as a simple numerical correction to $e^+e^- \to q\bar{q}$, with the identification

$$E(q) \equiv E(\bar{q}) \equiv Q/2 \tag{2.57}$$

The fact that the antiquark in $e^+e^- \to q\bar{q}G$ actually has a slightly smaller energy

$$E(\bar{q}) = \frac{Q^2 - t}{2\sqrt{Q^2}} \tag{2.58}$$

is ignored! The idea here is that all small mass effects (which, as argued above, cannot be described by perturbation theory) are presumed to be already included in whatever non-perturbative model is used to describe hadronization (e.g., fragmentation functions). As is discussed below in Section 2.7, the distinction between dressed jets and "bare perturbative quanta" is important in reconciling the seemingly contradictory initial results of different calculations of the $O(\alpha_s^2)$ QCD predictions for shape variable distributions in e^+e^- annihilation.

We can now give the dressed jet cross sections for e^+e^- annihilation to $O(\alpha_s)$, using the mass cut resolution criterion. The cross section for resolvable 3-jet production is

$$\frac{d\sigma^{3\text{-}jet}}{dt\,du} = \sigma_0 \left(\frac{2\alpha_s}{3\pi}\right) \times \left(\frac{1}{Q^4}\right) \times \tag{2.59}$$

$$\times \vartheta(t - t_c)\vartheta(u - t_c)\vartheta(s - t_c)F(t,u)$$

where

$$F(t,u) = \frac{u}{t} + \frac{t}{u} + \frac{2Q^2 s}{ut} \tag{2.60}$$

and $s = Q^2 - t - u$. The total 3-jet production rate is

$$\sigma^{3-jet}(t_c/Q^2) \equiv \int dudt \left[\frac{d\sigma^{3-jet}}{dudt}\right] \tag{2.61}$$

$$\equiv \sigma_0 \left[\frac{\alpha_s}{\pi}\right] A(t_c/Q^2) \tag{2.62}$$

where

$$A(\rho) = \frac{4}{3}\ln^2\rho + 2\ln\rho + \frac{5}{3} - \frac{2\pi^2}{9} + \frac{4}{3}B(\rho) \tag{2.63}$$

$B(\rho)$ is a bit messy;

$$B(\rho) = \ln\rho[3\rho - 2\ln(1-\rho)] \tag{2.64}$$

$$- \ln(1-2\rho)[\ln(1-2\rho) - 2\ln(1-\rho) + 3\rho + \frac{3}{2}]$$

$$- 3\rho - \frac{9}{4}\rho^2 + 2Li_2\left[\frac{-\rho}{1-2\rho}\right]$$

The form of $B(\rho)$ is not too important, and we note that

$$B(\rho) \underset{(\rho \to 0)}{\to} 0 \tag{2.65}$$

The function $Li_2(z)$ in Eq. (2.64) is the dilogarithm

$$Li_2(z) \equiv -\int_0^z \frac{dx}{x}\ln(1-x) \tag{2.66}$$

which frequently occurs in QCD phase space integrations (properties of $Li_2(z)$ are discussed in detail in [39]). The dressed 2-jet cross section is simply

$$\sigma^{2-jet}(t_c/Q^2) = \sigma_{TOT} - \sigma^{3-jet} \tag{2.67}$$

$$= \sigma_0 \left\{1 + \left[\frac{\alpha_s}{\pi}\right]\left[1 - A\left[\frac{t_c}{Q^2}\right]\right]\right\} \tag{2.68}$$

We have been a bit careless in our use of the word "jet" so far, and an important remark is in order:

"Jets" and "Jet Cross Sections" have no meaning without the specification of the resolution criterion and dressing algorithm.

Hadronic jets are certainly an experimental fact, in terms of approximately collinear sets of hadrons observed at PETRA, PEP and, quite spectacularly, at the CERN $\bar{p}p$ collider. It is widely accepted that these jets reflect the underlying hard parton production processes of perturbative QCD. However, lacking a complete theory of hadron production in QCD, it is not possible to make any precise quantitative connection between "experimental jets" (defined, e.g., by a cluster algorithm for associating final state hadrons) and "theoretical jets" (described by some dressing scheme in a perturbative calculation). The usual practice of generating perturbative jets, hadronizing these jets according to some model, then comparing the results to "experimental jets" tests not only perturbative QCD, but also the hadronization model itself. We shall see in Section 3 that the different hadronization models can lead to different results.

Since the idea of a "jet" is at best rather nebulous, we must be careful in choosing the resolution parameter t_c. Setting $t_c \to 0$ would yield $\sigma^{3-jet} \to \infty$, $\sigma^{2-jet} \to -\infty$. This is the same sad state of affairs we had for the undressed, bare parton cross section. A value $\sqrt{t_c} \gtrsim 7$ GEV is probably too large, since jet structure is quite visible at SPEAR for $E_{CM} \simeq 7$ GeV [27]. Based on the results of empirical cluster analyses at PETRA, we can estimate

$$\sqrt{t_c} \simeq 6 \text{ GeV} \tag{2.69}$$

as a reasonable value for the cutoff parameter. For this value we obtain, at $Q = 30$ GeV, (estimating $\alpha_s/\pi \simeq 1/20$)

$$\sigma^{3-jet} \simeq (6.1)\left[\frac{\alpha_s}{\pi}\right]\sigma_0 \simeq 0.30\sigma_0 \tag{2.70}$$

$$\sigma^{2-jet} \simeq \left[1 - (5.1)\frac{\alpha_s}{\pi}\right] \simeq 0.75\sigma_0 \tag{2.71}$$

These crude estimates are in reasonable agreement with the results of empirical cluster algorithm analyses of PETRA data [40,41].

To conclude this section on virtual corrections, we note that loop corrections modify the $q \to qG$ and $G \to GG$ Altarelli-Parisi splitting functions discussed

in Section 2.1. The effects of the leading virtual corrections can be included by changing these functions to

$$P_{q/q}(z) = C_F\left[\frac{1+z^2}{(1-z)_+} + \frac{3}{2}\delta(1-z)\right] \tag{2.72}$$

$$P_{G/G}(z) = 2C_G\left[\frac{z}{(1-z)_+} + \frac{(1-z)}{z} + z(1-z)\right] \tag{2.73}$$

$$+\left[\frac{11}{6}C_G - \frac{2T_R}{3}\right]\delta(1-z)$$

The splitting function for $G \to q\bar{q}$ does not have virtual corrections. The generalized function $[(1-z)_+]^{-1}$ in Eqs. (2.72-2.73) is defined by its integrals with (suitably regular) test functions:

$$\int_0^1 dz \frac{f(z)}{(1-z)_+} \equiv \int_0^1 dz \frac{f(z)-f(1)}{1-z} \tag{2.74}$$

Note that

$$\int_0^1 dz P_{q/q}(z) = 0 \tag{2.75}$$

This is interpreted as meaning that the probability of finding a quark inside a "quark jet" does not change. The leading mass singularities of perturbative QCD only affect the energy distributions of quarks within the quark jet.

2.3 Gauges and "All Orders" Summations

Gauge invariance is an important symmetry of QCD, related to the invariance of L_{QCD} under rotations in color space. The requirement that this rotation invariance be local (i.e., allow different color rotations at different space-time points) determines the form of the qqG, GGG and $GGGG$ vertices in Fig. (1) [42]. Moreover, it can be shown that only non-abelian gauge theories like QCD can have the important property of "asymptotic freedom" [43,44], which is crucial if there is to be any hope of reconciling a parton model picture with an underlying, bona fide field theory.

The fact that L_{QCD} is invariant under a class of gauge transformations means that the Lagrangian in Eq. (1.1) is, by itself, insufficient for specifying the quantization of the theory. In practice, this results in some minor "technical

complications" in the Feynman rules for gluons. However, the gauge freedom in the definition of the gluon propagator can be exploited to produce a simple physical picture of the leading terms in high order perturbative QCD processes.

The free equation of motion for the gluon field G_μ is, suppressing color indices

$$[\Box\, g^{\mu\nu} - \partial^\mu\partial^\nu]G_\mu = 0 \tag{2.76}$$

The gluon propagator should naively be given by the inverse of the operator in Eq. (2.76). However, this operator does not have any well-defined inverse. In order to define an inverse operator for Eq. (2.76) it is first necessary to remove the degeneracy of L_{QCD} under gauge transformations.

Before describing the solutions of this gauge degeneracy problem, it is instructive to have a slightly different picture of what is happening [45]. Lorentz invariance requires that the gluon field be described by a 4-vector G_μ, which corresponds to 4 different polarization states: two transverse polarizations, as well as longitudinal and scalar degrees of freedom. However, a massless vector particle has only the two transverse polarization states as physical degrees of freedom. Thus, the excess polarizations contained in the Lorentz structure "G_μ" have to be removed. The removal of the gauge degeneracy in L_{QCD} is related to the removal of unphysical gluon polarizations.

A Lorentz-covariant way of specifying the gauge is given by enforcing the transversality condition,

$$\partial^\mu G_\mu = 0 \tag{2.77}$$

This constraint can be incorporated by adding to L_{QCD} a gauge fixing term

$$\Delta L_{GF} = -\frac{1}{2\lambda}\sum_{\text{colors}}(\partial^\mu G_\mu)^2 \tag{2.78}$$

where $\frac{1}{\lambda}$ is a Lagrange multiplier. The gluon propagator is then given in momentum space by

$$D_{\mu\nu}(k) = \frac{i}{k^2}\left[-g^{\mu\nu} + (1-\lambda)\frac{k^\mu k^\nu}{k^2}\right] \tag{2.79}$$

The term in brackets is proportional to the sum on gluon polarizations. The parameter λ is unconstrained, and thus, must disappear in the final results for physical, gauge invariant quantities. Common particular values for λ are $\lambda = 1$

(Feynman Gauge) and $\lambda = 0$ (Landau Gauge).

Note that the gauge fixing condition in Eq. (2.77) can be written in momentum space as

$$\partial^\mu G_\mu \sim k \cdot \varepsilon \sim |k|\,(\varepsilon_0 - \varepsilon_L) = 0 \tag{2.80}$$

Thus, the constraint in Eq. (2.78) removes unphysical polarizations only in the combination (scalar)-(longitudinal). For abelian gauge theories like QED, this turns out to be sufficient. For non-abelian theories like QCD, one has to work a bit harder in order to remove the unwanted polarizations. A covariant way of doing this is by introducing a set of fictitious scalar fermions (Fadeev-Popov ghosts [46]) in the Lagrangian. These ghosts couple only to gluons and propagate in closed loops. These additional "particles" show up as additional Feynman graphs which must be evaluated while computing physical amplitudes. It can be shown that these ghost contributions precisely cancel the contributions from the last remaining unphysical gluon polarization state.

An alternative, ghost-free way of removing unphysical polarizations is to use some non-covariant device for fixing the gauge [47]. For example, one can introduce an auxiliary 4-vector n^μ and demand that $n^\mu G_\mu = 0$. Together with Eq. (2.77), this is sufficient to remove both unphysical polarization states. The gluon polarization sum is now given by

$$\sum_{\text{spins}} \bar{\varepsilon}^\mu \varepsilon^\nu = -g^{\mu\nu} + \frac{n^\mu k^\nu + k^\mu n^\nu}{(n \cdot k)} - \frac{n^2 k^\mu k^\nu}{(n \cdot k)^2} \tag{2.81}$$

Gauges specified by the additional constraint $n^\mu G_\mu = 0$ are called "axial gauges". Axial gauges are particularly useful in providing a simple, probabilistic interpretation of the leading mass singularities in the perturbative QCD expansion.

To illustrate this, we return to the simple example of $e^+e^- \to q\bar{q}G$ from Section 2.1 and define

$$H_{ij} \equiv \left[\sum_{\substack{\text{gluon}\\ \text{spins}}} \bar{\varepsilon}^\mu \varepsilon^\nu\right] \mathbf{M}_{ij}^{\mu\nu} \tag{2.82}$$

where

$$\mathbf{M}_{ij}^{\mu\nu} \equiv -\frac{1}{8} g^{\alpha\beta} \sum_{\substack{\text{quark}\\ \text{spins}}} \bar{\mathbf{M}}_i^{\mu\alpha} \mathbf{M}_j^{\nu\beta} \tag{2.83}$$

and the $\mathbf{M}_i^{\mu\alpha}$ are the matrix elements listed in Eq. (2.15-2.16). {The $-g^{\alpha\beta}$ in Eq. (2.83) effectively performs the contraction over the lepton current term, and the factor $\frac{1}{8}$ is included for simplicity.} The complete, spin-averaged squared matrix element is, up to a constant factor

$$|\mathbf{M}_1 + \mathbf{M}_2|^2 = \sum_{ij} H_{ij} = H_{11} + H_{22} + 2H_{12} \tag{2.84}$$

We first evaluate the H_{ij} using the covariant form of the gluon spin sum, given by the numerator in Eq. (2.79). In Feynman gauge ($\lambda = 1$), the result is

$$H_{11}^{(F)} = \frac{u}{t} \tag{2.85}$$

$$H_{22}^{(F)} = \frac{t}{u} \tag{2.86}$$

$$2H_{12}^{(F)} = \frac{2Q^2 s}{ut} \tag{2.87}$$

which sums up to $F(t,u)$ in Eq. (2.60). Evaluating these same terms using the axial gauge spin sum in Eq. (2.81), we obtain instead

$$H_{11}^{(A)} = \frac{1}{t}\left\{u + (2s+u)\frac{D_1}{D_3} + s\right\} - \frac{D_2}{D_3} - \frac{2n^2 s}{D_3^2} \tag{2.88}$$

$$H_{22}^{(A)} = \frac{1}{u}\left\{t + (2s+t)\frac{D_2}{D_3} + s\right\} - \frac{D_1}{D_3} - \frac{2n^2 s}{D_3^2} \tag{2.89}$$

$$2H_{12} = \frac{2Q^2 s}{ut} + \frac{D_1}{D_3} + \frac{D_2}{D_3} + \frac{4n^2 s}{D_3^2} - \frac{1}{t}\left\{s + (2s+u)\frac{D_1}{D_3}\right\}\frac{1}{u}\left\{s + (2s+t)\frac{D_2}{D_3}\right\} \tag{2.90}$$

where

$$D_j \equiv 2n \cdot p_j \tag{2.91}$$

and we again have

$$H_{11}^{(A)} + H_{22}^{(A)} + 2H_{12}^{(A)} = F(s,t) \tag{2.92}$$

The axial gauge expressions are considerably more complex than the Feynman gauge results in Eqs. (2.85-2.87), so one might well ask "Why bother with axial gauges at all?". The value of axial gauges comes from the simplifications

which arise in the collinear limit $t \to 0$.

Evaluating the covariant gauge results in the limit $t \to 0$, and using the simplified kinematics of Eqs. (2.29-2.30), we obtain

$$H_{11}^{(F)} \to \frac{Q^2}{t}[1-z] + \text{finite} \tag{2.93}$$

$$H_{22}^{(F)} \to \text{finite} \tag{2.94}$$

$$2H_{12}^{(F)} \to \frac{Q^2}{t}\left[\frac{2z}{1-z}\right] + \text{finite} \tag{2.95}$$

These terms sum to the required universal pole structure of Eq. (2.31) (up to a normalization constant previously discarded). However, we note that the singularity receives non-zero contributions from $|\mathbf{M}_1|^2$ and the interference term $2Re[\mathbf{M}_1^*\mathbf{M}_2]$.

We now repeat the $t \to 0$ evaluation using the axial gauge results in Eqs. (2.88-2.90). We note that, as long as $n \cdot p_3 \neq 0$,

$$D_1/D_3 \underset{t\to 0}{\to} z/(1-z) \tag{2.96}$$

$$D_2/D_3 \underset{t\to 0}{\to} 1/(1-z) \tag{2.97}$$

Thus

$$H_{11}^{(A)} \to \frac{Q^2}{t}\left\{\frac{1+z^2}{1-z}\right\} + \text{finite} \tag{2.98}$$

$$H_{22}^{(A)} \to \text{finite} \tag{2.99}$$

$$2H_{12}^{(A)} \to \frac{Q^2}{t}[0] + \text{finite} \tag{2.100}$$

The sum, of course, is the same as before, but we note that the leading pole contribution comes entirely from $|\mathbf{M}_1|^2$.

If we calculate in an axial gauge, so that only physical polarization states are included in the gluon spin sum, then, the interference term does not contribute to the dominant singularity. This is the simplification which makes the use of axial gauges worthwhile. In a sense, the full quantum mechanics of the problem--in which interference terms are important--can be replaced by a simple, essentially classical multiplication of probabilities associated with individual Feynman diagrams.

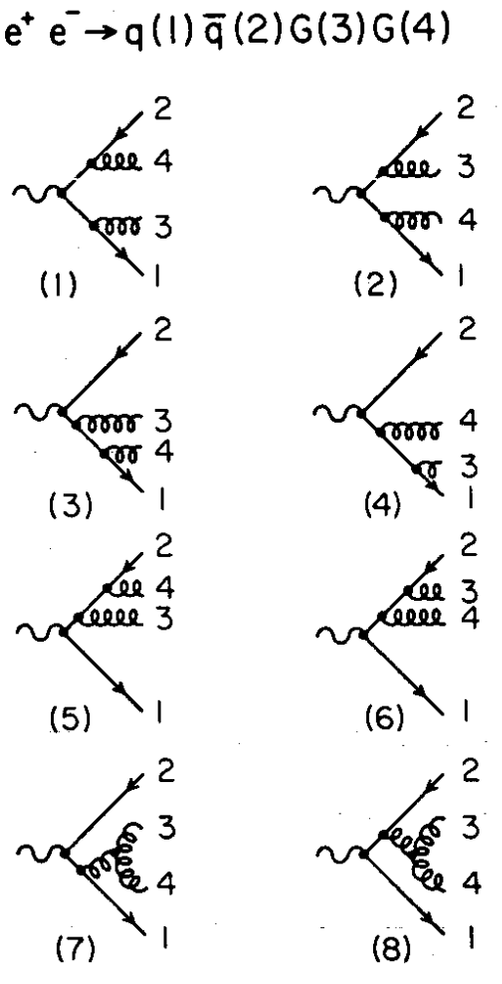

Fig. 8. $O(\alpha_s^2)$ Feynman graphs for $e^+e^- \to q\bar{q}GG$.

The explicit $O(\alpha_s)$ results examined above can be shown to generalize to arbitrary orders in QCD perturbation theory [32]. Consider the 4-parton process

$$e^+e^- \to q(p_1) + \bar{q}(p_2) + G(p_3) + G(p_4) \tag{2.101}$$

There are 8 different graphs, to $O(\alpha_s^2)$ associated with this process, as shown in Fig. (8). The perturbative singularities correspond to the vanishing of the masses of certain internal propagators

$$t_{ij} \equiv (p_i + p_j)^2 \to 0 \tag{2.102}$$

or

$$t_{ijk} \equiv (p_i + p_j + p_k)^2 \to 0 \tag{2.102}$$

Using an axial gauge, the leading pieces of the complete squared matrix elements can again be associated with the squares of individual diagrams, and the form of the singularity can be written down by inspection.

For example, the singularity for $t_{13} \to 0$, $t_{24} \to 0$ comes entirely from the square of the first graph in Fig. (8), and the leading term in the cross section is

$$d\sigma \to \sigma_0 \left[\frac{\alpha}{2\pi} \frac{dt_{14}}{t_{13}} dz P_{q/q}(z_1) \right] \times \left[\frac{\alpha}{2\pi} \frac{dt_{24}}{t_{24}} dz P_{q/q}(z_2) \right] \tag{2.104}$$

The total probability factors in terms describing the independent evolutions

$$q^*(p_1 + p_3) \to q(p_1) + G(p_3) \tag{2.105}$$

and

$$\bar{q}^*(p_2 + p_4) \to \bar{q}(p_2) + G(p_4) \tag{2.106}$$

Similarly, the leading singularities for $t_{134} \to 0$, $t_{13} \to 0$ are

$$d\sigma \to \sigma_0 \left[\frac{\alpha_s}{2\pi} \frac{dt_{134}}{t_{134}} dz_{13} P_{q/q}(z_{13}) \right] \times \left[\frac{\alpha_s}{2\pi} \frac{dt_{13}}{t_{13}} dz_1 P_{q/q}(z_1) \right] \tag{2.107}$$

which describes the nested sequence of gluon bremsstrahlungs

$$q^*(p_1 + p_3 + p_4) \to q^*(p_1 + p_3) + G(p_4) \tag{2.108}$$

followed by

$$q^*(p_1 + p_3) \to q(p_1) + G(p_3) \tag{2.109}$$

The "Leading-Logarithm" approximation to QCD perturbation theory comes about from summing up the individual pole contributions, such as Eqs. (2.104-2.107), where the sum is done to all orders in the perturbative coupling.

Before we can finally add up all the leading singularities of perturbative QCD, however, we must say a few words about the renormalization of the QCD coupling.

QCD COUPLING RENORMALIZATION

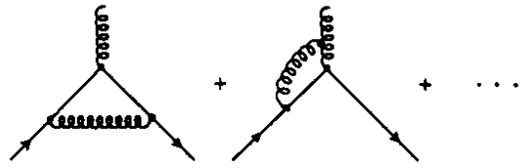

Fig. 9. Perturbative contributions to coupling renormalization.

Like the quark wave function discussed in Section 2.2, the coupling constant in perturbation theory is renormalized by higher order corrections. For example, the graphs shown in Fig. (9) lead to a renormalization of the $q\bar{q}G$ coupling. Following the general procedure used in Section 2.1, the divergences associated with the perturbative graphs in Fig. (9) are interpreted via an identification of the form

$$g_R \sim g_0 Z_g \tag{2.110}$$

[The notation in Eq. (2.110) is not standard, but this does not affect our qualitative discussions.] However, in order to give Eq. (2.110) a precise meaning, it is necessary to specify the exact kinematic configuration of the quarks and gluons in Fig. (9).

To avoid certain infrared problems in QCD, it is conventional to perform the renormalization in Eq. (2.110) with the external particles off mass-shell

$$p^2 = -\mu^2 \qquad (\mu^2 > 0) \tag{2.111}$$

The renormalized coupling defined in this way is usually denoted by

$$\alpha_s(\mu^2) \equiv \frac{g^2(\mu^2)}{4\pi} \tag{2.112}$$

The value of $\alpha_s(\mu^2)$ will change if we change the value of the renormalization point. The exact nature of this change is described by a powerful technique known as the Renormalization Group [48-50]. The evolution of $g(\mu^2)$ with changing μ is described by the differential equation

$$\frac{dg(t)}{dt} = \beta(g) \tag{2.113}$$

where $t \sim \frac{1}{2}\ln(\mu^2/\mu_0^2)$ and μ_0 is an initial point at which the value $g_R(\mu^0) = g_0$ is specified. The function β in Eq. (2.113) can be calculated in perturbation theory and has the form [43,44]

$$\beta(g) = -\frac{b_0}{4\pi}g^3 + 0(g^5) \tag{2.114}$$

where

$$b_0 = \frac{11C_G - 4T_R}{12\pi} \underset{QCD}{=} \frac{33 - 2N_F}{12\pi} \tag{2.115}$$

For QCD, with $N_f < 16$, $b_0 > 0$. This fact is crucial and leads to "asymptotic freedom"--the decrease in the size of $g(\mu^2)$ with increasing μ^2.

Keeping only the lowest order part for $\beta(g)$ in Eq. (2.114), Eq. (2.113) can be solved to give

$$\alpha_s(Q^2) = \frac{1}{b_0\ln(Q^2/\Lambda^2)} \tag{2.116}$$

where $\Lambda^2 = \mu_0^2 \exp(-4\pi/b_0 g_0^2)$.

Why have we bothered with the idea of a scale dependent coupling? The answer comes from the fact that the renormalization group automatically sums a number of large logarithms which must be included when we try to evaluate the correct leading-log predictions of perturbative QCD. Suppose we calculated with a fixed coupling $g^2(\mu_0^2)$, defined by renormalization at a specified configuration for the external legs in Fig. (9). Then, given a different configuration for the external legs in Fig. (9), the effect of the higher order

terms would be to replace g^2 (lowest order) by

$$g^2 \to g^2 + 0\left[\ln\left(\frac{\mu^2}{\mu_0^2}\right)\right] \tag{2.117}$$

where μ^2 is the scale for the new configuration. Large logarithms as in Eq. (2.117) would occur frequently in higher order diagrams, spoiling our attempt to sum the leading-logarithm contributions. The fact that the renormalization group sum of these terms gives a coupling which actually decreases with increasing μ^2 is the "miracle" of asymptotic freedom.

The proper leading-logarithm probability factor for $q \to q + G$ splittings is

$$dP = \frac{\alpha_s(t)}{2\pi}\frac{dt}{t}dz P_{q/q}(z) \tag{2.118}$$

with obvious generalizations for other QCD transitions.

Suppose now that we have a quark with maximum off-shell mass (virtualness) t_p. For example, the quark for $\gamma^* \to q + \bar{q} +$ gluons has virtualness $t_p = Q^2$. We want to evaluate the leading-log probability that this quark does not radiate any gluons and is in fact a final state parton.

The problem as posed above is not well-defined. Due to the divergences in Eq. (2.118), especially for $z \to 1$, the probability for emitting soft gluons would appear to diverge. To have a well-defined probability for "gluon radiations", we must first specify a resolution criterion for resolvable radiations.

A transition

$$q^*(p) \to q(zp) + G((1-z)p) \tag{2.119}$$

will be called resolvable if

$$z_c \le z \le 1 - z_c \tag{2.120}$$

for some cutoff parameter $z_c > 0$. We then define

$$\prod(t_p, t_c; z_c) \equiv \text{Probability [No Resolvable Emissions]} \tag{2.121}$$

as the probability that a quark evolves from an initial virtualness t_p to some minimum resolvable (mass)^2 t_c emitting only irresolvable gluons. $\prod$ is now well-defined and can be easily evaluated.

The leading-log probability for a single irresolvable emission at fixed t is given by integrating Eq. (2.118) over the z-range for irresolvable radiations

$$dP_1(t) = \frac{dt}{t}\frac{\alpha_s(t)}{2\pi}\left\{\int_0^{z_c} dz P_{q/q}(z) + \int_{1-z_c}^{1} dz P_{q/q}(z)\right\} \tag{2.122}$$

$$= \frac{dt}{t}\frac{\alpha_s(t)}{2\pi}\left\{-\int_{z_c}^{1-z_c} dz P_{q/q}(z)\right\} \tag{2.123}$$

$$\equiv \frac{dt}{t}\frac{\alpha_s(t)}{2\pi}\left\{-\gamma_{q/q}(z_c)\right\}. \tag{2.124}$$

where we have used Eq. (2.75) to obtain Eq. (2.123). The probability for having a single irresolvable emission somewhere between $t = t_p$ and $t = t_c$ is then given by

$$P_1 = \int_{t_c}^{t_p} \frac{dt}{t}\frac{\alpha_s(t)}{2\pi}\left[-\gamma_{q/q}(z_c)\right] \tag{2.125}$$

The probability for two irresolvable emissions is, by analogy

$$P_2 = \int_{t_c}^{t_p} \frac{dt_1}{t_1}\frac{\alpha_s(t_1)}{2\pi}\int_{t_c}^{t_1} \frac{dt_2}{t_2}\frac{\alpha_s(t_2)}{2\pi}\left[-\gamma_{q/q}(z_c)\right]^2 \tag{2.126}$$

This expression sums over all possible pairs of irresolvable emissions first at fixed t_1 then at $t_2 < t_1$ (the constraint $t_2 < t_1$ follows from simple kinematics).

The desired probability $\prod$ is obtained by simply summing over all possible numbers of irresolvable radiations

$$\prod(t_p, t_c; z_c) = \sum_{n=0}^{\infty} P_n \tag{2.127}$$

If we use the leading-logarithm expression for $\alpha_s(t)$ in Eq. (2.116), the nested t-integrations in Eq. (2.126-2.127) can be done analytically, and we obtain [51]

$$\prod(t_p, t_c; z_c) = \left[\frac{\ln(t_c/\Lambda^2)}{\ln(t_p/\Lambda^2)}\right]^{\frac{\gamma_{q/q}(z_c)}{\beta_0}} \tag{2.128}$$

where

$$\gamma_{q/q}(z_c) \equiv \int_{z_c}^{1-z_c} dz P_{q/q}(z) \tag{2.129}$$

and

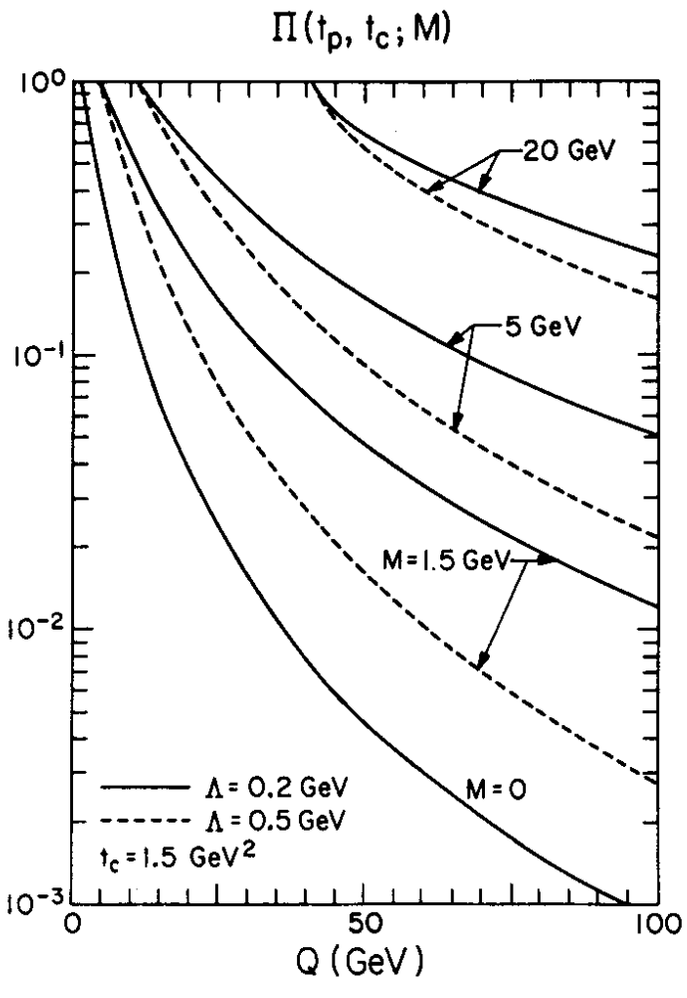

Fig. 10. Probabilities for no resolvable perturbative radiations according to Eq. (2.128) and the mass dependent generalization from Ref. [65]. The virtualness is $\sqrt{t_p} = Q - M$.

$$\beta_0 \equiv 4\pi b_0 = 11 - 2N_f/3 \tag{2.130}$$

The result in Eq. (2.128) is the basic formula used in the Monte Carlo parton shower models discussed in Section 2.5. $\prod$ is illustrated in Fig. (10) for various parameter values.

2.4 The QCD-Improved Parton Model

We need to give a physical interpretation to all the formalism of the preceding section. This is best done with a specific example.

Consider π° production in neutrino-nucleon scattering

$$\nu N \to \mu\pi^\circ X \tag{2.131}$$

(where X denotes any additional set of hadrons). The parton model description of this process is illustrated in Fig. (11a) and is described by an incoherent sum over contributing subprocesses

$$d\sigma[\nu N \to \mu\pi^\circ X] \sim \tag{2.132}$$

$$\sum \int dx_q\, dz_\pi\, [x_q G_{q/N}(x_q)][d\hat{\sigma}(\nu q \to \mu q')][D(z_\pi)]$$

$xG_{q/N}(x)$ is the probability for finding a particular quark "q" carrying a fraction x of the target nucleon's energy, $d\hat{\sigma}$ describes the scattering of this quark by the incident neutrino, and $D(z_\pi)$ describes the probability that the scattered quark will "decay" into a pion carrying a fraction z of the quark's energy. The functions $G(x)$ and $D(z)$ are assumed to be universal--that is, independent of the specific hard scattering subprocess.

The parton model provides a very successful description of a wide variety of data. However, the parton model is certainly not a "theory" of the strong interactions in any sense of the word. If, on the other hand, we believe that QCD is the proper theory of hadrons we must ask the question:

Is the parton model compatible with QCD theory?

The answer to this important question is a (qualified) "yes".

Once we allow quarks and gluons to interact we can imagine an enormous number of possible corrections to Fig. (11a) coming from gluons attached to the various quark lines. It is not *a priori* inconceivable that the quantum mechanical interference terms among the various QCD corrections could destroy the simple, probabilistic form of Fig. (11a) and Eq. (2.132).

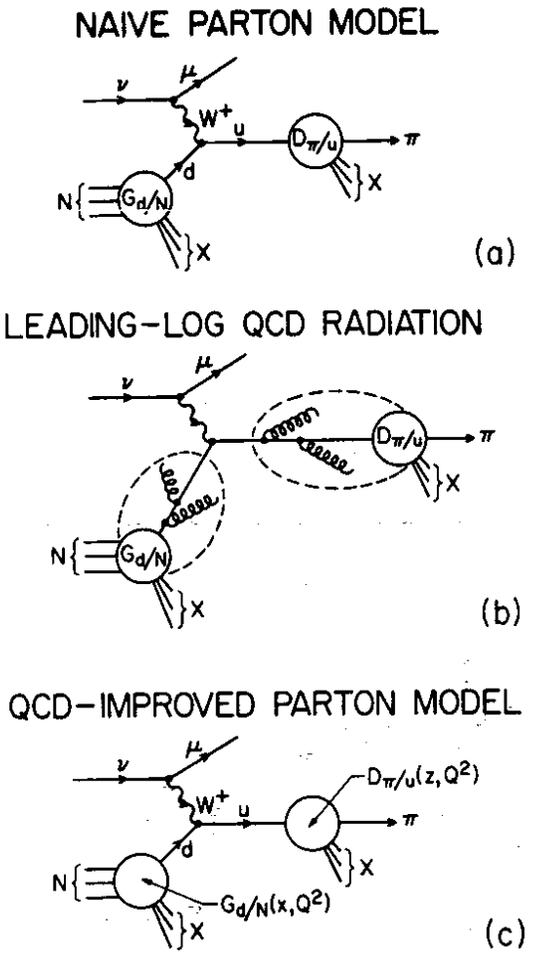

Fig. 11. Schematic illustration of QCD modifications to the parton model expansion for $\nu N \to \mu\pi X$.

However, we know from the results discussed in Section 2.3 that the parton model does survive QCD corrections if we restrict attention to the most important, leading-logarithm terms of the full QCD perturbative expansion.

In the leading-logarithm approximation (using an axial gauge), the QCD corrections to Eq. (2.132) can all be associated with gluon radiations along the incoming and outgoing quark lines in the hard scattering subprocess. These radiations can then be "factorized" into the distributions $G(x)$ and $D(z)$, as illustrated by the dotted lines in Fig. (11b). The result is the so-called "QCD-Improved" parton model.

The leading-log QCD corrections do predict certain modifications to the naive parton model formula in Eq. (2.132). If the parton subprocess $d\hat{\sigma}$ involved QCD interactions (e.g., $qq \to qq$, which enters in descriptions of hadron-hadron scattering), then we must use the scale-dependent QCD coupling

$$d\hat{\sigma}\,[\alpha_s] \to d\hat{\sigma}\,[\alpha_s(Q^2)] \tag{2.133}$$

where Q^2 is some typical momentum scale appropriate to the hard scattering.

Moreover, QCD corrections predict that the distribution and fragmentation functions G and D should change as the scale of the hard scattering changes [52-58]

$$G_{a/A}(x) \underset{QCD}{\to} G_{a/A}(x,Q^2) \tag{2.134}$$

$$D_{B/b}(z) \to D_{B/b}(z,Q^2) \tag{2.135}$$

This is, in fact, intuitively clear. As Q^2 increases, we expect that a larger and larger number of gluon radiations must be absorbed into $G(x)$ and $D(z)$ (the dashed lines in Fig. (11b)). Since these parallel gluon emissions carry off some fraction of the "original" quark's momentum, we thus expect the distribution $xG(x)$ to be shifted toward smaller x as Q^2 increases. This qualitative effect is indeed observed experimentally [59], as shown in Fig. (12).

A quantitative description of this Q-dependence is given in terms of the moments of the quark and gluon distributions. For example, let

$$u_{NS}(x,Q^2) \equiv G_{u/p}(x,Q^2) - G_{\bar{u}/p}(x,Q^2) \tag{2.136}$$

be the difference between the up-quark and anti-up-antiquark distributions in the proton (this particular combination is simple since it does not mix with

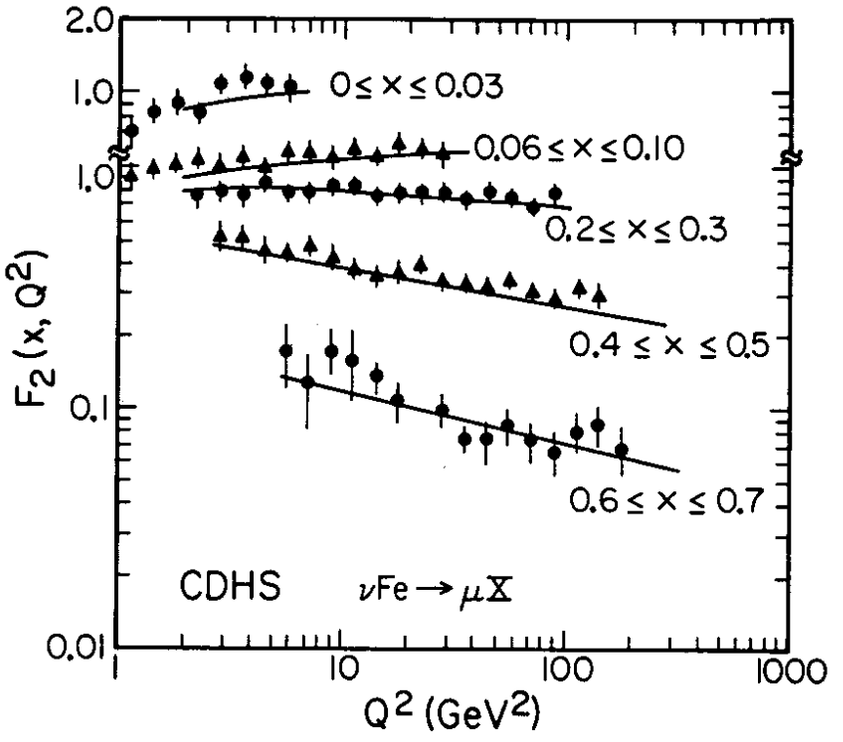

Fig. 12. Q^2 dependence of the nucleon structure function in deep inelastic scattering, as measured by the CDHS experiment [59].

gluons in the proton). Define the moments of the distribution

$$M_N(Q^2) \equiv \int_0^1 dx\; x^{N-1} u_{NS}(x,Q^2) \tag{2.137}$$

Then, the Q^2 evolution of these moments is predicted to be [60,61]

$$\frac{M_N(Q^2)}{M_N(Q_0^2)} = \left[\frac{\alpha_s(Q^2)}{\alpha_s(Q_0^2)}\right]^{\frac{\gamma_N}{2\pi b_0}} \tag{2.138}$$

where b_0 is given in Eq. (2.115) and

$$\gamma_N \equiv \int dz\; z^{N-1} P_{q/q}(z) \tag{2.139}$$

The prediction in Eq. (2.138) has been compared with data from deep-inelastic lepton-nucleon scattering with varying degrees of success. As the "lever arm" in Q^2 has increased, with higher energy experiments, the values of Λ determined via Eq. (2.138) have steadily fallen from $\Lambda \simeq 500$ MeV in 1978 [62] to $\Lambda \simeq 100$ MeV for the EMC $\mu N \to \mu N$ data [63].

Quantitative "failures" of Eq. (2.138) hardly disprove QCD. Within the framework of perturbative QCD alone we expect a number of corrections to Eq. (2.138), arising from sub-leading-logarithms, "higher twist" power corrections, etc., etc. Moreover, we must remember that at some point, the perturbative QCD on which Eq. (2.138) is based must be incomplete. We can hope that non-perturbative confinement corrections to Eq. (2.138) are important only at small Q^2. However, without a full solution to QCD, we can never really know what the domain of applicability of QCD perturbation theory really is.

Thus, even qualitative success of predictions such as Eq. (2.138) is important, in that it shows that the widely used parton model description of hard scattering processes is not inconsistent with QCD, and we are somewhat justified in using one thing (the parton model description) to try to test something else (QCD perturbation theory).

The QCD-Improved parton model was formalized in a number of theoretical papers written in about 1979 [30-33]. Among these was the work of Ellis, Georgi, Machacek, Politzer and Ross [32] which demonstrated perturbative factorization to all orders. It is interesting to note that this important paper comes perilously close to violating the Volkswagen Principle, as quoted by Politzer:

> "Never trust a theory paper whose authors cannot simultaneously fit inside a Volkswagen."

2.5 Parton Shower Monte Carlo Models

In the leading-log approximation to perturbative QCD, parton evolution can be treated as a probabilistic branching process, with individual transitions such as

$$q^*[p] \to q[zp] + G[(1-z)p] \tag{2.140}$$

described by simple probability factors as in Eq. (2.118). This branching formalism can be used to develop simple recursive Monte Carlo models [51,64-68] for the generation of parton showers.

The precise formulation of these shower models involves some important uncertainties. Recall that the basic splitting formula in Eq. (2.118) is derived only in the limit $t \to 0$. However, we want to generate "realistic" parton showers, as illustrated in Fig. (13), in which the internal parton lines have non-zero masses,

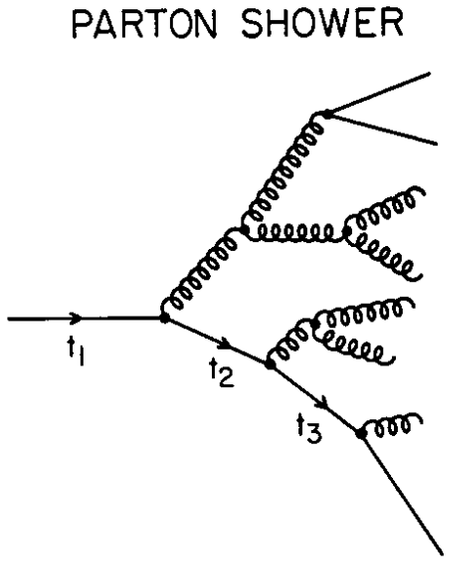

Fig. 13. Schematic illustration of a "realistic" parton shower, with the generation of non-zero parton transverse momenta.

thus allowing the production of non-zero parton transverse momenta. The masses of the internal lines will be ordered (by kinematics),

$$t_1 > t_2 > \ldots > t_n > \ldots \tag{2.141}$$

This ordering will generally be strong ($t_1 \gg t_2$, etc.), due to the $\alpha_s(t)/t$ weighting in Eq. (2.118). Unfortunately, leading-log perturbative QCD does not provide any insight as to how these non-zero masses should be included (all $t > 0$ pieces are formally "sub-leading"). We must instead try to make some reasonable choice, guided by "intuition" and exact results from low order QCD calculations.

An important uncertainty involves the identification of the variable "z" in Eq. (2.140). In the exactly collinear limit $t = p^2 \to 0$, all reasonable definitions of

z (energy fraction, $E + p_z$ fraction,...) coincide. For non-zero t, the definition of z can be related to the choice of n used in the axial gauge polarization sum in Eq. (2.81).

In Refs. [67,68], z is identified as the light-cone reaction,

$$z = \frac{E(q) + p_z(q)}{E(q^*) + p_z(q^*)} \tag{2.142}$$

for Eq. (2.140). This choice has the advantage that z is manifestly Lorentz invariant for boosts along the direction of q^*. There are some disadvantages, however.

It can be shown that z in Eq. (2.142) is the natural identification for $e^+e^- \to q\bar{q}G$ if we work in an axial gauge with gauge vector $n \sim p(\bar{q})$. As is discussed in Refs. [67,69], this choice implies that all radiation in $e^+e^- \to q + \bar{q}$ + (many gluons) comes from the quark. In the probabilistic interpretation of Sections 2.3 and 2.4, the antiquark does not radiate at all.

A more practical objection to Eq. (2.142) has to do with the precision of the identification in Eq. (2.31). Using z as defined in Eq. (2.142) and grinding through the kinematics, we have

$$|\mathbf{M}(e^+e^- \to q\bar{q}G)|^2 \underset{\substack{t \to 0 \\ z=(E+p_z)-\text{fraction}}}{\to} \frac{dt}{t} dz\ P_{q/q}(z) + O(t^0) \tag{2.143}$$

The pieces of $|\mathbf{M}|^2$ left out in the light-cone formalism are actually quite important for the $t > 0$ kinematic region of interest, and the Monte Carlo model of Refs. [67,68] routinely gives too few partons produced at high-p_T with respect to the jet axis.

The Monte Carlo model in Refs. [51,64-66] makes a different choice of z, with

$$1 - z \equiv \frac{E(G) + |\vec{p}(G)|}{E(q^*) + |\vec{p}(q^*)|} \tag{2.144}$$

for Eq. (2.142). To $O(\alpha_s)$, it can be shown that this identification comes from evaluating Eq. (2.88) with a gauge vector $n \simeq Q$ along the incident virtual photon. This gauge is clearly symmetric, so that q and $\bar{q}$ radiate equally. More importantly,

$$|\mathbf{M}(e^+e^- \to q\bar{q}G)|^2 \underset{\substack{t \to 0 \\ z=(E+|\vec{p}|)-\text{fraction}}}{\to} \frac{dt}{t} dz\ P_{q/q}(z) + O(t^1) \tag{2.145}$$

so that the leading-log formalism reproduces the exact $O(\alpha_s)$ result with better precision than the light-cone result in Eq. (2.146).

The discussions of the identification of z in the preceding paragraphs are typical of the uncertainties involved in generating "realistic" parton showers based on leading-log perturbative QCD. We should stress that these ambiguities are no worse than the uncertainties in " purely theoretical " predictions of leading-log perturbative QCD (e.g., no worse than the theoretical uncertainties in the classic moment relations in Eqs. (2.138-2.139)). The leading-log factorized QCD picture described in Section 2.4 cannot give precisely correct predictions.

To add to the confusion, we should note that a rather different parton shower formalism has been developed in Ref. [70], based on a different summation of perturbative QCD in Refs. [71-74]. This different summation attempts to add up not only the leading-log poles of the perturbative series, but also singularities from the emission of soft gluons.

Which formalism is correct? There is no easy answer. Without understanding how the full theory of QCD works, we cannot really address the question. For example, the parton shower formalisms in Refs. [51,65,67,70] differ primarily in the treatment of soft gluon emissions (where Ref. [70] does a better job of summing important perturbative terms). However, soft gluons have large wavelengths

$$\lambda \sim \frac{\hbar c}{E} \sim \frac{0.2\ \text{GeV-fm}}{E} \tag{2.146}$$

In the regions of phase space entering soft gluon summations, these wavelengths can become larger than the distance scale $\lambda \sim O(1f)$ of confinement, and some breakdown of perturbation theory is expected.

Why bother with parton Monte Carlos at all? This question is easier to answer. The Monte Carlo formalism provides the best tool, at present, for systematically including higher order QCD effects in realistic simulations of high energy processes. The necessity of including multiple QCD radiation has already been demonstrated in analyses of the NA5 full azimuth E_T events [75-77] and the enhanced "background" E_T signals associated with high energy jets at the CERN collider [1-3,78,79]. These qualitative features of the data cannot be understood using simple parton models without gluon bremsstrahlung.

We must remember, though, that the shower Monte Carlos are an approximation to perturbative QCD, and that perturbative QCD is itself an

approximation to "true QCD". Until we understand how confinement works, our best approach is probably to study various perturbative models, trying to understand which features of the models are most important in understanding the data.

The e^+e^- annihilation model described in Section 4 of this work uses the parton shower formalism of Ref. [51]. The starting point is the expression for the probability that a parton of maximum off-shell mass $\sqrt{t_p}$ does not undergo perturbative branching

$$\prod(t_p, t_c; z_c) = \left[\frac{\ln(t_c/\Lambda^2)}{\ln(t_p/\Lambda^2)} \right]^{\gamma(z_c)/\beta_0} \tag{2.147}$$

where for $A \to B + C$ splittings

$$\gamma(z_c) = \int_{z_c}^{1-z_c} dz \; P_{B/A}(z) \tag{2.148}$$

These formulae were derived for $q \to q + G$ in Section 2.3. The implementation of this formalism is basically straightforward.

We define resolvable perturbative radiation by a mass cut criterion. For example, the transition in Eq. (2.140) is resolvable only if

$$p^2 \equiv t > t_c \tag{2.149}$$

where t_c is a parameter of the model. With z chosen to be the $E + |p|$ fraction in Eq. (2.144), the cutoff z_c in Eq. (2.148) is given by

$$z_c = \min_{t_0 < t < t_p} \left\{ \frac{t}{(E + |p|)^2} \right\} \tag{2.150}$$

A random number $0 \le \xi \le 1$ is then generated, and the equation

$$\prod(t_p, t_0; z_c) = \xi \tag{2.151}$$

is solved for t_0. If $t_0 < t_c$, the initial parton does not radiate, and is instead put on mass shell as a final state parton. If $t_0 > t_c$, we have resolvable radiation, and the z-value for the branching is chosen according to

$$dP = dz \; P_{B/A}(z) \tag{2.152}$$

The daughters of the decay have individual virtualness fixed by the decay variables z and t. The branching process is then simply repeated until all partons

have evolved down to their appropriate on-shell masses.

Details of the shower formalism are discussed in Refs. [51,64]. Generalizations for massive quarks are examined in Ref. [65]. The parton shower Monte Carlo has only two parameters--the leading-log QCD scale Λ in Eq. (2.147) and the cutoff t_c in Eq. (2.149) for resolvable perturbative radiation.

The quark-gluon final state generated according to the parton shower formalism must be "converted" into hadrons before comparisons with experiment can be made. This is the subject of Section 4. For now, we simply remark that, because the hadronization scheme discussed in Section 4 is quite different from more conventional approaches, the value of Λ appropriate to the QCD-shower models is not generally the same as values found in conventional, Feynman-Field hadronization models.

2.6 Shape Variables for e^+e^- Annihilation

In the naive parton model, the process $e^+e^- \to q\bar{q} \to$ hadrons produces two back-to-back, identical, limited-p_T jets of hadrons. Including perturbative QCD, this simple picture for the shape of an event changes. For $e^+e^- \to q\bar{q}G$ events, e.g., events with moderately large $t = (p_q + p_G)^2$ lead to asymmetric two-jet systems, with a "fat jet" (the $q + G$ subsystem) recoiling against a "slim jet" (the antiquark). At sufficiently high energies, the hard emission of a wide-angle gluon leads to distinct 3-jet structure.

Shape variables provide a simple means of quantifying and measuring the overall flow of energy in e^+e^- annihilation events. The classic shape variables are determined from the eigenvalues of the momentum tensor [80]

$$M^{\alpha\beta} \equiv \sum_{j,k=1}^{N} p_j^\alpha p_k^\beta \quad (\alpha,\beta = x,y,z) \tag{2.153}$$

where the sum is over all charged particles in the event. Let Q_j denote the eigenvalues of M, with

$$Q_1 \le Q_2 \le Q_3 \tag{2.154}$$

and normalized such that

$$Q_1 + Q_2 + Q_3 = 1 \tag{2.155}$$

Letting $\hat{n}_j$ be the normalized eigenvectors, we have

$$Q_j = \sum_j (\vec{p}_j \cdot \hat{n}_i)^2 / \sum_k |\vec{p}_k|^2 \tag{2.156}$$

The direction $\hat{n}_3$ is called the sphericity axis of the event. From Eq. (2.156) it follows that the sphericity axis minimizes the squared transverse momentum sum

$$S = \frac{3}{2} \underset{\hat{n}}{Min} \{\sum_j |\vec{p}_j \times \hat{n}|^2\} / \sum_k |\vec{p}_k|^2 \tag{2.157}$$

$$= \frac{3}{2}(Q_1 + Q_2) \tag{2.158}$$

The quantity S defined above is called the sphericity of the event. For a completely collinear 2-jet system we have

$$S(2\text{-jet}) \to 0 \tag{2.159}$$

Historically, the departure of measured sphericity distributions from expectations of phase space hadronization provided the first evidence for 2-jet structure in e^+e^- annihilation [27].

A measure of the extent to which the event structure is not planar is given by the aplanarity

$$A = \frac{3}{2} Q_1 \tag{2.160}$$

which gives the minimum squared momentum out of the event plane.

Sphericity and its related variables are easy to calculate from experimental data. However, these variables have the defect of being incalculable in QCD perturbation theory. Since the sum in Eq. (2.153) is quadratic in particle momenta, $M^{\alpha\beta}$ changes if we replace one momentum by a parallel sum:

$$p_1 \to p_1^a + p_1^b = p_1 \tag{2.161}$$

We recall from Sections 2.2 and 2.3 that perturbative QCD has characteristic singularities for parallel splittings. In the calculation of dressed jet cross sections, the divergences from real emissions were canceled by divergences in the virtual corrections. However, for $M^{\alpha\beta}$, the real and virtual corrections correspond to different values of the tensor M, and the cancellation of divergences cannot occur.

To overcome this problem, the class of infrared-safe shape variables was proposed [29,51,81-89]. In general, a shape variable is simply some function of the particle momenta in an event

$$V = V(p_j) \tag{2.162}$$

A shape variable V is said to be infrared safe if it satisfies the conditions

1) V is unchanged if a single particle is replaced by a collinear pair of the same total momentum;

2) V is unchanged by the addition of an arbitrary number of soft (zero momentum) particles.

For massless final state particles, these conditions imply

$$V(p_1, p_2, p_3, \ldots) \underset{(p_1 + p_2)^2 \to 0}{\to} V(p_1 + p_2, p_3, \ldots) \tag{2.163}$$

This condition allows the cancellation of perturbative divergences to occur, and distributions $d\sigma/dV$ for parton final states can be calculated in a meaningful way.

The most commonly used infrared-safe jet variable is the thrust (or maximum directed momentum) [82],

$$T = \underset{\hat{n}_T}{Max} \{\sum_j \vartheta(\hat{n} \cdot \vec{p}_j) |\vec{p}_j \cdot \hat{n}_T|\} / \sum_j |\vec{p}_j| \tag{2.164}$$

The sum is again over all particles, but the ϑ function restricts contributions to particles in a given hemisphere. The physical region for thrust is $\frac{1}{2} \le T \le 1$, with $T \to 1$ for ideal, collinear 2-jet systems. For the 3-parton process $e^+e^- \to q\bar{q}G$, neglecting masses, one can easily show

$$T = \max\{x_j\} = \max\{2E_j/Q\} \tag{2.165}$$

To $O(\alpha_s)$, only a fraction of the full physical region is populated, $2/3 \le T \le 1$.

The $O(\alpha_s)$ perturbative thrust distribution for $e^+e^- \to q\bar{q}G$ is [29]

$$\frac{1}{\sigma_0} \frac{d\sigma^{(3)}}{dT} = \frac{2\alpha_s}{3\pi} \left[A(T) \ln\left[\frac{1}{1-T}\right] + B(T) \right] \tag{2.166}$$

where

$$A(T) = \frac{2(3T^2 - 3T + 2)}{T(1-T)} \tag{2.167}$$

$$B(T) = A(T) \ln(2T - 1) - \frac{3(3T-2)(2-T)}{1-T} \tag{2.168}$$

Note that $d\sigma/dT$ diverges for $T \to 1$. This, of course, is related to the

perturbative mass singularities examined in Section 2.2. The $O(\alpha_s)$ virtual corrections to 2-jet events yield additional divergences at $T = 1$. The real and virtual divergences are canceled by introducing a cutoff T_c and integrating out the large-T real contributions of Eq. (2.166)

$$\Delta\sigma_2(T_c) \equiv \sigma^V + \int_{T_c}^{1} dT \, \frac{d\sigma}{dT} \tag{2.169}$$

This gives a finite $O(\alpha_s)$ correction to the $T = 1$ 2-jet cross section which depends on the resolution parameter T_c.

The complete $O(\alpha_s)$ perturbative thrust distribution is then

$$\frac{1}{\sigma_0}\frac{d\sigma}{dT} = [1 + \sigma^V(T_c)]\,\delta(1-T) \tag{2.170}$$

$$+ \vartheta(T_c - T)\left\{\frac{1}{\sigma^0}\frac{d\sigma^{(3)}}{dT}\right\}$$

Note the "gap" in this result: there is no reliable $O(\alpha_s)$ prediction within the resolution region

$$T_c \le T < 1 \tag{2.171}$$

The solid line in Fig. (14) shows the perturbative prediction from Eq. (2.166). At present energies, non-perturbative fragmentation is expected to smear the results in Eq. (2.170). In particular, assuming the fixed-p_T^2 Field-Feynman fragmentation model, the $\delta(1-T)$ 2-jet term in Eq. (2.170) is smeared into something like a gaussian, with a characteristic width

$$\Delta T(\text{Non. Pert.}) \sim \frac{\langle p_T \rangle}{Q} \tag{2.172}$$

The effects of this simple model for non-perturbative hadronization are crudely indicated by the dashed lines in Fig. (14). Note that the general trend of hadronization smearing is to make the prediction less 2-jet like.

In the Hoyer model [23] for e^+e^- annihilation (which includes only 2-parton and $O(\alpha_s)$ 3-parton configurations), the thrust cut formalism is used to separate 2-jet and 3-jet events, with the value T_c chosen to coincide with the extremum of the non-perturbative (Feynman-Field) thrust distribution for $q\bar{q}$ systems. Thus, T_c increases from $T_c \simeq 0.92$ at $Q = 15$ GeV to $T_c \simeq 0.98$ at $Q = 90$ GeV. This roughly corresponds to $T_c \sim 1 - t_c/Q^2$, as expected for a fixed mass resolution

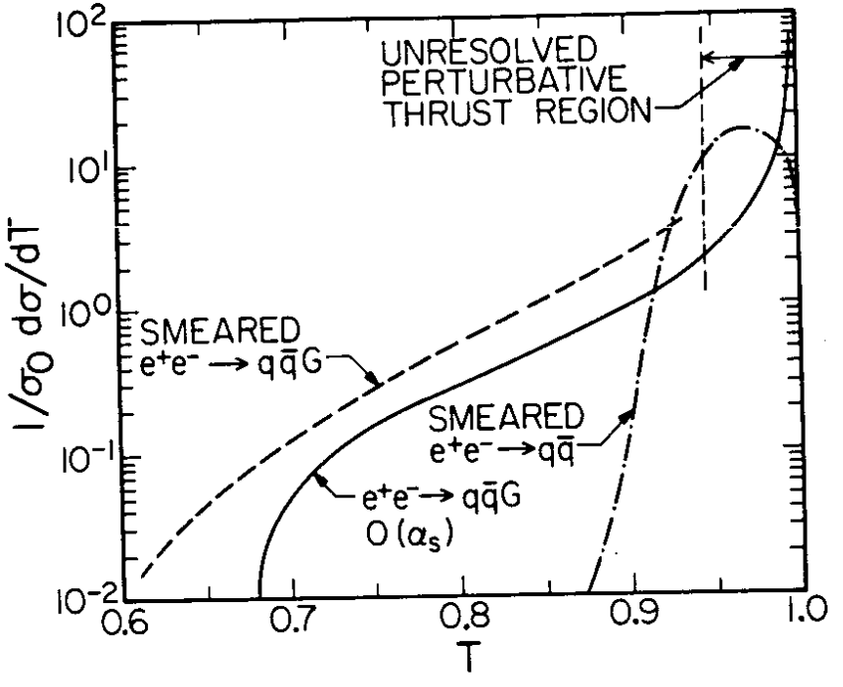

Fig. 14. The perturbative thrust distribution for $e^+e^- \to q\bar{q}G$ as given in Eq. (2.170). The dashed and dashed-dotted lines illustrate the smearing of perturbative results arising from parton hadronization.

criterion.

A rather large number of infrared safe variables have been proposed in the literature (many are reviewed in Ref. [64]). Of these, we will mention only one more, the Fox-Wolfram variables

$$H_l \equiv \sum_{i,j=1}^{n} \frac{|\vec{p}_i||\vec{p}_j|}{Q^2} P_l(\cos\vartheta_{ij}) \tag{2.173}$$

where ϑ_{ij} is the (CM) angle between $\vec{p}_i$ and $\vec{p}_j$ and P_l is the l-th Legendre polynomial. Unlike the thrust in Eq. (2.164), H_l can be evaluated without finding a preferred jet axis by some minimization technique. This makes H_l much easier to calculate for high multiplicity events.

Originally, it was hoped that the study of infrared safe shape variables could provide a test of perturbative QCD which would be relatively insensitive to hadronization corrections. That is, as Q increases, the non-perturbative smearing in Eq. (2.172) was expected to decrease, hopefully becoming irrelevant very quickly for large Q. The full result for $\langle 1 - T \rangle$ was expected to behave as

$$\langle 1 - T \rangle \simeq \alpha_s(Q^2)a_0 + \alpha_s^2(Q^2)a_1 + \ldots + A\,\frac{\langle p_T \rangle}{Q} \tag{2.173}$$

where the a_j are calculable in perturbation theory. Assuming that A is not too large, this simple expression appears to provide a simple way of determining α_s from the data.

Unfortunately, A is large, as shown by the results [90] in Fig. (15). Moreover, it seems plausible that the denominator for the non-perturbative term in Eq. (2.173) should be $\langle E(\text{parton}) \rangle$, not Q. As multijet configurations become important, $\langle E(\text{parton}) \rangle$ can be considerably less than Q.

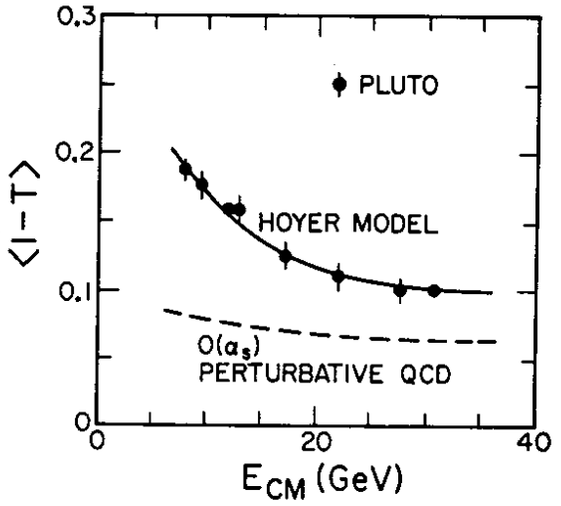

Fig. 15. Energy dependence of $\langle 1 - T \rangle$ as measured by the PLUTO collaboration [90]. The dashed curve is the $O(\alpha_s)$ perturbative QCD result. The solid curve includes estimates of non-perturbative hadronization effects.

Finally, there is the important point discussed in the next section that the $O(\alpha_s^2)$ corrections to Eq. (2.166) receive sizable corrections from small mass parton pairs--a kinematic regime where perturbation theory is not expected to give a good description of QCD.

The initial optimism that infrared safe observables could provide "hadronization-free" tests of perturbative QCD was probably too naive. Hadronization could well have significant effects at all relevant energies, and there is then little reason to prefer infrared safe variables over the "unsafe" ones related to $M_{\alpha\beta}$. (In fact, as discussed in Ref. [91], the $M_{\alpha\beta}$ variables may well provide better, more sensitive tests of jet structure at PETRA/PEP energies.)

2.7 Some Lessons from Higher Orders

The elements of perturbative QCD examined so far have been either exact lowest order calculations or approximate, leading-log sums of perturbation theory. Neither of these approaches is exact or complete. It is thus important to ask how exact higher order calculations will alter the lowest order predictions.

Higher order QCD corrections are in fact needed in order to give any precise meaning to the scale parameter Λ in Eq. (2.116). That is, it can be shown [92] that a change of scale

$$\Lambda \to \Lambda' = a\Lambda \tag{2.174}$$

is formally a sub-leading correction to the leading-log approximation. This means that leading-log values of Λ deduced from analyses of different processes need not be the same! (This is but one of several reasons why Λ is not a very good "fundamental parameter".)

In order to give Λ a precise meaning, we must consider higher order calculations. This brings us to the issue of renormalization scheme dependence [93]. Recall from Section 2.3 that bare perturbation theory leads to divergent expressions, such as

$$\sum \sim A \ln\left[\frac{\Lambda^2}{\mu^2}\right] + B \tag{2.175}$$

for the fermion self-energy in Fig. (6). These divergences were formally absorbed into the definitions of the fields

$$\psi_r \equiv Z_\psi^{-\frac{1}{2}} \psi_U \tag{2.176}$$

where

$$Z_\psi = 1 + i\alpha_s \sum \tag{2.177}$$

In fact, there is some freedom as to just how much of $\sum$ in Eq. (2.175) we wish to absorb in the renormalization in Eq. (2.176), and how much we "leave behind" to describe higher order effects. Certainly, the divergent part $A \ln(\Lambda^2/\mu^2)$ must be absorbed into ψ to get finite predictions, but we are free to absorb as much of the finite part B as we want.

Different methods for defining the finite parts of Z_ψ are known as different renormalization schemes. If we could sum all orders of perturbation theory exactly, there would be no scheme dependence in our predictions for physical cross sections. However, to any finite order in perturbation theory, we can expect our predictions to be sensitive to details of the renormalization scheme.

(Actually, things are slightly more complicated, as the form of Eq. (2.175) actually depends on the regularization scheme used to render divergent perturbative expressions "temporarily finite". For our purposes, however, this is an "inessential complication". The interested reader is referred to Ref. [7] for a nice, fairly elementary discussion.)

Renormalization scheme dependence enters in the $O(\alpha_s^2)$ expression for R (as defined in Eq. (2.9))

$$R = R_0\left[1 + \frac{\alpha_s}{\pi} + C_2\left(\frac{\alpha_s}{\pi}\right)^2\right] \tag{2.178}$$

The coefficient C_2 [94-96] depends on the renormalization scheme with

$$C_2(\overline{MS}) \simeq 1.98 - 0.115\, N_f \tag{2.179}$$

$$C_2(MOM) \simeq 0.739\, N_f - 4.637 \tag{2.180}$$

for the Modified Minimal Subtraction ($\overline{MS}$) and the Momentum (MOM) renormalization schemes discussed in Ref. [7]. Fortunately, the coefficient C_2 in Eq. (2.178) is reasonably small for most schemes. Eq. (2.178) thus provides a fairly good theoretical prediction of perturbative QCD. (Unfortunately, systematic difficulties make measurements of R at the few percent level rather difficult to achieve.)

Including higher order effects modifies the form of $\alpha_s(Q^2)$ from Eq. (2.116). There is some freedom, in higher orders, as to how Λ should be defined. One approach [97] gives

$$\frac{\alpha_s(Q^2)}{4\pi} \simeq \frac{1}{b_0 \ln(Q^2/\Lambda^2)} - \frac{b_1 \ln\ln(Q^2/\Lambda^2)}{b_0^3 \ln^2(Q^2/\Lambda^2)} \tag{2.181}$$

where, for QCD, $b_0 = 11 - 2N_f/3$ and $b_1 = 102 - 38N_f/3$.

Eq. (2.181) can be inverted to give Λ as a function of Q and α_s

$$\Lambda(Q,\alpha_s) = Q \exp\left\{-\frac{2\pi}{b_0\alpha_s} - \frac{b_1}{2b_0^2}\ln(4\pi\alpha_s)\right\} \tag{2.182}$$

compared to the lowest order result

$$\Lambda_{LO} = Q \exp\left\{\frac{-2\pi}{b_0\alpha_s}\right\} \tag{2.183}$$

If we estimate α_s (30 GeV) $\simeq 0.2$, Eq. (2.182) gives $\Lambda \simeq 200$ MeV while Eq. (2.183) gives $\Lambda_{LO} \simeq 500$ MeV. This comparison is not strictly fair (different values of α_s would result from lowest order and higher order fits to the same data), but these wide variations are typical of the results of more refined analyses.

Aside from these peculiarities in extracting a numerical value of Λ, QCD predictions for e^+e^- annihilation are generally not very sensitive to the question of renormalization prescriptions. This is not true for other observables which have been calculated in QCD perturbation theory, such as the decay widths of heavy mesons. The issue of prescription dependence is addressed in detail in, e.g., Ref. [93]. An appealing approach to this problem--based on the ansatz that finite order perturbative predictions should be stable against "small variations" in the renormalization scheme--has been proposed by Stevenson. An elementary introduction to this "Principle of Minimal Sensitivity" is given in Ref. [98].

The renormalization scheme dependence discussed above is entirely an issue of QCD perturbation theory, and the issue of how one should organize partial summations of QCD perturbation theory in the "best" possible manner. We conclude this section with an important example which shows that "perturbative" predictions can also be quite sensitive to the manner in which the perturbative calculation and (required) non-perturbative fragmentation models are joined together.

The specific issue involves the $O(\alpha_s)$ corrections to perturbative shape variable distributions. The calculations involved are quite complex and were first done in 1980 by groups at Caltech [99] and DESY [100]. The Caltech results were later verified in an independent calculation [101]. The results of these calculations appeared to be contradictory, with the DESY group finding considerably smaller corrections than the Caltech results. While some of the initial controversy was due to some simple errors in the early DESY preprints, it seems that the bulk of the disagreement is real: i.e., neither group has made any errors, yet they come to rather different conclusions.

The resolution of this discrepancy [102,103] comes from realizing that the Caltech group and DESY group actually evaluated results for <u>different</u> observables. Specifically, the Caltech group calculated shape variable distributions for <u>bare parton jets,</u> while the DESY group calculated the shape variable distributions for <u>dressed jets,</u> defined using a resolution criterion similar to that discussed for $O(\alpha_s)$ jets in Section 2.3.

We now briefly show just how the perturbative results can be so sensitive to the question of the dressing scheme.

There are a number of parton processes contributing to the e^+e^- cross section to $O(\alpha_s^2)$. To simplify the discussion, we consider only that part of the cross section proportional to the group theoretic factor C_F^2--which means that we ignore $G \to GG$ and $G \to q\bar{q}$ transitions. The $O(\alpha_s^2)$ squared matrix element for $e^+e^- \to q(1)\bar{q}(2)G(3)G(4)$ has a number of perturbative singularities associated with the vanishing of the variables

$$y_{ij} \equiv (p_i + p_j)^2 / Q^2 \tag{2.184}$$

for ij = 13, 14, 23 *or* 24. After some straightforward partial fractioning (as done to $O(\alpha_s)$ in Eq. (2.36)), the perturbative poles for the singular $q \to qG$ transitions can be isolated, and the complete squared matrix element can be written in the symmetric form

$$|\mathbf{M}|^2 \simeq \frac{1}{y_{13}} F(y_{ij}) + (1 \leftrightarrow 2) + (3 \leftrightarrow 4) + (1,3 \leftrightarrow 2,4) \tag{2.185}$$

where F is finite for $y_{13} \neq 0$.

In view of the general perturbative factorization results from Section 2.2, we know the limiting behavior of F

$$\lim_{y_{13} \to 0} F(y_{ij}) \to P_{q/q}(z) |\mathbf{M}(ee \to q\bar{q}G)|^2 \tag{2.186}$$

The perturbative real emission singularities in Eqs. (2.185, 2.186) are canceled by the singular $O(\alpha_s^2)$ corrections to the 3-jet process $e^+e^- \to q\bar{q}G$.

To obtain <u>finite</u> 3-jet and 4-jet cross sections, we introduce a resolution criterion on the 4-parton cross section. Specifically, introduce a scaled mass cutoff y_c. If $y_{ij} > y_c$, the 4 partons in $e^+e^- \to q\bar{q}GG$ are said to be distinct <u>jets,</u> and we thus define

$$d\sigma^{4\text{-jet}} \equiv \vartheta(y_{ij} - y_c)\, d\sigma(e^+e^- \to q\bar{q}GG) \tag{2.187}$$

If $y_{ij} < y_c$, we do <u>not</u> resolve the two nearly collinear partons. Instead, we interpret the (integrated) small mass configurations as part of the $O(\alpha_s^2)$ correction to the 3-jet cross section

$$d\sigma^{3\text{-jet}} \equiv d\sigma^V(e^+e^- \to q\bar{q}G) + \sum_{ij} \int_0^{y_c} \frac{dy_{ij}}{y_{ij}} F(y_{mn}) \tag{2.188}$$

The integration and summation on the right hand side allows the cancellation of real and virtual perturbative singularities to occur. The jet cross sections in Eqs. (2.187, 2.188) are <u>finite</u> (but depend on the resolution parameter y_c).

It is important to remember that Eq. (2.188) is interpreted as the $O(\alpha_s^2)$ correction to the production rate for 3 <u>massless</u> partons. As discussed in Section (2.2), the fact that the real emission part of Eq. (2.188) involves slightly different parton kinematics is ignored, and assumed to be beyond the realm of perturbation theory.

Given the finite jet cross sections in Eqs. (2.187, 2.188), the calculation of the $O(\alpha_s^2)$ shape variable distributions is a straightforward task. The solid lines in Fig. (16) show the $O(\alpha_s^2)$ corrections to the shape variable

$$C \equiv 1 - H_2 \tag{2.189}$$

where H_2 is the Fox-Wolfram shape variable defined in Eq. (2.173). We note that the shape and size of the net corrections depends very strongly on the value of y_c. The limit

$$y_c \to 0 \tag{2.190}$$

corresponds to the bare-parton Caltech results (the "data points"in the figure). The DESY group actually used a slightly different resolution criterion based on

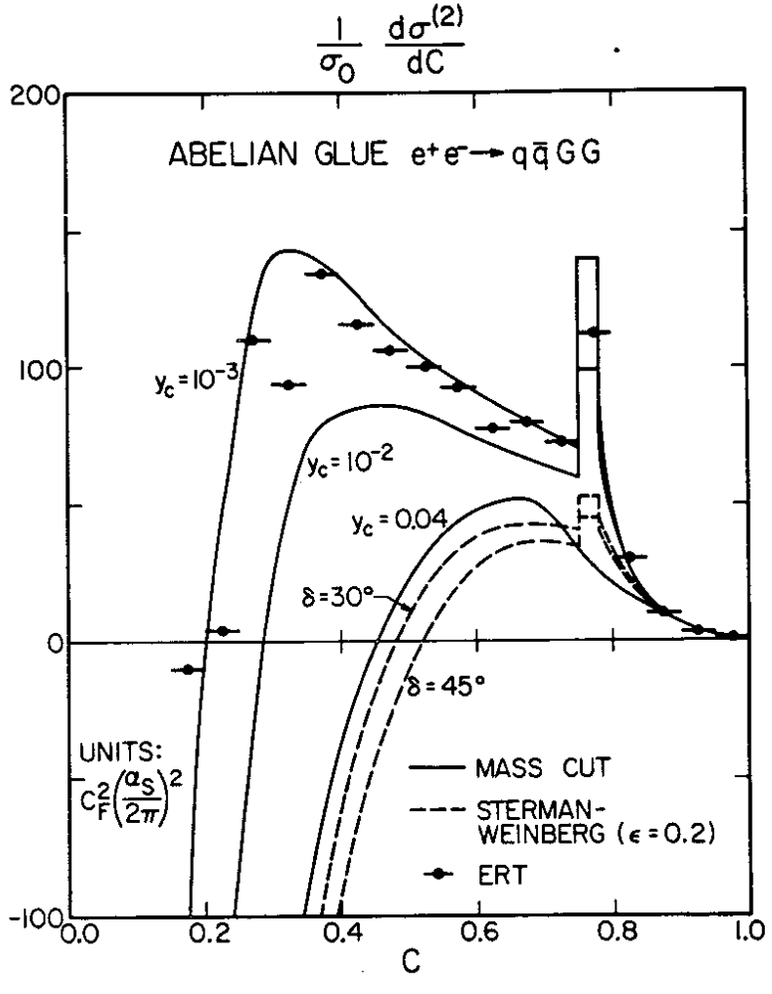

Fig. 16. Dependence of the $O(\alpha_s^2)$ perturbative corrections to $d\sigma/dC$ on the dressing scheme used in the calculation. Only the C_F^2 part of the full QCD result is shown.

Sterman-Weinberg energy and angle resolution parameters. The $\delta = 30°$ SW curve is the DESY result.

The differences between the $y_c = 0.04$ and $y_c = 10^{-3}$ results in Fig. (16) are all due to the differences between the 3-parton shape variable values assigned to all of Eq. (2.18B) and the actual 4-parton shape variable values which were "integrated out" on the right hand side of Eq. (2.18B). That is:

> The large Caltech correction in Fig. (16) is due, in part, to resolving low mass parton pairs.

In this kinematic configuration, however, we suspect that perturbation theory is not reliable. For small masses (long times) confinement is somehow the most important feature of "Complete QCD", and the interpretation of the bare parton results in Fig. (16) is thus not clear.

Due to the dressing cutoff sensitivity demonstrated in Fig. (16), the issue of $O(\alpha_s^2)$ corrections to shape variable distributions is rather difficult. Recently, Gutbrod, Kramer and Schierholz [104] have repeated the dressed jet calculation, using the mass cut resolution criterion. They demonstrated that their results coincide with the full Caltech result (all color factors) in the limit $y_c \to 0$. Due mainly to the $G \to GG$ transitions (not included in Fig. (16)), their total correction to $d\sigma/dT$ is quite large (though only about half the size of the 100% correction in the bare parton calculation). There is, in addition, some sensitivity in their results, resulting from the particular choice of the dressing scheme (mass cut vs. Sterman-Weinberg).

Because shape variable distributions do receive sizable corrections from low-mass, "non-perturbative" parton configurations, it is impossible to give a completely reliable prediction for, say, $d\sigma/dT$ without first considering the important issue:

> How do "perturbative" and "non-perturbative" aspects of QCD merge in the full theory?

At present, we have no answer to this important question.

3. Conventional Hadronization Models

The generation of hadrons from a parton final state can not yet be calculated in QCD, and some phenomenological parameterization of hadron production must be used instead. This section examines the two most widely used fragmentation models: the Feynman-Field quark jet model and the LUND model.

3.1 The Feynman-Field Quark Jet Model

Before describing what the Feynman-Field (FF) model [19] is, we should mention what it is not. Specifically, the FF model is not a "theory" of how hadronization works. Rather, it is simply a parameterization of hadron formation in jets which reproduces two important experimental facts:

1) Approximate scaling of the energy distributions of hadrons within a jet.
2) Limited transverse momenta of the produced hadrons with respect to the jet axis.

These qualitative features of hard scattering data are not "explained" or "derived" in the FF model. Rather, the FF model is a parameterization of hadron production from fast quarks which is constructed in such a manner that the above experimental observations are reproduced. As is discussed in Section 3.3, the simple picture of hadron production in the FF model suffers from a number of conceptual problems. (These problems were well understood by Feynman and Field, as noted in Section 4.3 of their paper.)

The FF model describes hadron production in quark jets through the iteration of the fundamental transition

$$q_a \rightarrow M(q_a,\bar{q}_b) + q_b \tag{3.1}$$

in which the incident quark fragments into a meson M and a "residual" quark q_b. This transition can be viewed as resulting from the creation of a $(q_b\bar{q}_b)$ pair from the vacuum, as illustrated in Fig. (17). Iterations of the basic transition in Eq. (3.1) lead to the production of a chain of primary hadrons (and a low energy "leftover" quark), as illustrated in Fig. (17).

The description of the basic vertex in Eq. (3.1) is chosen so as to reproduce the scaling and limited-p_t behavior of jets. Fig. (18) shows some relatively low energy data [105-107] for the scaled energy distributions of pions produced in e^+e^-, ep and νN interactions. The function $D(z)$ is defined by

$$D(z) \equiv \frac{1}{\sigma_{TOT}}\frac{d\sigma}{dz} \tag{3.2}$$

where σ_{TOT} is the appropriate total cross section. With this definition, $D(z)$ is normalized such that

$$\int dz D(z) = \langle N(\pi^\pm)\rangle \tag{3.3}$$

where $\langle N\rangle$ is the average multiplicity of pions produced in the interaction.

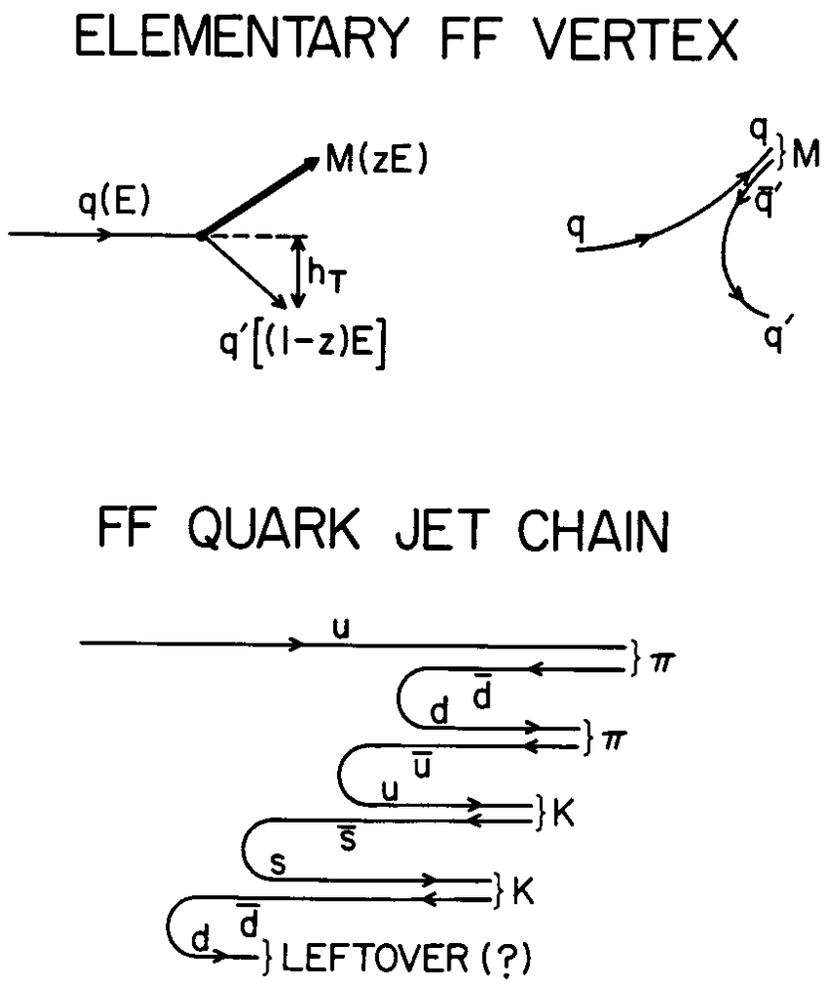

Fig. 17. Illustration of quark jet hadronization in the Field-Feynman (FF) model.

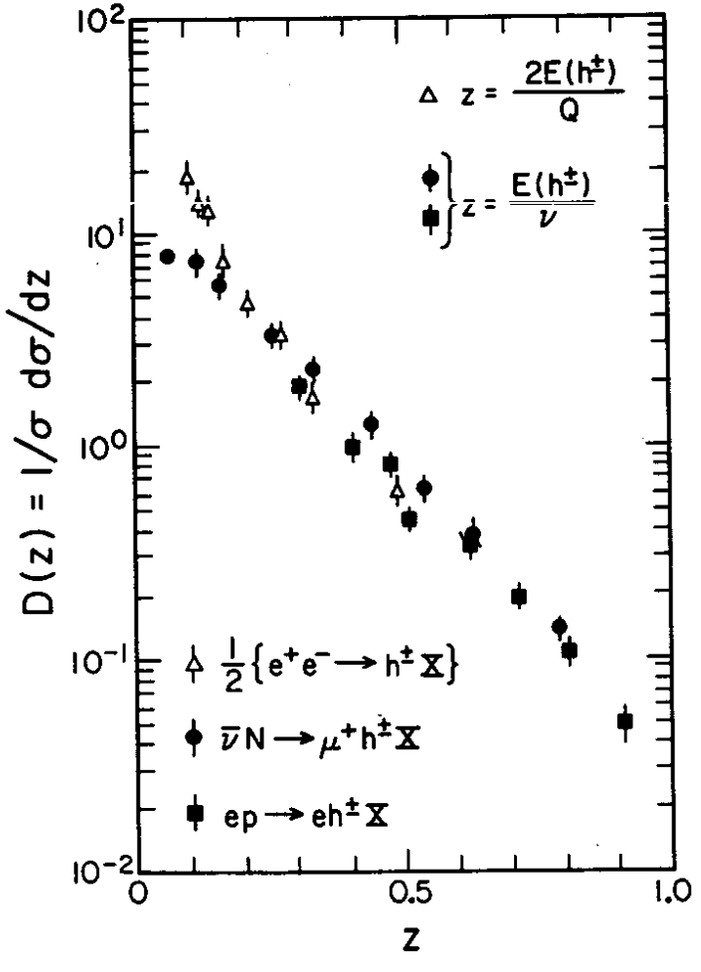

Fig. 18. Approximate process independence of the scaled energy distributions of charged hadrons produced in various hard scattering processes.The data are from Refs. [105-107].

The data points in Fig. (18) define a universal curve, to within 10-20%. At first glance, the process independence of $D(z)$ might seem remarkable, since the variables z for $\nu N \rightarrow \mu\pi X$ and $e^+e^- \rightarrow \pi X$ are not the same:

$$z_\nu = \frac{E(\pi)}{E(\nu) - E(\mu)} \tag{3.4}$$

for $\nu N \rightarrow \mu\pi X$, with energies measured in the rest frame of the target nucleon, and

$$z_{e^+e^-} = \frac{2E(\pi)}{Q} \tag{3.5}$$

for $e^+e^- \rightarrow \pi X$.

The relationship between $z_{\nu N}$ and $z_{e^+e^-}$ is clarified if we consider the parton model descriptions of e^+e^- → hadrons and $\nu N \rightarrow \mu$ + hadrons shown in Fig. (2). In each case we have

$$z \simeq \frac{E(\pi)}{E(\text{quark})} \tag{3.6}$$

If we neglect masses and transverse momenta, the energy ratio in Eq. (3.6) is invariant under Lorentz boosts along the direction of the quark momentum. In appropriate frames, Eq. (3.6) coincides with both Eq. (3.4) and Eq. (3.5). Thus, the process independence of Fig. (18) is plausible if we adopt the parton model picture of fragmenting quarks.

To reproduce the approximate scaling of the experimental $D(z)$ results, FF postulate that the energy sharing in Eq. (3.1) is described by a simple probability function

$$\frac{dP}{dz} = f(z) \tag{3.7}$$

where $z \simeq E(\text{meson})/E(\text{quark})$ (the precise form of z is discussed below). The residual quark q_b in Eq. (3.1) thus retains a fraction $\eta \equiv 1 - z$ of the original quark's energy. The probability function f is normalized such that

$$\int_0^1 dz\ f(z) = 1 \tag{3.8}$$

The splitting function $f(z)$ and the resulting fragmentation function for the (primary) hadrons in the decay chain of Fig. (17) are related by an integral equation

$$D(z) = f(z) + \int_z^1 d\eta \{ f(1-\eta) D(z/\eta) \} \tag{3.9}$$

The first term on the right hand side of Eq. (3.9) gives the probability that the observed hadron is the first hadron produced in the decay chain of the initial quark, and the second term sums over emission of the hadron deeper in the decay chain.

If we adopt a simple polynomial form for $f(z)$,

$$f(z) = (d+1)(1-z)^d \tag{3.10}$$

then Eq. (3.9) can be solved for $D(z)$, giving

$$D(z) = (d+1)\,\frac{(1-z)^d}{z} \tag{3.11}$$

The minimum z for hadron production is of the form

$$z_{MIN}(E_{CM}) \simeq m_\pi / E_{CM} \tag{3.12}$$

Thus, Eq. (3.3) and the fragmentation function in Eq. (3.11) give

$$\langle N_{ch}(E_{CM})\rangle \simeq A + B\ln(E_{CM}) \tag{3.13}$$

This logarithmic growth in multiplicity is consistent with e^+e^- experimental results for 2 GeV $\lesssim E_{CM} \lesssim$ 10 GeV. The increase in N_{ch} with increasing E_{CM} comes entirely from the low-z region of $D(z)$--where the data are not expected to scale.

Fig. (19) shows some experimental results [108,109] for the transverse momenta of charged hadrons with respect to the jet (sphericity) axis in e^+e^- annihilation at $E_{CM} \sim 15$ GeV and K^+p scattering at $p_{LAB} = 70$ GeV. The data are sharply cut off in p_t^2, with $\langle p_T\rangle \sim 320$ MeV. This observed limited-p_T behavior is parameterized in the FF model as follows.

The momentum of the original quark is taken to define the $+z$ axis. The $(q_j\bar{q}_j)$ pairs in Fig. (17) are assumed to have no net transverse momentum with respect to the z-axis, but the individual $q_j, \bar{q}_j$ are given equal magnitude transverse momenta distributed according to the probability

$$dP \simeq d^2p_t\, e^{-p_t^2/2\sigma_q^2} \tag{3.14}$$

The transverse momentum of a primary hadron is given by the vector sum of the transverse momenta of its constituent quark and antiquark, and

$$\langle p_t \text{ (Primary Meson)}\rangle = \sqrt{\pi}\sigma_q\ . \tag{3.15}$$

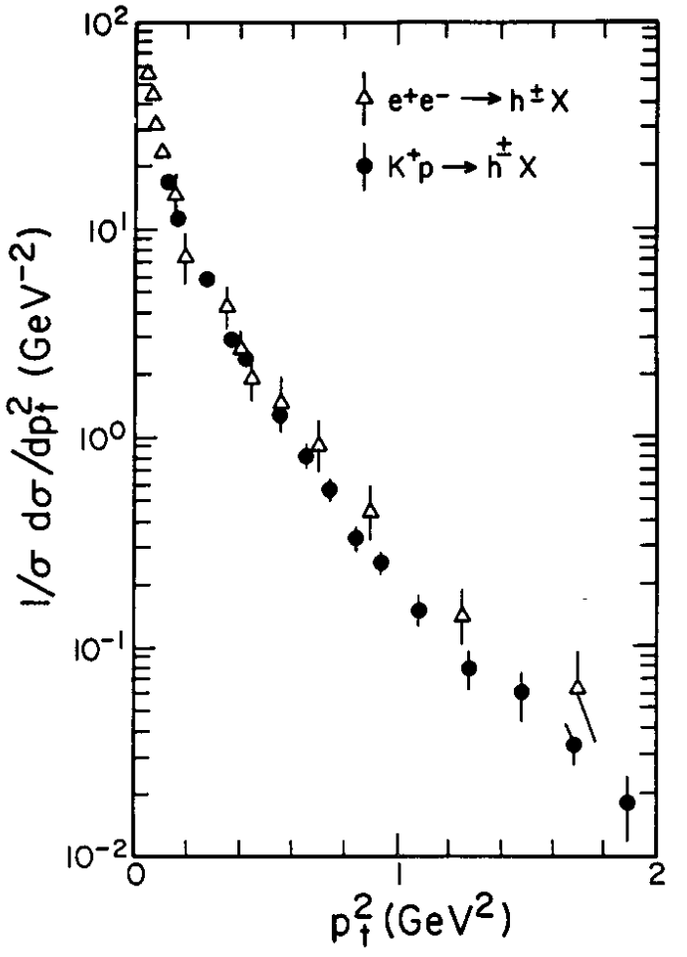

Fig. 19. Approximately universal behavior of the transverse momentum distributions of charged hadrons produced in e^+e^- annihilation and hadron-hadron scattering. The data are from Refs. [108, 109].

The transverse momentum smearing parameter σ_q in Eq. (3.14) is assumed to be independent of the incident quark energy.

The FF model assumes that all primary hadrons produced in the decay chain are either pseudoscalar or vector mesons. The relative production probability for these two spin states is taken to be a fixed number

$$\alpha_v \equiv \frac{N[\text{Vectors}]}{N[\text{Vectors}] + N[\text{Pseudoscalars}]} \tag{3.16}$$

Note that the value chosen for α_v will affect the determination of the optimal form of $f(z)$ in Eq. (3.7). That is, the decays of primary vector mesons ($\rho \to \pi\pi$, e.g.) will soften the net $D(z)$ distribution, distorting the shape away from that predicted by the integral equation, Eq. (3.9).

The quark pairs produced in the decay chain are allowed to have flavors $(u\bar{u})$, $(d\bar{d})$ or $(s\bar{s})$, with $(u\bar{u})$ and $(d\bar{d})$ produced with equal probabilities. The strangeness production probability

$$\gamma_s \equiv \frac{N[s\bar{s}]}{N[u\bar{u}] + N[d\bar{d}] + N[s\bar{s}]} \tag{3.17}$$

is a free parameter of the model. Its value is adjusted to reproduce the observed rate of strange particle production in quark jets. We note that the values of α_v in Eq. (3.16) and γ_s in Eq. (3.17) are correlated. That is, since the vector meson decays

$$K^* \to K\pi \tag{3.18}$$

$$\rho \to \pi\pi \tag{3.19}$$

yield excess pions, γ_s cannot be determined from experimental $N[K]/N[\pi]$ rates unless α_v is known.

To complete our specification of the FF model, we must address two technical details: the precise definition of z in Eq. (3.7) and the manner in which the decay chain in Fig. (17) is stopped when the residual quark in Fig. (17) becomes sufficiently soft. Feynman and Field identify z with the light cone fraction

$$z = \frac{(E + p_z)\text{Meson}}{(E + p_z)q_a} \tag{3.20}$$

for the transition in Eq. (3.1). The manner in which the cascade is stopped is rather arbitrary. Typically, a minimum value $W_0 \equiv (E + p_z)_{MIN} \simeq 1$ GeV is introduced, and the cascade is terminated once the $E + p_z$ of the residual quark falls

below W_0. (The scheme used in Ref. [19] is in fact rather different—if not slightly peculiar.)

All elements of the basic FF model have now been specified. The model involves one phenomenological function, $f(z)$ in Eq. (3.7), and three phenomenological parameters, σ_q in Eq. (3.14), α_v in Eq. (3.16) and γ_s in Eq. (3.17). The function $f(z)$ is conventionally parameterized as

$$f(z) = 1 - \alpha_F + 3\alpha_F(1 - z)^2 \tag{3.21}$$

introducing the fourth (and final) parameter α_F. The structure of the model is remarkably simple. The chain of primary hadrons in Fig. (17) is generated using the simple, iterative formalism described above. Unstable vector mesons produced in the decay chain are then allowed to decay according to the decay modes and branching ratios found in the particle data tables [110].

Values of the four parameters in the model were determined by fits to various data. The values

$$\gamma_s = 0.4 \tag{3.22}$$

$$\alpha_v = 0.5 \tag{3.23}$$

$$\sigma_q = 320 \text{ MeV} \tag{3.24}$$

$$\alpha_F = 0.77 \tag{3.25}$$

were found to provide a reasonable fit to experimental results. We take these values as specifying the "standard" Feynman-Field quark jet model. The FF model provides no physical insight into any energy dependence of these parameters, and it is generally simply assumed that the values in Eqs. (3.22-3.25) are independent of the initial quark's energy.

In using the FF model to analyze results from high energy PETRA/PEP experiments, several extensions and modifications of the basic FF formalism are required.

The first extension concerns gluon fragmentation. In the Ali [24-25] and Hoyer [23] models, gluons are hadronized by first splitting the gluon into a quark-antiquark pair

$$G[E] \to q[zE] + \bar{q}[(1 - z)E] \tag{3.25}$$

The daughter quark and antiquark are then fragmented independently, using

the FF scheme. The flavor of the $q\bar{q}$ pair in Eq. (3.26) is taken to be $u\bar{u}$, $d\bar{d}$ or $s\bar{s}$ with equal probability (gluons are "flavor blind"). In the Ali model, the energy sharing in Eq. (3.26) is distributed according to the Altarelli-Parisi splitting function in Eq. (2.35),

$$\frac{dP}{dz} \sim z^2 + (1-z)^2 \tag{3.27}$$

The Hoyer model simply assigns all the gluon energy to either q or $\bar{q}$ with equal probability. This means that gluons are effectively viewed as quarks of random flavor. This assumption has no theoretical motivation, but it does reproduce some experimental results for energy distributions within the individual jets of 3-jet events and hadrons produced in upsilon decays [111,112].

Heavy quark production is important in e^+e^- annihilation, with charm and bottom production accounting for more than 40% of the cross section. It is clearly necessary to generalize the FF model--in particular, Eqs. (3.21, 3.25)--to give a reasonable description of heavy flavor fragmentation.

On general, almost kinematic ground, Bjorken [113] and Suzuki [114] have argued that the heavy meson M produced in heavy quark fragmentation

$$Q \to q' + M(Q\bar{q}') \tag{3.28}$$

should carry most of the energy of the heavy quark Q. In particular, Bjorken suggests the estimate

$$\langle z_E \rangle \sim 1 - \frac{1\ \mathrm{GeV}}{M_Q} \tag{3.29}$$

where

$$z_E \equiv E[M(Q\bar{q})]/E(Q) \tag{3.30}$$

and M_Q is the heavy quark mass. Charm, however, is not tremendously heavy ($M_Q \sim 1.5$ GeV), and it is not likely that the $M_Q \to \infty$ arguments in Refs. [113,114] can be applied. The Ali and Hoyer models instead typically use the ansatz

$$f_c(z) = 1 \tag{3.31}$$

for the splitting function for charm in Eq. (3.7). This assumption is consistent with the indirect observations of charm production and semileptonic decay in neutrino dimuon events, $\nu N \to \mu\bar{\mu}X$ [115-117].

In place of Eq. (3.31), some recent analyses use the estimate [118]

$$f_c(z) = \frac{1}{z\left[1 - \frac{1}{z} - \frac{\varepsilon}{1-z}\right]^2} \tag{3.32}$$

which was suggested by a calculation using a simple vertex function to connect, e.g., a c-quark and a $\bar{d}$-antiquark with a D^+ wave function. The parameter ε in Eq. (3.32) is estimated to be

$$\varepsilon \simeq (m_u/m_c)^2 \tag{3.33}$$

and the value $\varepsilon \simeq 0.15$ provides a reasonable fit to recently measured $D(z_E)$ distributions for $e^+e^- \to D^{*\pm}X$ events at PEP and PETRA.

The final extension of the FF model to be considered here concerns the question of baryon production in quark fragmentation. Naïvely, we might view baryon production as arising from a generalization of Eq. (3.1)

$$q_a \to B[q_a, q_b, q_c] + \bar{q}_b + \bar{q}_d \tag{3.34}$$

This "vertex" involves many more participants than Eq. (3.1). Based on, e.g., the counting rule formalism of Brodsky and Farrar [119,120]; it was generally assumed that baryons produced in the fragmentation of quark jets would be fairly soft, with,

$$\frac{D_{p/u}(z)}{D_{\pi/u}(z)} \overset{?}{\sim} (1-z)^N \tag{3.35}$$

for $N \gtrsim 2$, where $D_{p/u}$ describes a u-quark fragmenting into a proton, etc. This rather widely accepted expectation is not realized in the PETRA data, where $N(p)/N(\pi)$ is found to actually increase with $z \to 1$ [121,122].

3.2 Applications of the (Extended) FF Model

In Section 3.3 we will discuss a number of important conceptual shortcomings in the FF model. Before "attacking" the model, though, it seems fair that we spend some time showing that the model does do a reasonable job at the task for which it was originally intended: the parameterization of the important qualitative features of jet fragmentation in a manner which lets us explore the nature of underlying hard processes.

The examples discussed below basically use the $O(\alpha_s)$ Hoyer model described in Sections 3.1, 2.6, and, in detail, in Ref. [23]. Both examples deal

with experimental evidence for hard gluon radiation in e^+e^- annihilation. Events with distinct 3-jet topology had been observed at PETRA essentially as soon as the machine was turned on. In order to demonstrate that these events could not be understood as, e.g., occasional statistical fluctuations in high energy 2-jet events, a detailed analysis of the event properties was necessary.

A particularly nice analysis was done by the TASSO group, as reported in Refs. [123,124]. Multihadron events at E_{CM} = 12 GeV and E_{CM} = 30 GeV were analyzed, using the sphericity tensor formalism described in Section 2.6. The first stage in the analysis involved a careful redetermination of the FF parameters for the dominant 2-jet events. These events were selected from the entire data sample by a cut on the sphericity

$$S(2\text{-}jets) \leq 0.25 \tag{3.36}$$

These data were then compared with simulated FF events, which were analyzed using the experimental acceptances, resolutions, etc.

The TASSO analysis in [124] did not distinguish hadron flavors, so no information on γ_s in Eq. (3.22) was obtained. Experimental results on the aplanarity A (Eq. (2.160)), the scaled momentum distributions dN/dx_p for charged hadrons, and the mean charged multiplicity were found to be particularly sensitive to values of the FF parameters σ_q, a_F and α_v, respectively. Simultaneous fits to the 12 GeV and 30 GeV 2-jet data samples gave the values

$$a_F = 0.57 \pm 0.20 \tag{3.37}$$

$$\sigma_q = 0.32 \pm 0.04 \text{ GeV} \tag{3.38}$$

$$\alpha_v = 0.56 \pm 0.15 \tag{3.39}$$

These values are consistent with the "standard" FF values from Section 3.1.

At 30 GeV, the 2-jet events do not reproduce the tail at large S in the experimental sphericity distributions. Such large-S events are expected from wide-angle gluon bremsstrahlung, and are incorporated into the analysis using the Hoyer model in Monte Carlo simulations. With the FF parameters fixed from the analysis of low-sphericity events, the coupling α_s in Eq. (2.20) is the only free parameter in the model, and the value

$$\alpha_s = 0.17 \pm 0.02 \tag{3.40}$$

was determined. The resulting Hoyer model fits were found to agree well with

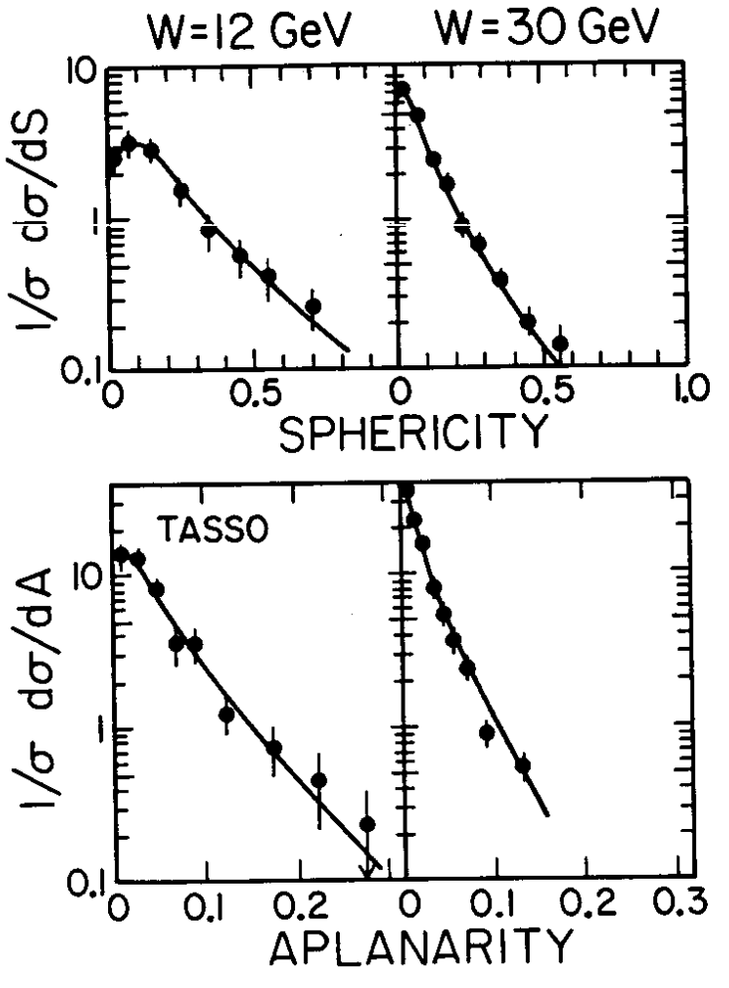

Fig. 20. Independent fragmentation fits to shape variable data from the TASSO analysis in Ref. [120].

the data, as illustrated in Fig. (20). We must remark, however, that the determination in Eq. (3.40) is not "absolute", but depends on the many particular assumptions of the Hoyer Model.

Further evidence for hard gluon bremsstrahlung is provided by the shapes of large sphericity events within the event plane (the plane normal to the aplanarity axis $\hat{n}_3$). In perturbative QCD, large sphericity events should arise from a single hard gluon bremsstrahlung, so that the momentum flow in an event should lie primarily in a plane determined by the underlying $q\bar{q}G$ parton system.

To test this expectation, the TASSO group measured the variables

$$\langle p_t^2\text{-}IN\rangle \equiv \frac{1}{N_{chg}}\sum_j (\vec{p}_j \cdot \hat{n}_2)^2 \qquad (3.41)$$

$$\langle p_t^2\text{-}OUT\rangle \equiv \frac{1}{N_{chg}}\sum_j (\vec{p}_j \cdot \hat{n}_3)^2 \qquad (3.42)$$

where the sum is over all charged particles in the event, and the $\hat{n}_j$ are the eigenvectors of the sphericity tensor. For planar events, one expects $\langle p_t^2\text{-}IN\rangle$ large and $\langle p_t^2\text{-}OUT\rangle$ small. {Two-jet events give small values for both.}

The TASSO results at 12 GeV and 30 GeV [91, 108] are shown in Fig. (21). The excess of large $\langle p_t^2\text{-}IN\rangle$ events at high energy is quite evident. Fig. (21a) shows that the $\langle p_t^2\text{-}IN\rangle$ signal cannot be reproduced in a 2-jet FF model, even if σ_q is increased to $\sigma_q \sim 450$ MeV (larger values of σ_q are excluded by the 30 GeV $\langle p_t^2\text{-}OUT\rangle$ data). Fig. (21b) shows that the full Hoyer model with $\alpha_s \simeq 0.17$ can reproduce the data.

The results in Fig. (21) do suggest an interesting question, however. How would the extracted value of α_s change if we generalized the FF model to allow systematic energy dependence of σ_q, with σ_q (12 GeV) $\simeq$ 300 MeV and σ_q (30 GeV) $\simeq$ 450 MeV. From the results in Fig. (21a), it seems plausible that this energy dependence might decrease the value of α_s required to reproduce the full $\langle p_t^2\text{-}IN\rangle$ distribution. A systematic energy dependence of σ_q cannot be excluded on the basis of any data examined thus far. In the FF model, σ_q is a constant--but this is simply an assumption. In Section 4 we will discuss a simple dynamical model for limited-p_T jets in which $\langle p_t^2\rangle$ does increase between Q = 12 GeV and Q = 30 GeV.

As a final example of use of the extended FF model, we consider the question of determining the spin of the gluon. Actually, the gluon spin is not directly

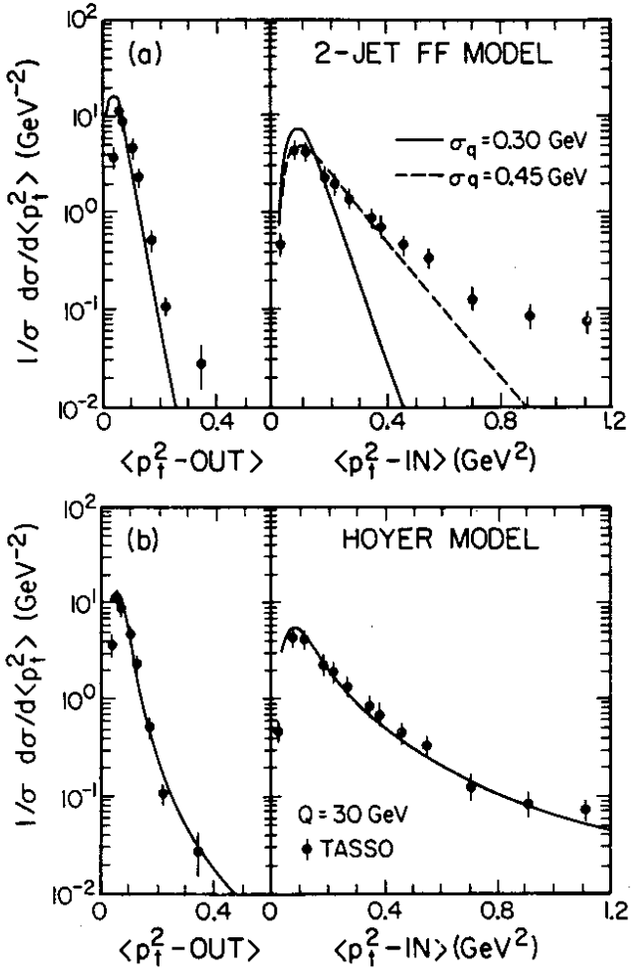

Fig. 21. Mean transverse momenta in and out of the event plane. The data are from TASSO [91, 108]. The curves in (a) are predictions of Field-Feynman 2-jet fits for different values of the transverse momentum smearing. The curves in (b) are results for the full Hoyer model.

measured. Instead, the basic 3-parton cross section in Eq. (2.23) is compared to predictions of a "toy" model in which the gluon is treated as a spin-zero object. The analogue of Eq. (2.23) for this spin-zero "gluon" is [29]

$$\frac{1}{\sigma_0}\frac{d\sigma}{dx_1 dx_2} \simeq \frac{x_3^2}{(1-x_1)(1-x_2)} \tag{3.43}$$

where $x_3 = 2 - x_1 - x_2$. The differences in the numerators in Eqs. (2.23), (3.43) reflect the differences between scalar and vector $q\bar{q}G$ couplings in Fig. (4). The question of determining the gluon spin is then the question of showing that Eq. (3.43) is strongly disfavored by the data.

The test can be done in terms of the Ellis-Karliner angle [125]. Consider the $q\bar{q}G$ configuration in Fig. (22), specified by particular fractional energies $x_1 > x_2 > x_3$. Now boost the $\bar{q}G$ subsystem to its own rest frame and define

$$\tilde{\vartheta} \equiv \vartheta(q,\bar{q}) \tag{3.44}$$

in that frame. One can show by simple kinematics

$$\cos\tilde{\vartheta} = (x_2 - x_3)/x_1 \tag{3.45}$$

The distribution $dN/d(\cos\tilde{\vartheta})$ can then be used to distinguish between Eqs. (3.43-2.23).

To implement this test, a number of cuts must first be made on the full data sample, in order to select events with well-defined 3-jet structure. Moreover, particles in the selected events must be associated with particular jets in order to define the jet energies x_j. This requires an empirical cluster-finding algorithm. In the analysis of TASSO [126,127], Monte Carlo events are generated, using both Eq. (3.43) and Eq. (2.23). The partons are hadronized using the FF prescription, and these simulated events are passed through the same acceptance criteria and cluster algorithms as used in the data analysis. Model predictions and experimental results for $dN/d(\cos\tilde{\vartheta})$ can then be compared, as shown in Fig. (23). It is seen that the perturbative QCD prediction is strongly preferred over results of the spin-zero model.

The gluon-spin analysis is a perfect example of the "conservative" use of the FF jet fragmentation model (for which the model was truly intended). In order to make a careful test of $dN/d(\cos\tilde{\vartheta})$, a number of cuts, etc. were needed on the data. The effects of these cuts on the theoretical predictions can be estimated by the Monte Carlo simulations. Moreover, since the same

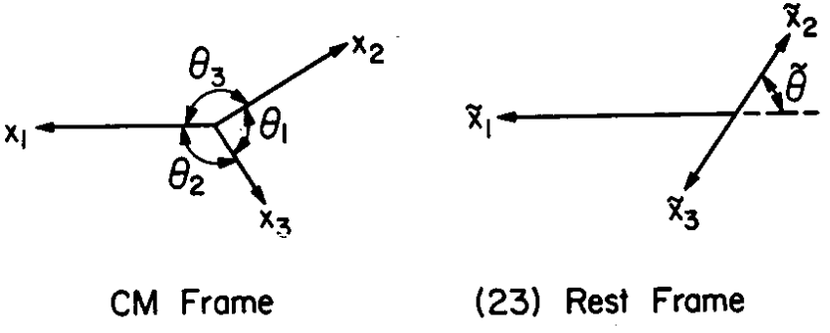

Fig. 22. Definition of the Ellis-Karliner angle $\tilde{\vartheta}$.

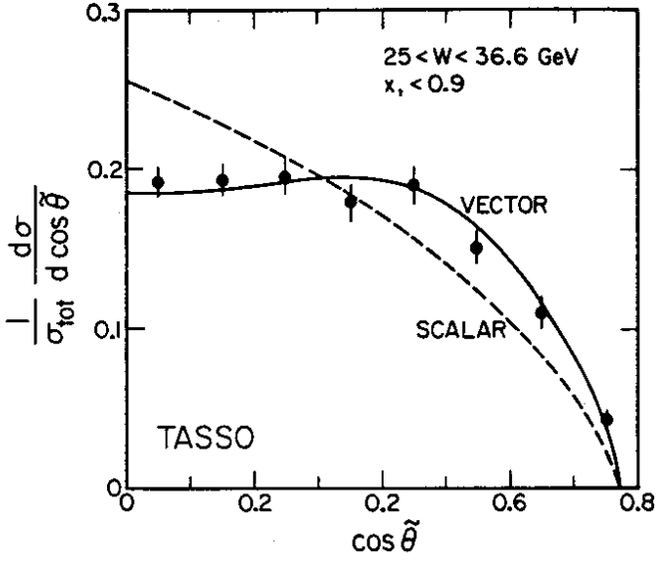

Fig. 23. TASSO results [126, 127] for $d\sigma/d\cos\tilde{\vartheta}$ compared with predictions of perturbative QCD and the scalar gluon model.

hadronization scheme was used for both the scalar and vector models, the differences between the predictions shown in Fig. (23) are not overly sensitive to details of the hadronization model. Variations in, e.g., α_s or σ_q do not affect the strong positive conclusion of the analysis.

3.3 Problems with the FF Model

There are a number of basic conceptual problems with the (extended) FF model, which are somewhat well known, though not necessarily well-appreciated. These problems can become serious when we assume that the FF prescription provides a "precise" description of hadronization and push predictions of the model too far. Among the major problems in the FF parameterization we have:

1) Energy is not conserved.
2) The model is not Lorentz invariant.
3) Flavor, charge and color are not conserved.
4) The evolution of hadron production in space-time seems wrong.
5) Multiple counting problems arise for nearly collinear parton systems.

We next briefly discuss these points.

The FF scheme does not conserve energy. This is obvious if we realize that the single massless quark is assumed to materialize as a massive jet of physical hadrons. The splitting algorithm in Eq. (3.1, 3.7) conserves the sum $E + p_z$, but neither E nor p_z separately. The imposition of energy conservation in FF Monte Carlo simulations is rather arbitrary. For example, in the FF 2-jet model used in the Mark II data analysis software, FF events are generated and then simply rejected if energy is not conserved within some tolerance. In other models (e.g., the Ali model), the "bare" event generated via the FF model is boosted and rescaled (in energy) to restore energy momentum conservation.

The FF fragmentation scheme is frame dependent. Most importantly, with the cascade terminated by a simple minimum value of $E + p_z$, the multiplicity in a quark jet depends on the quark's energy. Thus, the hadrons obtained by Lorentz-boosting the result of quark fragmentation are in general different from those obtained by hadronizing a boosted quark.

Due to the leftover soft quarks at the ends of FF decay chains, flavor and charge are not conserved. For $e^+e^- \to q\bar{q}$ events, this is frequently "repaired" by combining the leftover quark and antiquark into a single soft meson. For models involving a large number of underlying partons (e.g., the leading-log

shower model of Refs. [22,26]), the FF hadronization scheme produces a large number of leftover quarks, and the imposition of flavor and charge conservation requires a number of *ad hoc* algorithms. Predictions for, e.g., $\langle N_{ch}(E_{CM})\rangle$ thus cannot be made with much reliability.

There are some rather major objections to the space-time picture of hadronization which appears to follow from the FF model. Specifically, the iterative branching scheme in Fig. (17) seems to describe an "Outside-In" picture, in which fast hadrons are formed first and slow hadrons last. As discussed in detail in Ref. [128], this space-time picture seems very odd. In particular, if we assume that hadrons arise as a result of the screening of large-scale color separation, the expected space-time evolution is "Inside-Out", in which the first hadrons produced are the least energetic, in any reference frame.

Finally, there is an important practical issue related to the merging of resolved multijet systems into a single unresolved jet. Consider $e^+e^- \to q\bar{q}G$ and consider the particular symmetric configurations

$$E(q) = x_1 E_{CM}/2 \tag{3.46}$$

$$E(\bar{q}) = E(G) = (1 - x_1/2) E_{CM} \tag{3.47}$$

Suppose further that we use a mass-cut definition of resolvability, so that $\bar{q}$ and G are treated as distinct, resolvable jets only if

$$(p_{\bar{q}} + p_G)^2 \geq t_c \tag{3.48}$$

which means

$$x_1 \leq 1 - t_c/Q^2 \tag{3.49}$$

for the kinematic configuration in Eqs. (3.46-3.47).

Consider the case where t_c/Q^2 is small (e.g., $t_c/Q^2 \sim (6/30)^2$ for PETRA/PEP energies) and consider the multiplicity of the final state hadrons in the $\bar{q}G$ subsystem just above and just below the resolution cutoff in Eq. (3.49).

For $x_1 > 1 - t_c/Q^2$, the $\bar{q}G$ system is viewed as a single antiquark jet of energy $E_{CM}/2$. Using the simple multiplicity estimate from Eq. (3.13) we obtain

$$\langle N(\bar{q} + G)\rangle \sim A + B \ln[E_{CM}/2] \tag{3.50}$$

For $x_1 < 1 - t_c/Q^2$, we have two distinct jets of energy $E_{CM}/4$, and

$$\langle N(\bar{q} + G)\rangle = \langle N(\bar{q})\rangle + \langle N(G)\rangle \tag{3.51}$$

$$\simeq 2A + 2B \ln[E_{CM}/4] \qquad (3.52)$$

The values in Eqs. (3.50, 3.52) are not the same. The independent (FF) fragmentation picture which is used in the Hoyer and Ali models is not continuous across the borders for resolvable perturbative radiations.

3.4 The LUND Model for String Fragmentation

The term "LUND Model" is actually a bit ill defined, in that Andersson, Gustafson and their collaborators have been extremely active and productive in this field for a number of years [129-141]. In this section, we examine specifically the LUND model for hadron production from simple $q\bar{q}$ systems: "string fragmentation". The LUND model for "gluon fragmentation" is treated in Section 3.5.

The LUND string model for $q\bar{q}$ systems [130] is basically a simple picture for hadronization of 2-jet systems (e.g., e^+e^- annihilation without wide angle gluon fragmentation). A very important difference between the FF and LUND approaches concerns the role of color confinement in the picture of hadron production. The FF model involves independent fragmentation of the quark and antiquark in $e^+e^- \to q\bar{q} \to$ hadrons events, while the LUND picture essentially begins with the point of view that these independent, isolated quarks and antiquarks are unphysical. In the LUND picture, the pair production illustrated in Fig. (17) is a result of the confining force between the quark and antiquark, and hadronization describes the evolution of this entire system, not just the individual quark and antiquark ends. By treating the colorless $q\bar{q}$ system as a whole, many aspects of the FF model can be "derived"--but in such a manner that several of the objections mentioned in the previous section are cured.

Color confinement is an essential initial aspect of the LUND picture, and some description of color confinement in QCD is needed in order to proceed. We have, as yet, no real solution to this fundamental problem, but considerable progress can nonetheless be made using simple, qualitative pictures of how confinement might work, if only we knew how to solve QCD.

Consider a (static) system composed of an oppositely colored quark-antiquark pair. The color force lines connecting these sinks and sources of color are expected to be qualitatively very different from the familiar dipole field configurations of QED illustrated in Fig. (24). Specifically, it can be argued in a number of ways that the flux lines in QCD should be confined to narrow tubelike configurations [142,143], as shown very schematically in Fig. (24). The energy

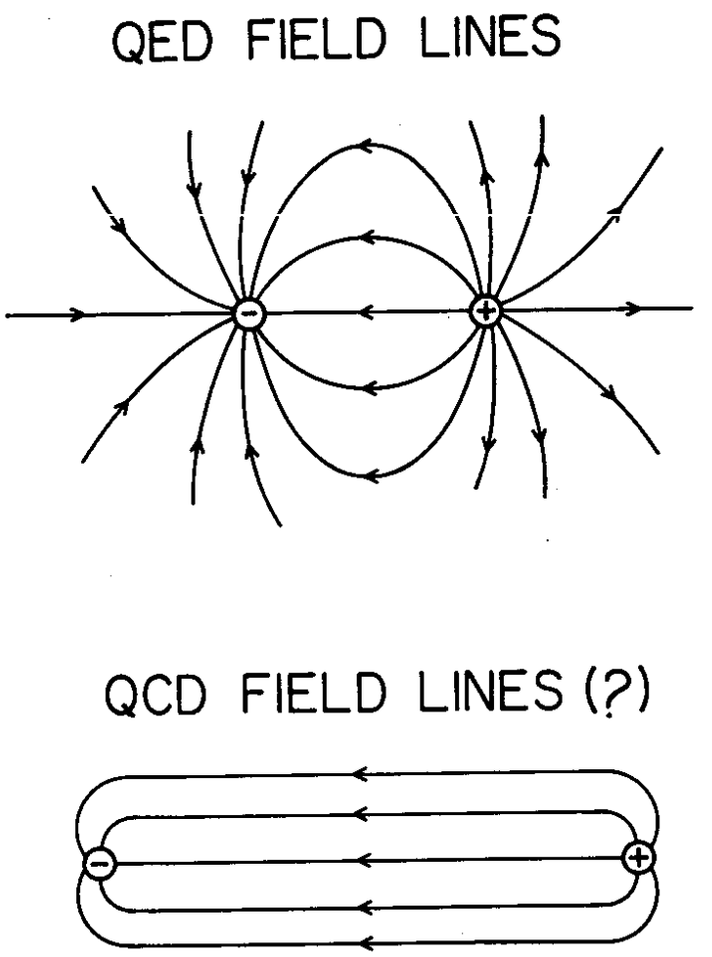

Fig. 24. Schematic illustrations of field lines between opposite charges in QED and QCD.

density per unit length inside these tubes is roughly constant, so that the energy needed to separate color (i.e., separate the quark and antiquark) is proportional to the separation distance ("linear confinement"). If the quark and antiquark are separated by too great a distance, the configuration of a single long flux tube becomes energetically unfavorable, and the ground state of the system is instead expected to be a configuration in which the elongated flux tube has broken into two smaller, individually colorless subsystems through the creation of a quark-antiquark pair.

In Ref. [130], the above qualitative picture of color screening is incorporated into a simple model of hadron production in 1+1 dimension (so-called "Simple-LUND" model).

Consider a system of two massless quarks, confined by a massless relativistic string [144,145] in 1+1 dimensions (i.e., a single space direction "x" and the time direction "t"). Let the total invariant mass of the system be W. The quark and antiquark are confined by a constant attractive force (string tension)

$$\frac{dp}{dt} = \pm\alpha \tag{3.53}$$

where the sign in Eq. (3.53) is such that the quark is always "pulled" toward the antiquark.

At time $t = 0$, suppose that the quark and antiquark are both at position $x = 0$, with initial opposite momenta of magnitude

$$p_0 = W/2 \tag{3.54}$$

The quark initially moves in the $+\hat{x}$ direction, and the antiquark along $-\hat{x}$. As the quark and antiquark move apart, they lose energy to the confining field. For times $t < p_0/\alpha$,

$$\vec{p}_q(t) = (p_0 - \alpha t)\hat{x} \tag{3.55}$$

$$\vec{p}_{\bar{q}}(t) = -(p_0 - \alpha t)\hat{x} \tag{3.56}$$

$$E_f = \alpha|x| = \alpha|x_q(t) - x_{\bar{q}}(t)| \tag{3.57}$$

$$= 2\alpha t \tag{3.58}$$

where E_f is the energy in the confining field (the string carries energy, but not momentum). At time

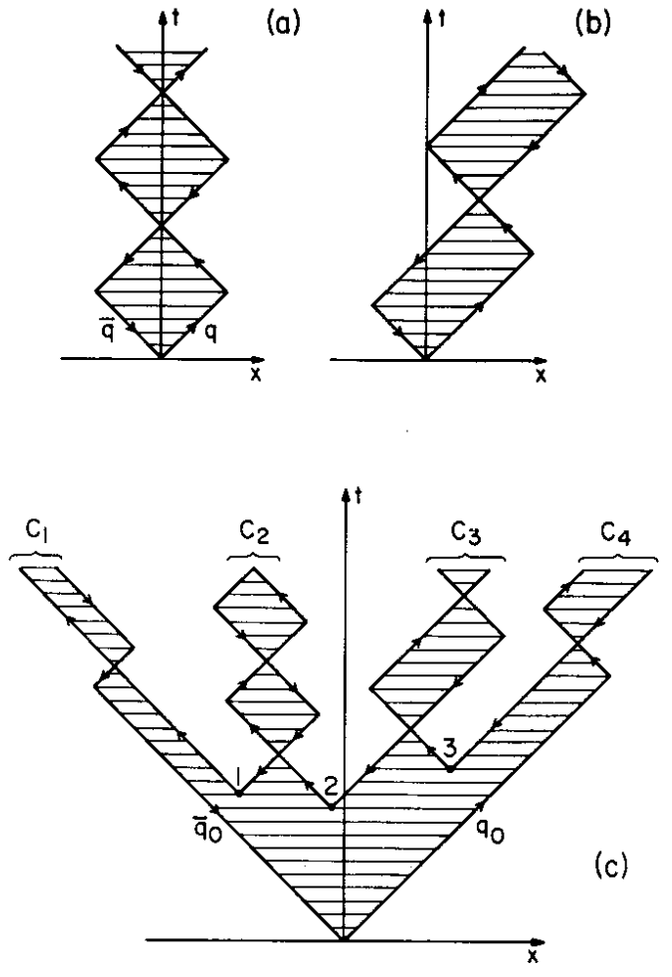

Fig. 25. Time evolution of colorless $q\bar{q}$ systems in the 1+1 dimensional string picture: (a) a simple $q\bar{q}$ system in its rest frame, (b) a system with net momentum along $+\hat{x}$, (c) a large mass system evolving through pair productions at points 1, 2, 3.

$$\tilde{t} \equiv p_0 / \alpha \qquad (3.59)$$

all the energy of the system is contained in the confining field. For $t > \tilde{t}$, the quark and antiquark reverse directions and begin gaining energy from the stretched string.

The time evolution of a simple $q\bar{q}$ system in its rest frame is shown in Fig. (25a). The shaded horizontal lines indicate the regions of space-time where the confining string field is non-vanishing. The area of an elementary rectangle in this diagram is related to the total mass of the system

$$A = W^2 / 2\alpha^2 \qquad (3.60)$$

As time increases, the system undergoes simple oscillatory motion ("yo-yo modes"). Fig. (25b) shows the time evolution of a simple $q\bar{q}$ system in a frame in which the system has net momentum along the $+\hat{x}$ direction. The mass of the system is still given by the area of a basic rectangle, according to Eq. (3.60). Note that the zero-momentum turning points of the quark and antiquark are not simultaneous in this frame.

The simple picture of quarks confined by strings is used in Ref. [130] to describe both stable $q\bar{q}$ mesons (e.g. pions) and the excited $q\bar{q}$ state formed initially in $e^+e^- \to q\bar{q} \to$ hadrons. The transition from the excited $q\bar{q}$ state to stable subsystems is described by allowing the confining string to break via the production of massless quark-antiquark pairs at points in space-time where the confining string field is non-vanishing. The probability for this pair production is assumed to be uniform in space-time

$$dP = \mathrm{P} dx dt \qquad (3.61)$$

The created quark and antiquark then link with the original quark and antiquark to produce individual colorless subsystems. This process breaks the confining string, as illustrated in Fig. (25c). Note that the color screening from pair production is assumed to be complete, in the sense that the string field vanishes in the forward light cone of the pair production point.

The LUND group uses the string picture to evolve the initial state of $e^+e^- \to q\bar{q}$ all the way down to a collection of primary hadrons. The requirement that the produced hadrons have the proper mass introduces correlations among adjacent pair production points. For example, suppose that the subsystem labeled "C_2" in Fig. (25c) is actually a final state pion. Then, the area of the

associated rectangle must be related to the pion mass according to Eq. (3.60), which requires the production points "1" and "2" in Fig. (25c) to satisfy the relation

$$(x_2 - x_1)^2 - (t_2 - t_1)^2 = m_\pi^2 / \alpha^2 \qquad (3.62)$$

The 2-dimensional probability in Eq. (3.61) is effectively replaced by a 1-dimensional production probability along kinematically allowed hyperbolae, as in Eq. (3.62).

By construction, this "Simple-LUND" string breaking model for hadronization is Lorentz Invariant, and conserves energy-momentum. It can be shown (see Ref. [130]) that the production of primary hadrons in this scheme has the proper "Inside-Out" space-time character, in which the slowest primary hadrons are created first in any Lorentz frame. Moreover, by boosting to a frame in which the leading meson (e.g., the meson containing the quark from the initial $e^+e^- \to q\bar{q}$ vertex) is slow (hence, produced first), it is possible to show that the simple LUND picture is equivalent to the FF $q \to q' + M$ splitting picture, and that the effective fragmentation function $D(z)$ for the simple LUND model satisfies the integral equation in Eq. (3.9). The elementary splitting function $f(z)$ (Eq. (3.7)) is completely determined in the string picture

$$f(z) = 1 \qquad \text{(Simple LUND)} \qquad (3.63)$$

for all primary hadron. As a result of satisfying Eq. (3.7), the simple LUND model predicts approximate scaling of fragmentation functions $D(z)$, in agreement with experimental results. The fact that $f(z)$ in Eq. (3.63) is harder than Eq. (3.21) (i.e., predicts more large z splitting) is compensated by an increased production of vector mesons.

The 1+1-dimensional Simple-Lund model effectively reproduces most of the FF formalism while at the same time "curing" several of the FF conceptual difficulties mentioned in Section (3.3). This important result is accomplished by hadronizing the entire $q\bar{q}$ system as a whole, rather than the independent fragmentation of q and $\bar{q}$ in the FF model. In Simple-LUND, color confinement plays a pivotal role in the dynamics of hadronization, in the form of the (simplistic-?) assumptions in Eqs. (3.53, 3.61, 3.62). In contrast, color confinement and color screening have essentially no role in the conceptual picture behind the FF model.

Before adding transverse momenta to the fragmentation scheme ("Standard-LUND"), we should point out that there are some potential problems with even the 1+1-dimensional Simple-LUND picture. Specifically, the mass shell constraint in Eq. (3.62) complicates the implementation of the intuitive, uniform string breaking probability in Eq. (3.61). Due to the kinematics of Eq. (3.62), the string hadronization scheme is not "symmetric". The hadronic state generated by working from the quark end of the string toward the antiquark end differs from that obtained by splitting off mesons from the other direction. (This symmetry issue is addressed in detail in Ref. [134], where a slightly different string breaking formalism is proposed.) The quantum mechanics responsible for the masses of observed hadrons cannot be reproduced by the simple, semiclassical picture of strings and string breaking. Production points generated solely according to Eq. (3.61) would produce a continuum of meson masses.

In practice, the LUND string fragmentation Monte Carlo generates hadrons from the outside in (as in the FF scheme), choosing at random whether to produce a hadron from the quark end of the string or the antiquark end. After each meson production, the invariant mass W of the leftover $q\bar{q}$ subsystem is evaluated. If W is greater than some cutoff (typically $W_0 \sim$ few GeV), string breaking meson production is allowed to continue. If $W \lesssim W_0$, a single $q_j\bar{q}_j$ pair is generated, breaking the residual system into two mesons. The kinematics of this last break are completely determined by mass-shell constraints, so that Eq. (3.60) does not enter.

Transverse momenta are added to the LUND model of string hadronization in Ref. [135]. We first note that, in Simple-LUND, energy conservation requires that the $q\bar{q}$ pair produced at, e.g., point "1" in Fig. (25c) must have zero invariant mass (i.e., the quarks are massless and carry no energy). In order to produce transverse momenta, the model must allow production of massive pairs:

$$M^2_{pair} = 2(M_q^2 + p_f^2) \tag{3.64}$$

(we now also allow for non-zero quark masses). To conserve energy in the total system, this mass must be produced over some finite length of the confining string. The pair "replaces" an entire segment of the string, not simply a point.

It is argued in Ref. [135] that this pair production over a distance can be viewed as a quantum mechanical tunneling phenomenon. In analogy with results of the exactly soluble Schwinger model [146] (QED in 1+1 dimensions), the probability for production of a massive $q\bar{q}$ pair is assumed to be

$$dP \sim dp_f^2\, e^{-\pi m_t^2/\kappa} \tag{3.65}$$

where

$$m_t^2 \equiv m_q^2 + p_f^2 \tag{3.66}$$

[This result cannot be derived for "real" 3+1-dimensional QCD.] We note that Eq. (3.65) implies that $q\bar{q}$ pairs are generated with fixed average transverse momenta of $q(\bar{q})$ with respect to the string, exactly as in the FF model (replacing "strings" by "incident quark direction").

The incorporation of transverse momenta modifies the Simple-Lund longitudinal splitting function of Eq. (3.62). That such modifications should occur is fairly clear: in order to produce a specified transverse momentum in Eq. (3.65), the original $q\bar{q}$ system must survive without breaking long enough that the field energy stored in the string is sufficient to make the production of the specified mass energetically possible. However, the precise form of the interplay between $f(z)$ and transverse mass production cannot be computed from first principles. Instead, Ref. [135] contains qualitative arguments for a connection

$$(q\bar{q}) \rightarrow \text{Meson} \tag{3.67}$$

relating partons to hadrons.

The discussion in Ref. [135] leads to the introduction of phenomenological "tunneling form factors" which modify the elementary result in Eq. (3.62) to a preferred form

$$f(z) \sim (1+c)(1-z)^c \quad \text{(Standard LUND)} \tag{3.68}$$

with $c \simeq 0.3$–0.5. (This result also incorporates expected effects from collinear gluon emissions [136].) The splitting functions for FF, Simple LUND and Standard LUND are compared in Fig. (26).

Using Eq. (3.65-3.66), it is fairly straightforward to add baryon production to the LUND model for string fragmentation. In Ref. [137], it is assumed that baryon production can be described by occasional creation of a diquark-antidiquark pair during the breaking of the color string. The diquark (qq bound state) is treated as a single object. Ignoring the transverse momenta, the probability of diquark production relative to (massless) quark production is, according to Eq. (3.65)

$$P[(q_a q_b),(\overline{q_a q_b})] = e^{-\pi m_{ab}^2/\kappa} \tag{3.69}$$

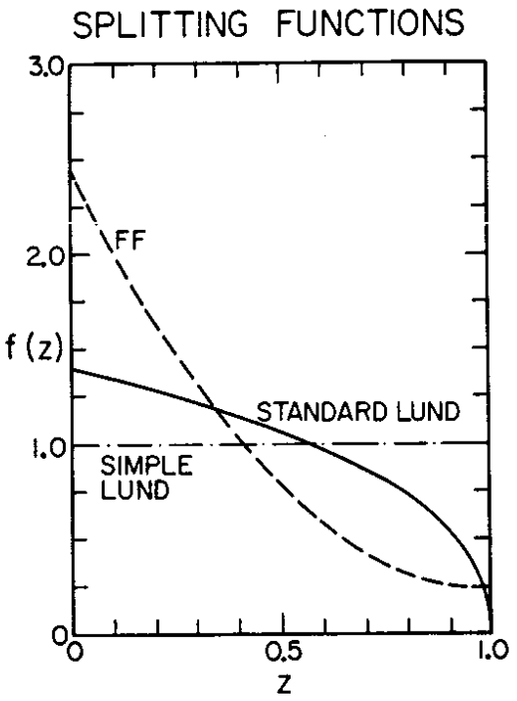

Fig. 26. Comparison of the elementary splitting functions in the Feynman-Field, Simple-Lund and Standard-Lund models.

The form in Eq. (3.69) is extremely sensitive to variations in the assumed value for the diquark mass. Values of these mass parameters were determined from observed low energy baryon production rates in Ref. [147].

The final form of the "Standard LUND" string fragmentation model is actually somewhat complicated. A number of phenomenological parameters are involved. The complete model is described in detail in Refs. [140-141]. Due largely to the exact kinematics required for the "proper" incorporation of particle masses and transverse momenta, the simple physical picture underlying Fig. (25) and Eqs. (3.53, 3.62) is quite obscured in the final product. Nonetheless, the basic conceptual difference between the FF jet model and the LUND string fragmentation model is simple, important, and worth repeating:

Hadrons do not form from the independent fragmentation of isolated quarks. Rather, hadron production is a "cooperative" phenomenon, involving a quark, an antiquark, and the confining color field between them (the string).

3.5 The LUND Model for Gluon Fragmentation

In the LUND picture, hadronization is viewed in terms of strings connecting oppositely colored quark-antiquark pairs. For events with a hard perturbative gluon (e.g., $e^+e^- \to q\bar{q}G$), the LUND prescription for hadronization again involves strings, and the question of "gluon fragmentation" essentially becomes the question of how a perturbative gluon is expected to modify the simple 1+1-dimensional string representation of $e^+e^- \to q\bar{q}$ developed in Section 3.4.

It is first useful to recall the color content of elementary QCD quanta. Quarks are assumed to transform according to the fundamental representation of SU(3), and come in three different colors (say, R, Y, B for red, yellow, blue). Antiquarks have the corresponding anticolors ($\bar{R}$, $\bar{Y}$, $\bar{B}$). Gluons transform according to the adjoint representation of SU(3), and can be characterized by a color index and an anticolor index (e.g., $R\bar{Y}$, $B\bar{R}$, etc.). (There are only eight gluons, since the completely symmetric combination $R\bar{R} + Y\bar{Y} + B\bar{B}$ transforms as a color singlet.)

The composite "color + anticolor" content of the gluon immediately suggests one possible way of associating color strings with a $q\bar{q}G$ system. Consider $e^+e^- \to q(p_1) + \bar{q}(p_2) + G(p_3)$, and suppose that we separate the color and anticolor components of the gluon by splitting it into an effective quark-antiquark pair,

$$G[p_3] \to q'[zp_3] + \bar{q}'[(1-z)p_3] \tag{3.70}$$

From the color lines, we see that the splitting in Eq. (3.70) has effectively replaced the initial $q\bar{q}G$ system by two strings, $(q\bar{q}')$ and $(q'\bar{q})$. The 4-momenta of the two strings are

$$k_1 = p_1 + (1-z)p_3 \tag{3.71}$$

$$k_2 = p_2 + zp_3 \tag{3.72}$$

Each string is massive, and can be (independently) hadronized in its own rest frame, using the simple 1+1-dimensional string hadronization model from

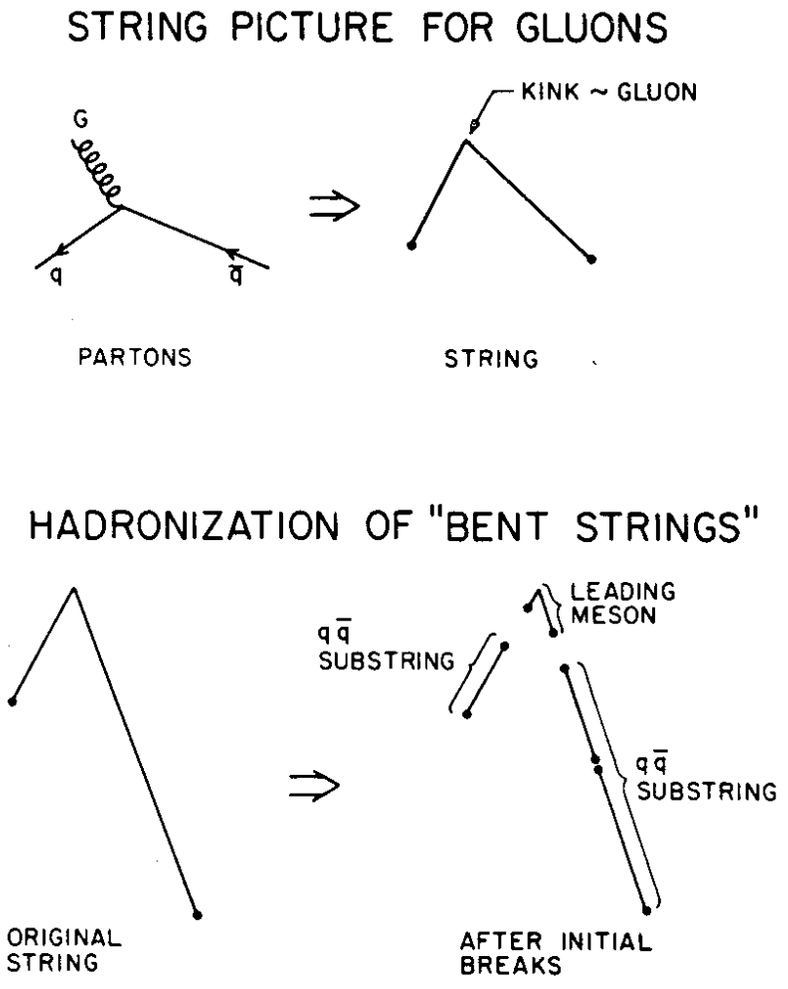

Fig. 27. Identification of a gluon with a kink in the confining string according to the LUND picture. The kink separates from the string through pair productions in the hadronization picture developed in Ref. [131].

Section 3.4.

This simple splitting scheme is in fact used in the QCD-Cluster Models described in Section 4. However, the simple string splitting in Eqs. (3.70-3.72) is not a precise description of the LUND gluon hadronization scheme (as is often wrongly assumed). The LUND picture of gluon fragmentation [131] is actually a bit more subtle.

For the simple 1+1-dimensional string picture of Section 3.4, the momentum of the system was carried entirely by the ends of the string (i.e., the quark and antiquark). In a covariant treatment of the massless relativistic string in higher dimensional spaces (in particular, in 3+1-dimensional, "real" space-time), it can be shown that more complicated patterns of motion are available for the string. In particular, there exist modes in which an infinitesimal element of the string itself can carry momentum as well as energy. In the string picture used by the LUND group in Ref. [131], the gluon in a $q\bar{q}G$ final state is identified as an infinitesimal, momentum-carrying "kink" in the string.

Fig. (27a) shows a crude representation of the time evolution of the "bent string" associated with a $q\bar{q}G$ event. Adopting the string-breaking hypothesis of Section 3.4, this bent-string "decays" into hadrons through the production of $q\bar{q}$ pairs at various points along the straight string subsegments, as illustrated in Fig. (27b). More specifically, the kink in the string is first separated from the system by pair production breaks on either side of the kink. The remaining substrings then evolve into hadrons in the same 1+1-dimensional manner as the strings from Section 3.4.

The "bent string" LUND gluon picture is somewhat similar to the naive splitting approach in Eqs. (3.70-3.72), with two important differences: (1) There is no freedom involved in choosing the splitting fraction z in Eq. (3.70). The positions of the string breaks in Fig. (27) are all (nominally) determined by generalizations of the uniform pair production probability in Eq. (3.61). (2) The LUND string breaking formalism produces a "leading meson" in gluon fragmentation--i.e., the meson which contains the kink in the original bent string. (Note, however, that this leading meson need not be flavor neutral.)

Unlike the Hoyer model or Ali model of Section (3.1), gluon fragmentation in the LUND model does not involve additional, unknown phenomenological functions, such as a fragmentation function $D(z)$ for gluon decay. Hadronization of a $q\bar{q}G$ system is instead completely specified by the results of hadronizing $q\bar{q}$ systems, once the bent string picture of color flow is adopted.

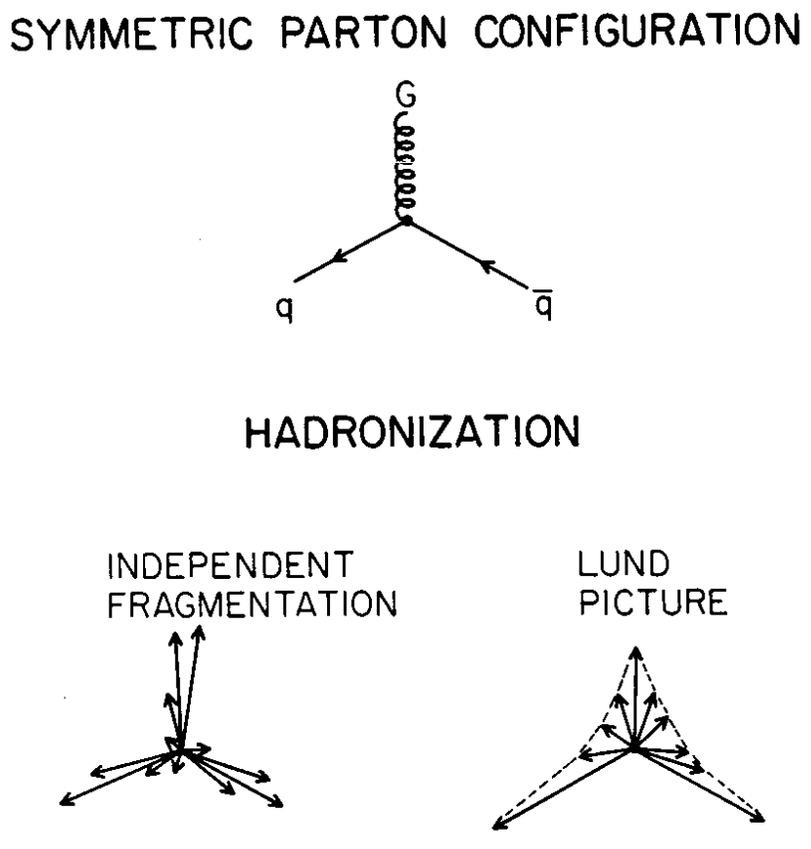

Fig. 28. Schematic illustration of the different topologies for three-jet events expected in the independent fragmentation and LUND pictures.

In the Hoyer model, the primary hadrons in $e^+e^- \to q\bar{q}G$ events follow the momentum directions of the underlying hard partons. This is not the case in the LUND model. The hadrons formed from the fragmentation of the substrings in Fig. (27) will tend to lie on hyperbolae in momentum space which stretch between the quark (antiquark) and gluon momentum vectors. (This follows from simply Lorentz-boosting the results of individually fragmenting the substrings in their own CM.) The qualitative difference between independent fragmentation and string fragmentation of $q\bar{q}G$ systems is illustrated in Fig. (28).

Finally, we should note that the LUND picture for hadronization provides a simple resolution of the "discontinuity" problem in independent fragmentation models (objection #5 from Section (3.3)). Consider a sequence of $e^+e^- \to q\bar{q}G$ events. As the $\bar{q}$ and G become more nearly collinear, the mass (length) of the associated string segment becomes smaller and smaller, eventually vanishing as the $\bar{q}G$ invariant mass vanishes. The "extra" string segment between the gluon kink and the antiquark end vanishes in a continuous manner (ultimately producing no additional hadrons) as the antiquark and gluon become irresolvable. At the same time, the long string from the quark to the gluon kink continuously changes to the proper string for a single $q\bar{q}$ system. The overlap/discontinuity problems of independent fragmentation models are thus naturally avoided.

3.6 Independent Fragmentation versus LUND

Both the LUND model and the Independent Fragmentation (Hoyer) model have been used extensively in analyses of experimental results from PETRA and PEP. Since each model involves a fairly large number of phenomenological parameters, it is generally possible to fine tune either model to agree with most experimental results. Due to the complexities of the hadronization models, it is not clear to what extent data fitting tests perturbative QCD and to what extent data fitting instead tests the assumptions and structures of the specific models. In this section, we use two specific examples to illustrate some of the difficulties and ambiguities involved with using hadronization models and Monte Carlos to test perturbative QCD.

The first example concerns the determination of α_s from the observed production rates for 3-jet events. An analysis comparing predictions of the Hoyer and LUND models was done by the CELLO group [148]. The procedure used is basically that outlined in Section 3.2. A cut on a jet variable (e.g., $S < 0.25$ (sphericity) or $T > 0.95$ (thrust)) is made to select a sample of 2-jet events.

Hadronization parameters are then fixed by requiring that the models reproduce the important features of the 2-jet sample (distributions in dN/dz, dN/dp_T^2, etc.). With the hadronization parameters fixed, the coupling α_s in Eq. (2.20) is determined by requiring that the full 2-jet plus 3-jet models reproduce the observation "perturbative" tails in shape variable distributions.

The CELLO group found that the Hoyer and LUND models gave rather different values for the QCD coupling

$$\alpha_s[\text{Hoyer}] \simeq 0.155 \pm 0.015 \tag{3.73}$$

$$\alpha_s[\text{LUND}] \simeq 0.235 \pm 0.025 \tag{3.74}$$

It had been suggested that the differences between Eqs. (3.73-3.74) might be due to the fact that the 2-jet FF model used in the analysis did not provide a good representation of the 2-jet data. The model comparison was repeated by the TASSO group [123,149], with particular attention given to careful determination of the hadronization parameters. The TASSO fit to the full data sample included $O(\alpha_s^2)$ perturbative QCD subprocesses. Results of the analysis gave

$$\alpha_s[\text{Hoyer}] = 0.16 \pm 0.015 \tag{3.75}$$

$$\alpha_s[\text{LUND}] = 0.21 \pm 0.015 \tag{3.76}$$

It should be noted that the statistical errors in these determinations are smaller than the model-dependent difference between the α_s values.

The qualitative trend

$$\alpha_s[\text{LUND}] > \alpha_s[\text{Hoyer}] \tag{3.77}$$

is found to be generally independent of the particular shape variable used in the analysis. There is a claim to the contrary by the Mark J group [150], who suggest that α_s can be determined in a model-independent way using the asymmetry in the (infrared-safe) energy-energy correlation function [84, 151]

$$A(\vartheta) \equiv \frac{1}{\sigma}\left[\frac{d\sum_E}{d\vartheta}(\vartheta - \pi) - \frac{d\sum_E}{d\vartheta}(\vartheta)\right] \tag{3.78}$$

where

$$\frac{1}{\sigma}\frac{d\sum_E}{d\vartheta} \equiv \frac{2}{\sigma}\sum_{i,j=1}^{N_{\text{ncd}}}\int \frac{d^3\sigma}{dz_i dz_j d\vartheta} z_i z_j dz_i dz_j \tag{3.79}$$

and the sum in Eq. (3.79) is over all hadrons with angular separation ϑ (within some resolution). However, the Mark J conclusion of fragmentation model independence is not supported by similar analyses from other PETRA/PEP experiments.

The qualitative result in Eq. (3.77) is easily understood in terms of the different underlying pictures of gluon fragmentation. Consider, for simplicity, a completely symmetric 3-jet perturbative event with

$$E(q) = E(\bar{q}) = E(G) = Q/3 \tag{3.80}$$

In the Hoyer hadronization scheme, the 3-fold symmetry of the parton event survives (aside from statistical fluctuations). The LUND picture does not preserve the 3-fold symmetry of the parton configuration. As noted in Section 3.5, hadronization of $q\bar{q}G$ systems in the LUND formalism predicts that particle momenta will lie along hyperbolae joining $q(\bar{q})$ to G, as shown in Fig. (28). The LUND scheme effectively "smears out" the perturbative energy flow of the gluon. Thus, in order to reproduce an experimental high-p_T signal (e.g., the observed rate of large thrust events), the LUND picture requires a larger cross section for underlying perturbative 3-jet events: a higher value of α_s.

The string (LUND) and independent fragmentation (Hoyer) hadronization pictures give different pictures of the momentum flow in "3-jet" events, as illustrated in Fig. (28). Recent analyses by the JADE group have attempted to measure these differences [152,153].

The JADE analysis begins with a sample of planar, 3-jet events extracted from their full data sample by cuts on the eigenvalues of the sphericity tensor

$$Q_2 - Q_1 > 0.07 \tag{3.81}$$

$$Q_1 < 0.06 \tag{3.82}$$

The planar events in this sample are then organized into three clusters according to triplicity [86],

$$T_3 \equiv \min_{c_1,c_2,c_3}\left\{\frac{|\sum_{j\in c_1}\vec{p}_j| + |\sum_{k\in c_2}\vec{p}_k| + |\sum_{l\in c_3}\vec{p}_l|}{|\sum_i \vec{p}_i|}\right\} \tag{3.83}$$

where the minimization is over all possible partitions of charged hadrons in an event into three disjoint clusters c_j. The (empirical) jet energies E_j are defined

as the sums of particle energies within each cluster. The jets are then ordered in energy, with

$$E_1 > E_2 > E_3 \tag{3.84}$$

Using Monte Carlo studies of fragmentation models, the JADE group estimates that 16% of the events selected by the cuts in Eqs. (3.81-3.82) are due to statistical fluctuations in underlying $e^+e^- \to q\bar{q}$ 2-parton events. Of the remaining (3-parton) events, the gluon jet from $e^+e^- \to q\bar{q}G$ is identified with jet 1, 2, or 3 with probability 12%, 22% and 53%. The softest jet from the triplicity analysis should thus contain an enhanced population of underlying "gluon jets".

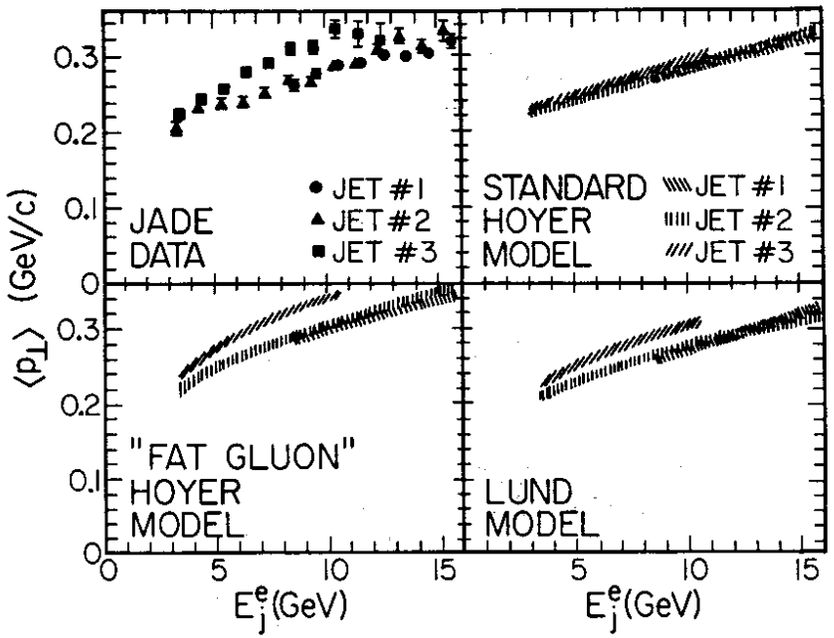

Fig. 29. Mean transverse momenta of individual hadrons within the distinct jets of three-jet events in e^+e^- annihilation at $E_{CM} \sim 30$ GeV. The JADE data are from Rev. [152]. Predictions of the LUND, Hoyer and "Fat Gluon" Hoyer models are shown.

The first experimental evidence for a difference in quark and gluon fragmentation comes from examining the mean transverse momenta of particles within a jet. Transverse momenta are measured with respect to the appropriate jet axis, which is defined by the sum of the momenta of all particles in the corresponding cluster.

Fig. (29) shows JADE results for $\langle p_t \rangle$ within each of the three jets, as a function of the jet energies. The $\langle p_T \rangle$ values within jets 1 and 2 are essentially identical, (as expected for underlying quark and antiquark jets), but the soft jet is found to have a systematically broader $\langle p_T \rangle$. This effect is naturally understood within the LUND string picture, while the standard Hoyer assumption that quarks and gluons fragment in the same manner cannot reproduce this trend. The experimental results in Fig. (29) do not rule out the idea of independent fragmentation hypothesis, however. The Hoyer model can fit these results if the transverse momentum smearing σ_G for gluon jets is simply taken to be larger than that for quark jets (e.g., $\sigma_q \simeq 350$ MeV and $\sigma_G \simeq 500$ MeV).

The JADE group has gone farther in their analysis [154], attempting to directly measure the different pictures of angular energy flow in the Hoyer and LUND models, as was illustrated in Fig. (28). The three jets defined by the triplicity analysis are used to define an orientation angle within the event plane, with the energetic jet #1 lying along $\vartheta = 0$, and jet #2 having a smaller ϑ value than jet #3. The angular energy flow

$$\frac{1}{E_{TOT}} \frac{dE}{d\vartheta} \simeq \sum_{j(\vartheta_j \sim \vartheta)} E_j \tag{3.85}$$

is then computed, and the data are compared to predictions of the Hoyer and LUND models, as shown in Fig. (30).

The LUND model predictions are consistent with the data, while the independent fragmentation results have systematic differences from the data, particularly in the regions between the jet peaks. In the region between the two "quark jet" peaks, the independent fragmentation prediction is too high. The LUND result is lower in this region since there is no string stretching from the quark directly to the antiquark.

The JADE results in Fig. (30) give some preference for the string picture of hadronization, rather than the independent fragmentation approach. We have tried to argue throughout Section 3 that the independent fragmentation scheme cannot be expected to give complete description of all features of hadron formation. Experimental preferences for strings over independent fragmentation

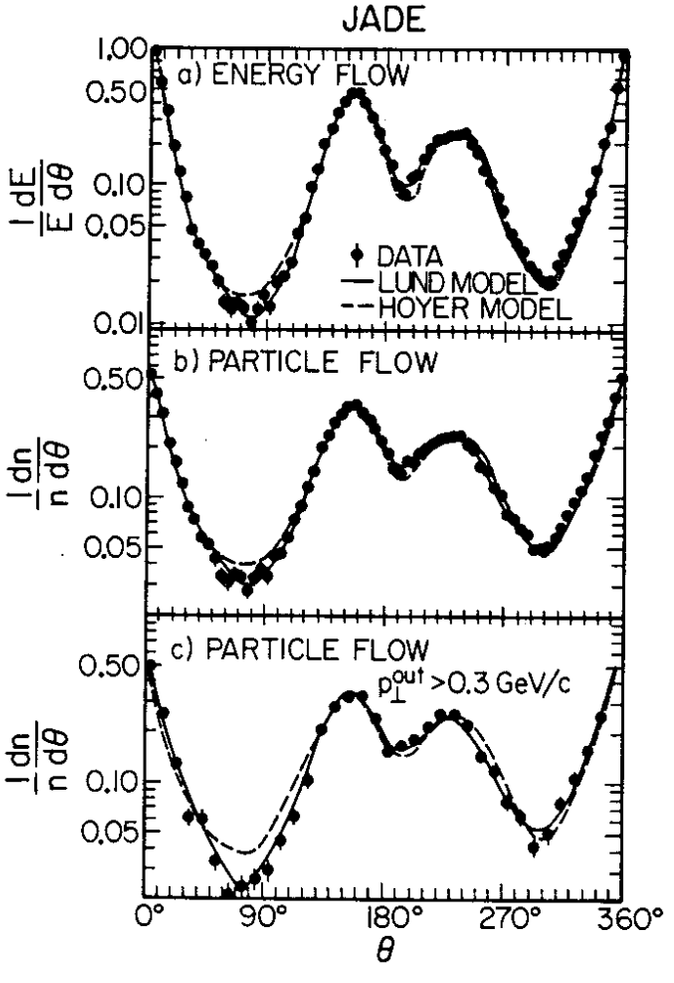

Fig. 30. Energy and particle flows for 2-jet events in e^+e^- annihilation. The JADE data [153] are compared with results of Hoyer and LUND model fits.

are thus rather gratifying.

4. QCD-Cluster Models

It was suggested in Section 3.4 that one way of viewing the differences between independent fragmentation (FF/Hoyer) and string (LUND) hadronization schemes concerned the differing dynamical roles of color confinement in the two pictures. Color confinement has essentially no role in the formulation of the FF picture, while confinement underlies a basic conceptual premise of the LUND picture: hadron production from colorless string systems, not from isolated, colored quarks.

In this section we examine a new class of hadronization models: QCD-Cluster models [154-160,65]. Like the LUND model, these new models describe hadronization through the production (then "decay") of massive colorless objects (the clusters). Unlike the LUND string hadronization scheme, the QCD-Cluster models do not require fragmentation functions, tunneling form factors, etc. Instead, the QCD-Cluster approach evolves the initial system into a collection of relatively low-mass colorless clusters. Hadron production from these clusters is then described using simple statistical/phase space parameterizations. Experimental distributions can be reproduced in the QCD-Cluster approach without the use of phenomenological fragmentation functions, transverse momentum smearing, tunneling form factors, etc.

4.1 Some General Considerations

The basic QCD-Cluster approach to hadron production can be described in terms of two rather general principles:

1) Hard color separations must be screened (neutralized) before hadrons actually form.

2) Hadron formation is a local, universal process.

The dynamical (i.e., QCD) content of the model is contained entirely in the first point--the manner in which color screening occurs in the evolution of an e^+e^- annihilation event.

An e^+e^- annihilation event begins with the hard separation of color and anticolor at the primary $\gamma^* \to q\bar{q}$ vertex. In order to prevent the separation of color and anticolor over distances greater than $O(1\,fm)$, some sort of color screening mechanism must begin very shortly after the initial $\gamma^* \to q\bar{q}$

production. One example of a color screening mechanism is the non-perturbative $q\bar{q}$ pair production described in the 1+1-dimensional string-breaking formalism of the LUND model. Another example would be the radiation of a large number of perturbative gluons, which could produce a system of small mass colorless strings in the manner described in Eqs. (3.70-3.73). In the (unsolved) world of QCD, we might well suspect that color screening occurs through some mixture of these idealized perturbative and non-perturbative mechanisms.

Leaving aside for now the issue of the proper color-evolution mechanism, the effect of the color screening process in point (1) is fairly simple:

> The initial state (i.e., a highly excited, colorless system of mass $W = E_{CM}$) has been evolved into a collection of low mass colorless clusters.

The role of dynamical QCD models is limited to describing the production of this cluster final state. Note that no specific assumptions are needed (or made) relating perturbative QCD quanta directly to physical hadrons. There are no fragmentation functions or hadronic were functions involved in this approach. This is perhaps the single most important difference between QCD-Cluster models and the more conventional hadronization schemes discussed in Section 3.

Since we do not yet know now hadrons are actually formed in QCD, it seems clear that diagrams such as Fig. (17) connecting pions and perturbative quarks have no truly fundamental meaning. As Bjorken notes in Ref. [128], it is not clear that a rigorous field theory exists with hadrons and partons as members of the same Fock space. The explicit use of a $q \to q' + M$ vertex in the FF picture (and its implicit use in Standard LUND) is in fact a rather strong assumption as to how hadron formation actually occurs. The role of QCD in the QCD-Cluster approach is much more conservative, much less ambitious: only rather gross features of the final state (the cluster final state) are described by the dynamical model.

Hadron formation from the cluster final state is described using principle (2) listed above. "Locality" means that each cluster is assumed to evolve into hadrons independently. This locality assumption is supported by the observed lack of long-range correlations in the final states produced in hadron-hadron scattering. Locality is implicitly assumed in all hard-scattering parton

models. That is, if hadronization somehow depended on the collective, underlying configuration of all partons, then the parton model approach would have no value.

The "universality" assumption in (2) essentially means that hadron production from a given cluster does not depend on the cluster production mechanism. Rather, hadron production can only depend on simple Lorentz-invariant cluster attributes, such as mass and flavor. A 1.8 GeV $u\bar{u}$ cluster should produce hadrons in essentially the same way as pions are produced in proton-antiproton annihilation at rest.

Universality is the key to separating (factorizing) the incalculable aspects of hadron production from the (hopefully) calculable production of a cluster final state. We need not understand how hadrons are formed at low mass scales. Instead, we need only have a reliable parameterization of low mass hadronization deduced from studies of extensive, low-energy experimental data. To the extent that the clusters produced by the QCD model have fairly small mass, we can hope that hadron formation from these clusters is basically a simple process, determined primarily by phase space and the statistical density of physical hadrons.

The basic structure of a "generic" QCD-Cluster model is fairly simple

1) The initial state is evolved into an ensemble of low mass colorless clusters, using some specific QCD-inspired model.
2) Final state hadrons are formed from the individual clusters, using a simple parameterization or statistical model.

There are by now a number of specific QCD-Cluster models [154-160]. Basically, these models differ in details of the cluster formation in step (1), as is discussed in the following sections.

4.2 The Field-Wolfram Model

The first QCD-Cluster model was presented by Field and Wolfram in Refs. [154,155]. In this model, e^+e^- annihilation into hadrons is described in three steps:

1) Production of a quark-gluon shower according to leading-log perturbative QCD.

2) Formation of the cluster final state via color strings associated with the parton shower.

3) Independent hadronization of each cluster using a simple two-body statistical ansatz.

The structure of the model is illustrated schematically in Fig. (31).

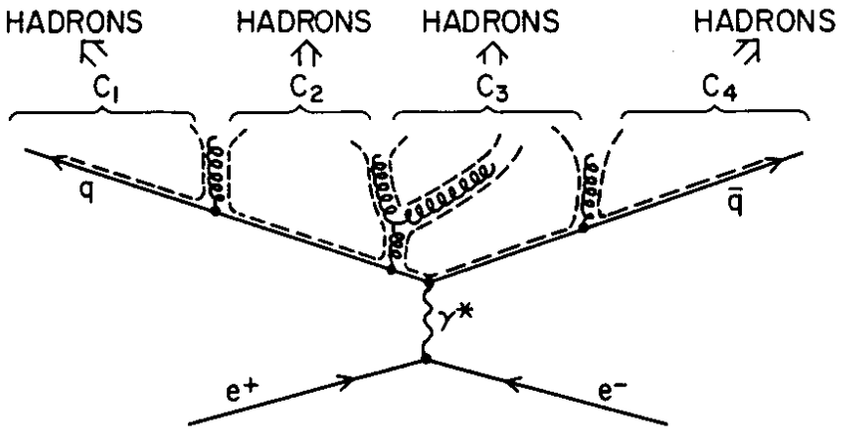

Fig. 31. Schematic illustration of the Field-Wolfram model. The dashed lines indicate the strings connecting oppositely colored elements of the parton final state.

The parton shower is generated using the Fox-Wolfram algorithm described in Section (2.5). Final state partons are put on mass shell, with light quarks (up, down and strange) and gluons assumed to be massless.

The color strings in step (2) are formed by first splitting final state gluons into collinear quark-antiquark pairs,

$$G[p] \rightarrow q[zp] + \bar{q}[(1-z)p] \tag{4.1}$$

Several choices were tried for dN/dz, the probability function for assigning z-values in Eq. (4.1), and the results of the model were found to be fairly insensitive to the choice made. The quark (antiquark) in Eq. (4.1) carries the color (anticolor) index associated with the gluon, in the manner described in Section (3.5). Due to the planar (probabilistic) structure of parton shower events, each

final state quark (perturbative, and those from Eq. (4.1)) is linked to a unique partner antiquark by a color string--the light dashed lines in Fig. (31). These strings have mass and 4-momenta determined by the sums of the 4-momenta of the quarks and antiquarks at the ends of the strings

$$p_{st_j} = p_{q_j} + p_{\bar{q}_j} \tag{4.2}$$

In the Field-Wolfram (FW) model, each perturbative string is treated as a distinct cluster and is hadronized independently. There is a small problem with this approach in that the parton shower formalism can produce some strings with small (even vanishing) masses. Fig. (32) shows some typical distributions in string masses in the FW model. Very low mass strings cannot "decay" into physical hadrons in a manner which conserves energy and momentum. In the extension of FW presented in Ref. [156], an algorithm was used for joining adjacent small mass strings to produce more massive clusters. Note that cluster C_3 in Fig. (31) contains two strings. As discussed in Ref. [156], the cluster masses in the model must not be too small if the model is to yield reasonable production rates for baryons and vector mesons.

The clusters C_j in Fig. (31) are characterized by a mass W, a quark flavor q_a and an antiquark flavor $\bar{q}_b$. In the FW model, these clusters are decayed by a simple 2-body ansatz illustrated schematically in Fig. (33). The probability for a particular 2-body decay mode

$$C_j[W;q_a,\bar{q}_b] \rightarrow H_1 + H_2 \tag{4.3}$$

is given by a product of three factors

$$P[C_j \rightarrow H_1 + H_2] = P_F \cdot P_S \cdot P_K \tag{4.4}$$

P_S is simply a spin-state counting factor

$$P_S = (2J_1 + 1)(2J_2 + 1) \tag{4.5}$$

determined by the spins of the final state hadrons. The factor P_K in Eq. (4.4) is a 2-body phase space suppression factor

$$P_K = \vartheta(W - M_1 - M_2)\ \frac{2|\vec{p}_1^{\,*}|}{w} \tag{4.6}$$

$$= \vartheta(W - M_1 - M_2)\ \frac{\lambda^{\frac{1}{2}}(w^2, M_1^2, M_2^2)}{w^2} \tag{4.7}$$

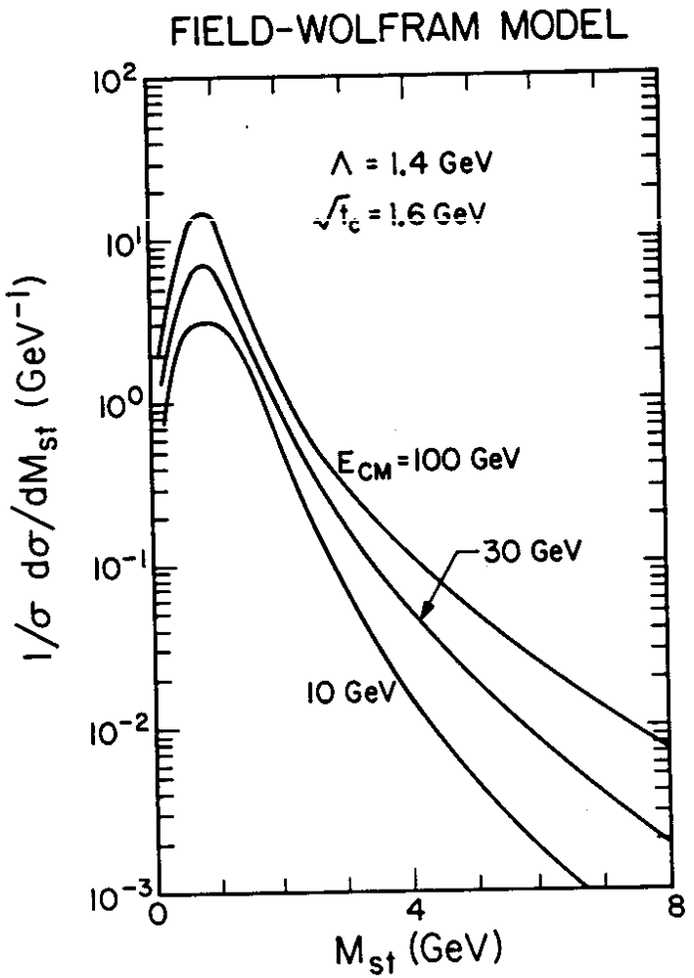

Fig. 32. Distributions in the string mass for $e^+e^- \to u\bar{u} \to$ partons at various CM energies. The parton shower and string formation formalisms are described in Refs. [154, 155].

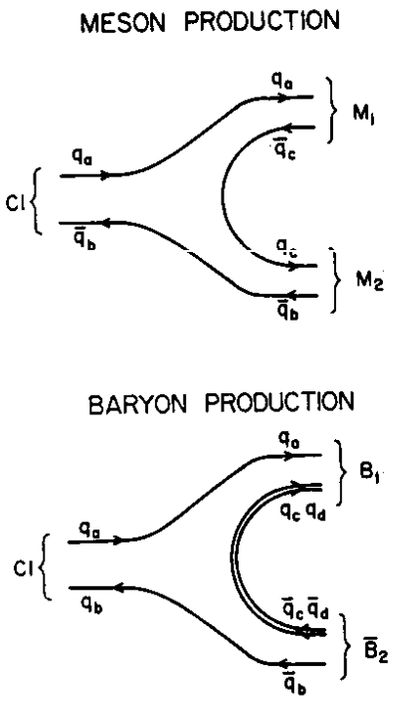

Fig. 33. Schematic illustration of the cluster hadronization scheme used in the Field-Wolfram model.

where $\vec{p}_1^*$ in Eq. (4.6) is the 3-momentum of hadron H_1 in the decay rest frame, and

$$\lambda(x,y,z) = x^2 + y^2 + z^2 - 2xy - 2xz - 2yz \tag{4.8}$$

The flavor selection factor P_F in Eq. (4.4) is a bit more complicated. We may imagine that the flavors of H_1 and H_2 in Fig. (33) are specified by the creation of a quark-antiquark pair (meson production) or a diquark-antiquark pair (baryon production). The flavor selection factor contains relative probabilities for these different creations, as well as flavor mixing factors, whenever quark contents do not specify a unique hadron (e.g., a pseudoscalar $u\bar{u}$ meson can be any of π^0, η or η').

The decay mode for a cluster is chosen at random from a list of "all" possible decays, with individual modes weighted by the factor in Eq. (4.4). The cluster decay is assumed to be isotropic in the cluster rest frame. Unstable hadrons produced in cluster decay are subsequently decayed using decay modes listed in the Particle Data Tables [110].

The two-body decay ansatz in Eq. (4.3) can give a reasonable description of low mass cluster hadronization only if a suitably rich spectrum of possible hadrons H_j is included. In the original FW model, the 0^{-+}, 1^{--}, 2^{++}, 1^{++}, 1^{+-} and 0^{++} meson nonets (u, d and/or s quarks only) and the light quark $1/2^+$, $3/2^+$ baryon multiplets are used. Heavy hadrons (c, b and/or t) are not included in the FW particle lists. Instead, heavy quarks are decayed weakly as part of the shower evolution, before string/cluster formation. The extension of FW in Ref. [156] does include heavy hadrons, with, e.g., 0^{+-}, 1^{--} and $1/2^+$ charmed hadron multiplets.

Aside from a small number of simple probability factors (e.g., the relative probability of strangeness production in the gluon splitting in Eq. (4.1)), the FW model has only two parameters: the leading-log QCD scale Λ and a mass-squared cutoff t_c for resolvable perturbative radiation. In Refs. [154,155], it was found that many 30 GeV PETRA results could be reproduced using the parameter values

$$\Lambda[FW] = 1.4 \text{ GeV} \tag{4.9}$$

$$t_c[FW] = 2.56 \text{ GeV}^2 \tag{4.10}$$

The extended FW model is Ref. [156] uses a slightly different parton shower formalism and has, besides Λ and t_c, an additional cluster size parameter W_{MIN}, which controls the joining of small mass strings into more massive clusters. Typical parameter values used in Ref. [156] are

$$\Lambda[FW - ex] = 0.2 \text{ GeV} \tag{4.11}$$

$$t_c[FW - ex) = 1.5 \text{ GeV}^2 \tag{4.12}$$

$$W_{MIN}[FW - ex] = 1.25 \text{ GeV} \tag{4.13}$$

(The substantial difference between Eq. (4.9)-(4.11) is discussed later in Section 4.5.)

Figs. (34)-(37) show some typical results for the Monte Carlo models in Refs.

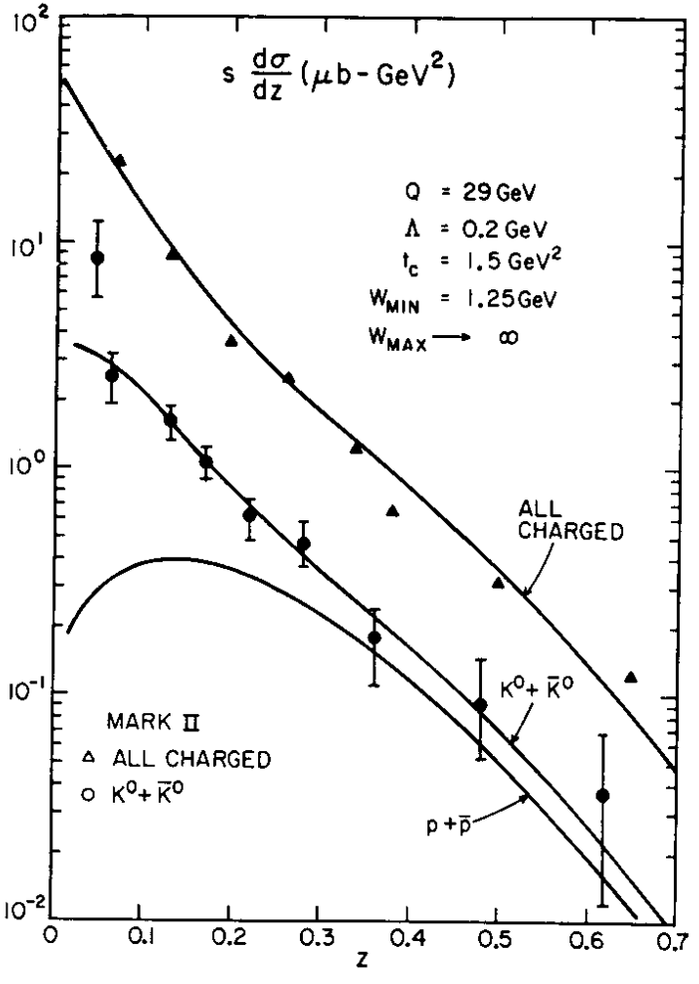

Fig. 34. Scaled momentum distributions for charged hadrons, neutral kaons and protons + antiprotons in the QCD-Cluster model of Ref. [156]. The Mark II data are from Ref. [161].

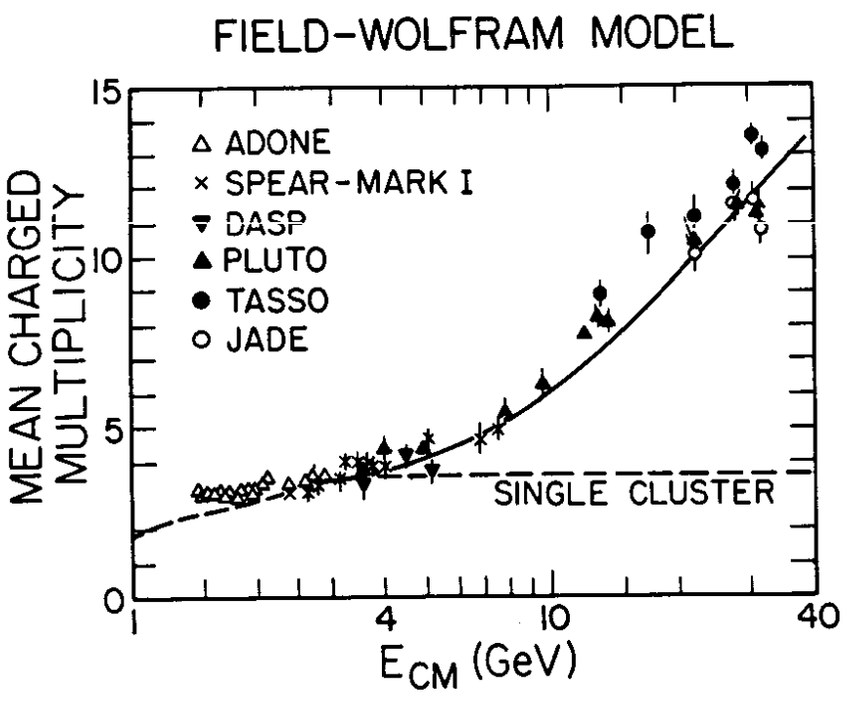

Fig. 35. Mean charged multiplicities in the Field-Wolfram model for e^+e^- annihilation. The data are from Refs. [162-167].

[154-156]. We should emphasize that these curves are computed without the use of phenomenological fragmentation functions or p_t-smearing functions. With the parton shower parameters fixed by inclusive particle studies, the energy distributions for charm production at $Q = 29$ GeV shown in Fig. (36) are essentially "zero-parameter" predictions of the model. The good agreement between model predictions and the data gives strong support to the basic philosophy of the QCD-Cluster description of hadronization.

There are, however, several reasons to view the results and predictions of the FW model with a bit of cautions skepticism. In particular,

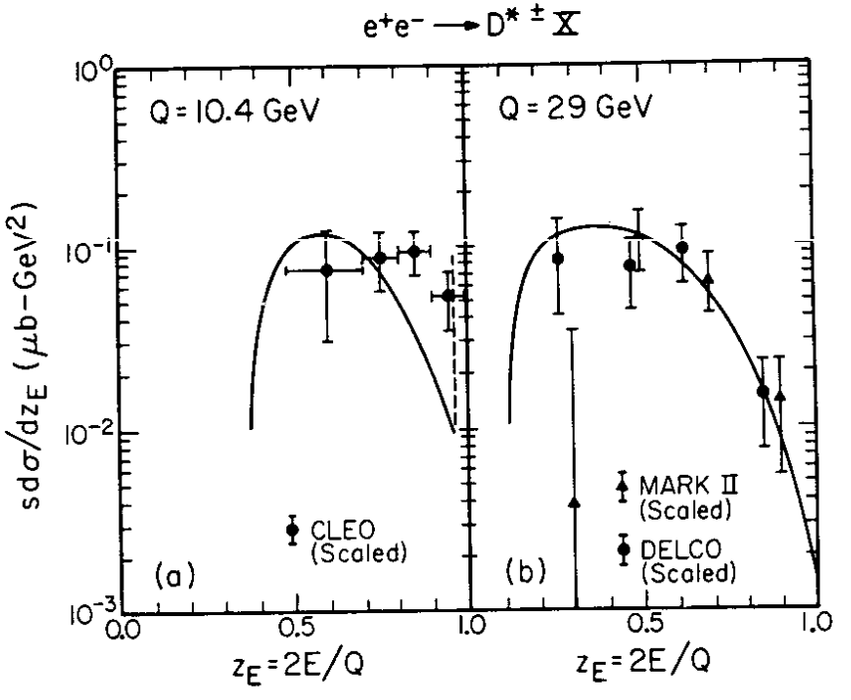

Fig. 36. Predicted energy distributions for D^* production according to the model of Refs. [156, 65]. The data are Refs. [168-170].

1) The 2-body cluster decay ansatz in Eq. (4.3) does not, in fact, provide a sufficiently precise description of low-mass hadronization (the "factorization" of soft physics needs to be done more carefully).

2) The results in Refs. [154-156] are very sensitive to the precise treatment of soft gluons during the perturbative parton shower (recall the differences between $\Lambda[FW]$ and $\Lambda[FW-ex]$).

3) The cutoffs on perturbative evolution in Eqs. (4.10, 4.12) are very small. From the qualitative discussions in Section 2.2, it seems that this implies pushing perturbative QCD ideas too far.

Recent developments in the QCD-Cluster formalism have generally been concerned with studies of these three major problem areas in the original (and extended) FW model.

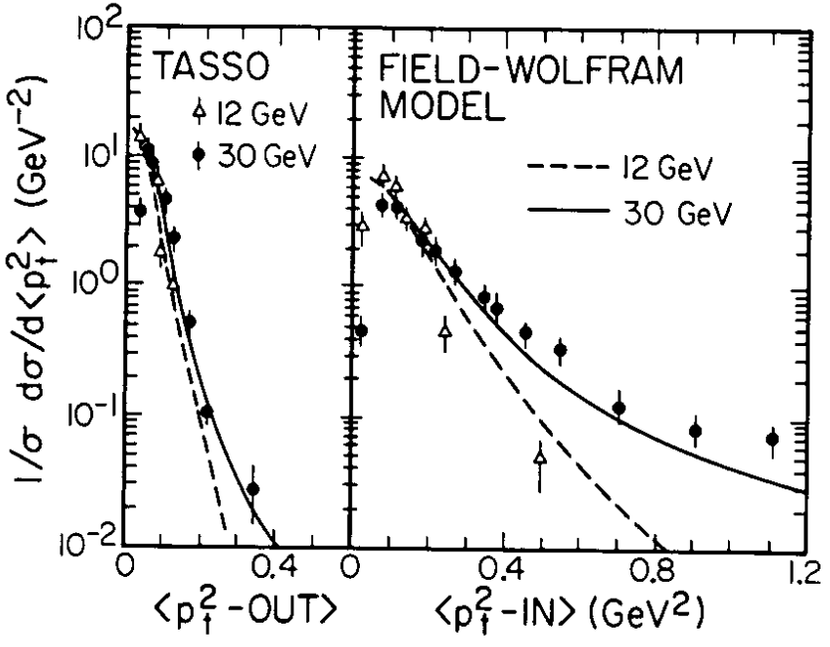

Fig. 37. Mean transverse momenta in and out of the event plane in the Field-Wolfram model. The TASSO data are from Refs. [91, 108].

4.3 Soft Gluons and the Webber Model

The leading-logarithm parton shower formalism of Sections 2.3 and 2.5 is determined by summing collinear mass singularities. These are not the only important singularities of perturbative QCD. These are also soft perturbative singularities associated with the emissions of low energy gluons. These soft perturbative singularities have been studied and carefully summed in a number of important papers.

The soft gluon analyses in Refs. [71-74] find very important interference effects. [The axial-gauge analysis of Section 2.3 eliminates only collinear interference, $t \to 0$, but $z < 1$.] The physical origin of these interference effects is actually somewhat easy to understand. Consider a fairly well developed shower of N nearly collinear gluons as illustrated in Fig. (38), and consider the effect of adding an additional soft gluon to the final state. In the incoherent,

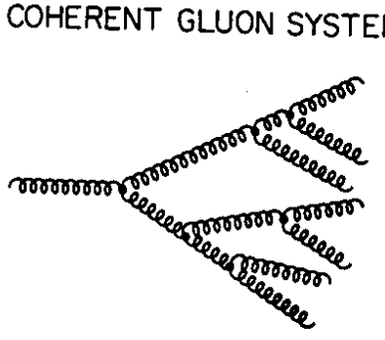

Fig. 38. Schematic illustration of a coherent gluon jet. A low energy (long wavelength) incident gluon cannot resolve the structure on the right hand side of the figure.

leading-log approximation, this soft gluon can couple to each of the N collinear gluons, with the same coupling $\mathbf{M} \simeq C_G \cdot g$, where C_G is the gluon-gluon color factor. Summing up these independent contributions, the total leading-log rate for the soft gluon addition to Fig. (38) behaves as, in the incoherent approximation,

$$|\mathbf{M}|^2_{INCO} \sim N g C_G \tag{4.14}$$

However, soft gluons have very long wavelengths. As the wavelength becomes sufficiently large, the incident, soft gluon cannot resolve all the different gluons on the right hand side of Fig. (38), and it "sees" instead only the single hard gluon at the base of the collinear shower. This "decreased resolution power" is evident in a summation which includes interference effects, and instead of Eq. (4.15), a coherent summation gives

$$|\mathbf{M}|^2_{CO} \sim 1 \cdot g C_G \tag{4.15}$$

In spite of the importance of interference effects, the coherent summation in Refs. [71-74] can still be phrased in terms of a probabilistic parton shower, as is discussed in Ref. [70]. Unlike the shower evolution in Fig. (13), in which there was strong ordering of the internal masses in the shower (see Eq. (2.141)), the coherent shower formalism is characterized by a strong ordering of gluon emission angles ϑ_j in Fig. (39), with

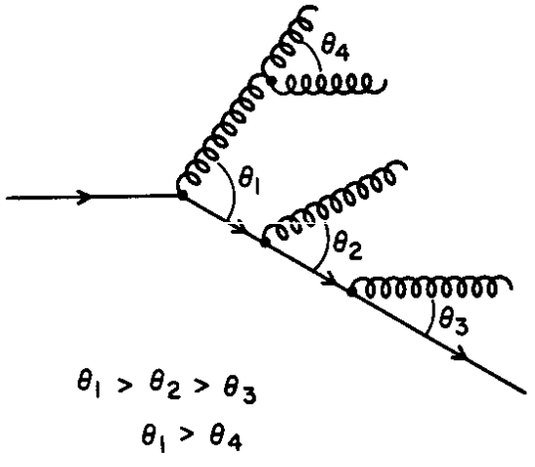

Fig. 39. Angular ordering of successive radiations in the coherent parton shower formalism of Ref. [70].

$$\vartheta_1 > \vartheta_2 > \vartheta_3 \ldots \tag{4.16}$$

In addition to this angular ordering, the formalism of Refs. [71-74] suggests that the proper argument of α_s in Eq. (2.118) is not $\alpha_s(t)$, but $\alpha_s[z(1-z)t]$. There is one peculiar technical complication in the shower formalism of Ref. [70], namely, e^+e^- annihilation events cannot be generated at a specified CM energy Q. Instead, Q^2 must be computed from a generated final state parton configuration, and the event either kept or regenerated if the produced value of Q is within some tolerance of the desired value.

A QCD-Cluster model using the coherent branching formalism has been presented by Webber in Refs. [157,159]. Aside from the use of the different shower model, the Webber model is broadly similar to the FW model. In particular, clusters are identified with individual color strings, heavy quarks are decayed weakly inside the shower, and final state clusters are again hadronized using the 2-body decay ansatz. The spectrum of hadrons used in the cluster parameterization is a bit smaller than in FW (only 0^{-+}, 1^{--}, 2^{++} mesons, but all FW baryons), and the weighting for specific modes is slightly different than that described in Section 4.2, (the Webber scheme seems to give baryon producing decays rather abnormally high probabilities).

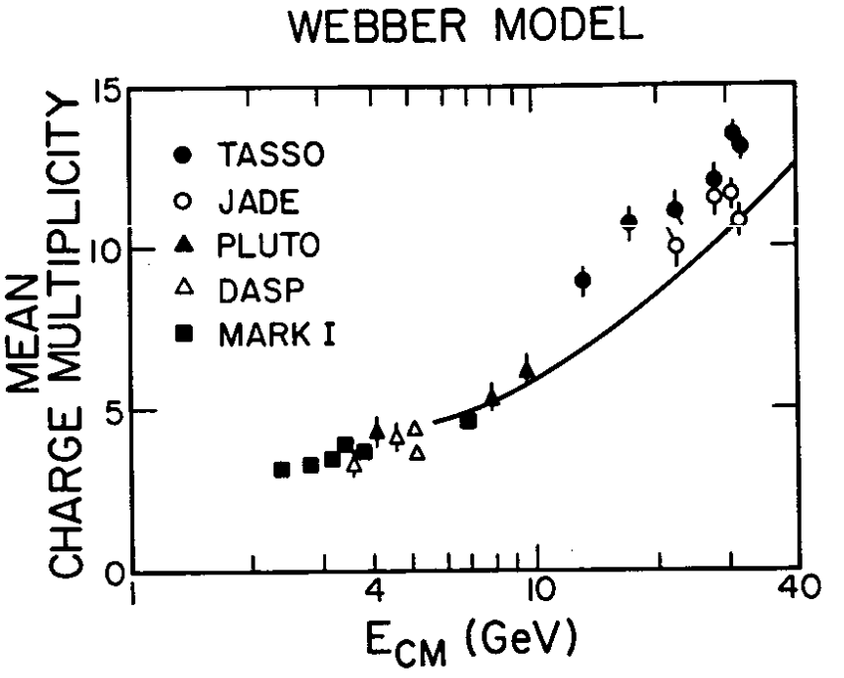

Fig. 40. Mean charge multiplicities in the Webber model for e^+e^- annihilation [157, 159]. The data are from Refs. [163-167].

The problems of very-light strings encountered in the FW model are avoided in the Webber model by an interesting set of tricks. Light quarks are not taken to be massless but are instead given constituent type masses $m_u = m_d \simeq m_\pi$, $m_s \simeq m_k$. This assignment ensures that all final state strings are massive enough to undergo 2-body decays. The argument of α_s in the probability for $G \to q\bar{q}$ splittings is chosen such that α_s diverges at the phase space boundary for the splitting. This means that all gluons ultimately split into $q\bar{q}$ pairs within the shower itself, and the additional splitting stage, Eq. (4.1), of the FW model is not needed. (The strangeness production rate in the Webber model is, however, fairly sensitive to the detailed implementation of these tricks.)

The Webber model can be tuned to agree with experimental results from PETRA/PEP, as shown in Figs. (40-41). The parameter values used in Ref. [157]

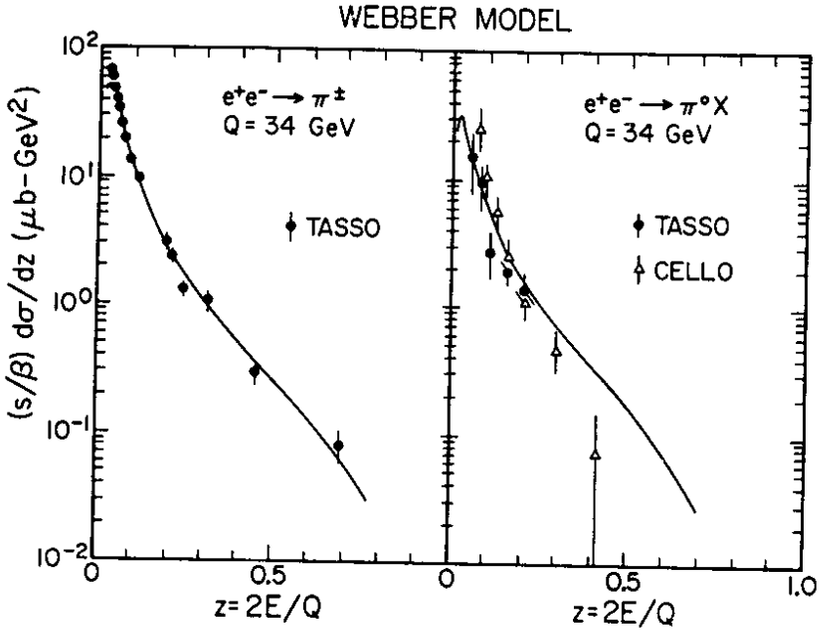

Fig. 41. Scaled energy distributions for pion production at E_{CM} = 34 GeV in the Webber model. The data are from Refs. [171-174].

were

$$\Lambda = 0.18 \text{ GeV} \tag{4.17}$$

$$t_c = (0.4 \text{ GeV})^2 = 0.16 \text{ GeV}^2 \tag{4.18}$$

Note that the cutoff on perturbative radiation is extremely small. More recent "fine tunings" of the model give slightly different parameter values.

If we accept the idea that it is reasonable to use purely perturbative QCD formalism on small mass scales, then the parton shower formalism in the Webber model is almost certainly preferable to that used in Refs. [154-156], in that a large number of perturbative singularities have been summed. However, the "if" at the start of the previous sentence must be examined rather carefully, since we do not yet know how to mix "perturbative" and "non-perturbative" QCD in the full theory.

4.4 An Improved Description of Low Mass Hadronization

The simple two-body statistical ansatz for cluster decays illustrated in Fig. (33) does not give a particularly precise description of low energy hadronization data. For example, a 1.88 GeV $u\bar{u}$ cluster which is decayed according to the schemes of Refs. [154-157] gives a mean charge multiplicity

$$\langle N_{ch}(u\bar{u};\, 1.88 \text{ GeV})\rangle \simeq 2.2 - 2.5 \tag{4.19}$$

This is significantly smaller than the soft hadronization result of a physical process at the same mass scale, proton-antiproton annihilation at rest [175],

$$\langle N_{ch}(\bar{p}p\,|_{rest})\rangle = 3.14 \pm 0.06 \tag{4.20}$$

A more dramatic failure of the 2-body cluster decay scheme is evident if we consider charm production in e^+e^- annihilation at E_{CM} = 5.2 GeV. This energy is low enough that the parton shower formalisms in [154-157] generally give no perturbative radiation, and the final state cluster ensemble has only a single $c\bar{c}$ cluster of mass $W = E_{CM}$. With the limited hadronic spectra in Ref. [154-157], this cluster can only decay into $D\bar{D}$, DD^* or D^*D^* channels, which would give

$$z_E(D) \gtrsim 0.95 \tag{4.21}$$

where

$$z_E(D) \equiv 2E_C / E_{CM} \tag{4.22}$$

This "prediction" is in sharp contrast to the results shown in Fig. (42). The data [176,177] are strongly peaked toward the kinematic minimum $z_{MIN} = 2M_D / E_{CM}$. The data indicate that multiparticle effects are important in low energy hadron production.

The shortcomings in Eqs. (4.19-4.20) and Fig. (42) do not undermine the basic QCD-Cluster approach. As emphasized in Section 4.1, the model does not (or, at least, should not) make any claim at understanding hadronization mechanisms on small mass scales. This aspect of hadron production has been factorized out of the models. The parameterizations in Refs. [154-157] do not, however, do a good job of representing low energy hadron production. This deficiency must be remedied if we are to reliably test the interesting dynamics of cluster formation in comparisons with high energy e^+e^- annihilation data.

The problem of accurately parameterizing low energy data is discussed in detail in Ref. [178]. The model developed there involves a simple generalization

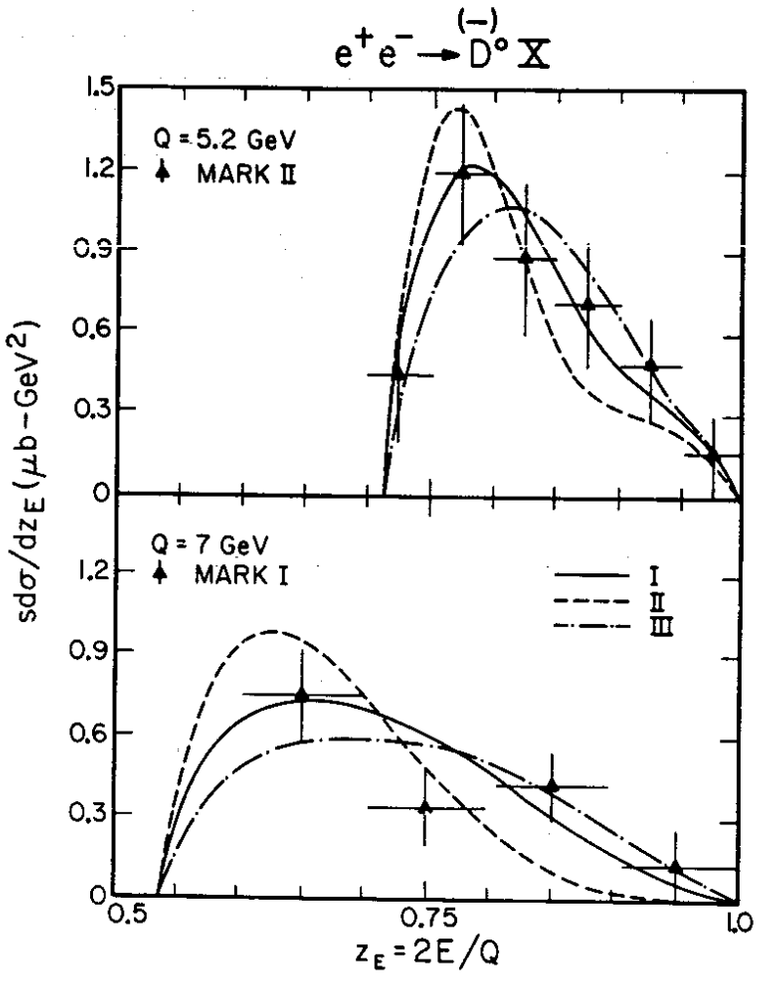

Fig. 42. Energy distributions for charmed mesons in the cluster decay parameterization of Ref. [178].The data are from Refs. [176, 177].

of Eq. (4.3) to allow the occasional production of "sub-clusters"

$$C \to H_1 + C_2 \tag{4.23}$$

For a specified cluster flavor (e.g., $u\bar{d}$, $c\bar{s}$, etc.), the density of clusters as a function of cluster mass is parameterized as

$$\rho(M) = A\vartheta(M - M_0)(M - M_0)^N \tag{4.24}$$

where M_0 is an empirical, flavor dependent cluster threshold. The analog of the probability factor in Eq. (4.4) is taken to be

$$P[C \to H_1 + C_2] = P_F \cdot P_S \cdot \hat{P}_K \tag{4.25}$$

The spin and flavor factors are precisely as defined before. Subclusters are taken to have spins 0 (meson clusters) or 1/2 (baryon clusters). The kinematic suppression $\hat{P}_K$ is given by a simple generalization of Eq. (4.7)

$$\hat{P}_K = \frac{1}{W^2} \int_{M_0}^{W - M_1} dM\, \rho(M) \lambda^{\frac{1}{2}}(W^2, M^2, M_0^2) \tag{4.26}$$

(The computer program developed in [178] uses an approximation to Eq. (4.26) to increase the program efficiency.)

Parameter values are determined in Ref. [178] through comparisons with a large number of low energy data, after first making some simplifying assumptions. In particular, the parameters A and N are taken to be independent of the cluster flavor. With this assumption, the charm data shown in Fig. (42) provide rather strong constraints on the exponent N in Eq. (4.24). The three curves in Fig. (42) correspond to best fits for the exponent values

$$N = 1/2 \quad \text{(I)} \tag{4.27}$$
$$N = 1 \quad \text{(II)} \tag{4.28}$$
$$N = 1/4 \quad \text{(III)} \tag{4.29}$$

Fits to various low energy data for these three exponent values are shown in Figs. (43, 44). The fit with $N = 1/2$ provides the best overall description of the data sample.

Included in Ref. [178] is a careful determination of the probability factors for creating the various quark-antiquark and diquark-antidiquark pairs in Fig. (33). In order to fit, e.g., $\bar{p}p \to K\bar{K}$ + pions and $e^+e^- \to K\bar{K}X$, at low energies, the suppression of strangeness production in cluster decay was found to be

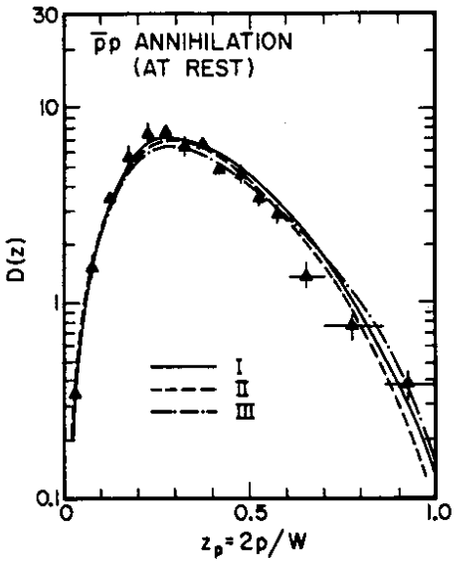

Fig. 43. Scaled momentum distributions for charged pions from $\bar{p}p$ annihilations at rest according to the cluster decay parameterization of Ref. [178]. The data are taken from Ref. [179].

$$P[s\bar{s}]/P[u\bar{u}] = 0.5 - 0.6 \tag{4.30}$$

(The value in Eq. (4.30) is correlated with other parameter values, such as N in Eqs. (4.27-4.29).) We note that this suppression factor is rather different from the corresponding value in the FF model [180]

$$P_{FF}\left[\frac{s\bar{s}}{u\bar{u}}\right] = 0.29 \pm 0.02$$

The reason for this is the kinematic suppression factors in Eqs. (4.7, 4.26) which are not part of the FF formalism. There is no such thing as a model-independent "fundamental value" for strangeness suppression in soft hadronization.

The physics behind the specific parameterization adopted in Ref. [178] is all quite reasonable: two-body dominance, phase space, statistical particle densities and Zweig's rule. From the more general point of view of the QCD-Cluster models, however, no physical justification is required. The parameterization in

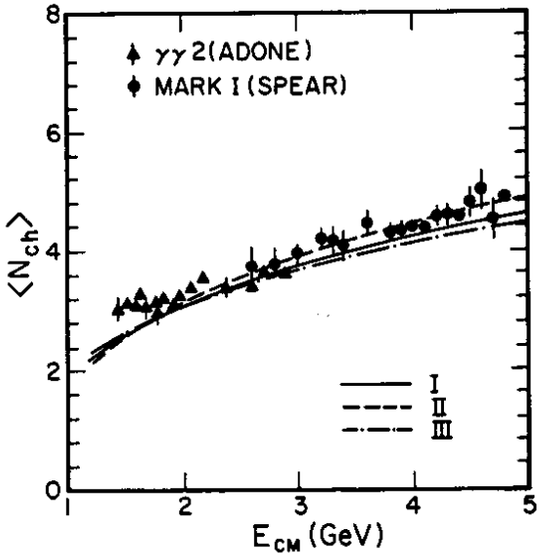

Fig. 44. Charge multiplicities for low energy e^+e^- annihilations according to the parameterizations in [178]. The data are from Refs. [162, 163].

Ref. [178] fulfills the required task mentioned in Section 4.1: the accurate representation of observed features of low mass hadron production data. The QCD-Cluster models described in Sections 4.5, 4.6 use this improved parameterization.

4.5 Limited p_T Jets Without the Feynman-Field Mechanism

The parton shower formalisms used in Refs. [154,156,157] differ primarily in the production rates for low energy gluons. These soft gluons are needed in order to break large mass clusters into smaller mass sub-clusters. For example, adding a fairly soft gluon to a large mass $q_i\bar{q}_j$ string, then forming substrings, breaks up the original large cluster in the manner previously discussed. Qualitatively, at least, soft gluon formation can be related to the screening of large scale color separations as a system evolves in space-time.

In Ref. [154], soft gluons are generated primarily at late times in the shower evolution. This would appear to give an improper, "outside-in" character to

hadron production in the event. In Ref. [156], the shower formalism was artificially modified to enhance the radiation of soft gluons at early times in the shower evolution. Fewer soft radiations are needed at later times, and the Λ value used in Ref. [156] is thus considerably smaller than that from Ref. [154] (compare Eqs. (4.9, 4.11)). It is interesting to note that the ad hoc modification of the shower formalism used in Ref. [156] has the same qualitative effect as the more careful resummation of soft gluons used in Ref. [157]: an enhancement of soft radiation at early times and a suppression at later times.

Since we do not yet understand how confinement actually works in QCD, the dependence of the shower formalisms on details of the treatment of soft perturbative radiation is a bit disconcerting. Soft gluons have long wavelengths, and it is generally believed that, at long distances, the important aspect of QCD is confinement, not perturbation theory. Several arguments against a "purely" perturbative formalism can be found in Ref. [128]. It thus seems important to investigate "non-perturbative" models for color screening/color evolution in the development of the cluster final state.

A simple, non-perturbative QCD-Cluster model is presented in Ref. [158]. The starting point for this model is the 1+1-dimensional string model used by the LUND group, and described previously in Section 3.4. The use of the string-picture in Ref. [158] is, however, quite different from what was done by the LUND group.

The 1+1 dimensional string picture is, at best, an overly simplified representation of (expected) qualitative features of confinement: narrow flux tubes and a linearly confining potential. It is argued in Ref. [158] that this very crude description of color screening should be used only to describe gross features of the space-time evolution of an excited $q\bar{q}$ system: the break-up of the large mass $q\bar{q}$ state into smaller mass, colorless subclusters. The detailed generation of hadrons according to the simple string formalism is an unnecessarily bold assumption in the LUND model--an assumption which requires extensive modifications and complications of the underlying string formalism.

The basic structure of the non-perturbative QCD-Cluster model in Ref. [158] is quite simple:

1) The string-model formalism is used to break large mass systems into smaller mass subclusters.

2) The clusters produced in step (1) are individually hadronized using the parameterization outlined in Section (4.4).

The separation of event evolution into "soft" (string model evolution) and "very soft" (cluster hadronization) phases is done using a mass-cut formalism, which is now described.

Consider a cluster characterized by a mass W, a quark flavor q_a and an antiquark flavor $\bar{q}_b$. If the cluster mass satisfies the relation

$$W \leq W_2[q_a,\bar{q}_b] + W_{MAX} \tag{4.32}$$

(W_2 is the 2-particle mass threshold specified by the cluster flavor), then the cluster is not evolved by the string model, but is instead hadronized directly using the parameterization of Ref. [178]. The parameter W_{MAX} sets the maximum cluster mass for "very soft" hadronization. In Ref. [178] the limit

$$W_{MAX} \lesssim 4 \text{ GeV} \tag{4.33}$$

was estimated. The value W_{MAX} = 4 GeV is used in Ref. [158].

Clusters more massive than the bound in Eq. (4.33) are allowed to break into two subclusters,

$$C \rightarrow C_1 + C_2 \tag{4.34}$$

using the string model prescription. Unlike the mass-shell constraints (Eq. (3.62)) imposed in the LUND formalism, the space-time position of the string break is unconstrained, except for the requirement that the daughter subclusters satisfy the mass inequalities

$$W_1 \equiv W[C_1] \geq W_2[q_a,\bar{q}_c] + W_c \tag{4.35}$$

$$W_2 \equiv W[C_2] \geq W_2[q_c,\bar{q}_b] + W_c \tag{4.36}$$

where W_c is a parameter of the model.

The minimum mass constraints in Eqs. (4.35, 4.36) restrict the position (x,t) of allowed string breaks to lie within a region of space-time bounded by curves corresponding to equalities in Eqs. (4.35, 4.36). This allowed region is illustrated by the shaded region in Fig. (45), where we consider the space-time of a 6 GeV $u\bar{c}$ cluster in its rest frame, using the coordinates

$$\chi \equiv \alpha x \tag{4.37}$$

$$\tau = \alpha t \tag{4.38}$$

where α is the string tension in Eq. (3.53). The shaded area in Fig. (45) is for W_c = 1.25 GeV.

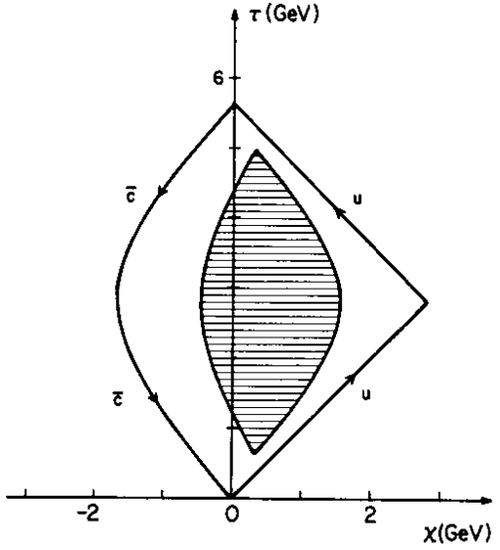

Fig. 45. Allowed space-time region for pair production in the string model evolution of a 6 GeV $u\bar{c}$ cluster, using the mass cut formalism of Eqs. (4.35, 4.36).

String breaking is allowed with uniform probability

$$dP = \mathrm{P} dx dt \tag{4.39}$$

within the space-time region specified by Eqs. (4.35-4.36). Working in the rest frame of the decaying cluster, Eq. (4.39) implies that the (proper) time of the first cluster break is distributed according to

$$dP = \mathrm{P}\, e^{-\mathrm{P}A(t)}\, dt \tag{4.40}$$

where $A(t)$ is the area (CM) of allowed string breaking points at times prior to t. Explicit formulae for $A(t)$ and the kinematic boundaries for Fig. (45) are given in the Appendix of Ref. [158].

The (CM) time for an allowed cluster break is generated according to the probability in Eq. (4.40), and the position variable x is then selected uniformly with the allowed x region for breaks at that time. With (x,t) thus chosen, the kinematics of $C \to C_1 + C_2$ are completely specified. The string model cluster evolution is simply repeated, as necessary, until no large mass (sub)clusters remain.

With the cutoff between string model evolution and soft cluster decay specified by the mass cuts in Eqs. (4.35-4.36), the string tension α in Eq. (3.53) and the pair production probability P in Eq. (4.39) enter

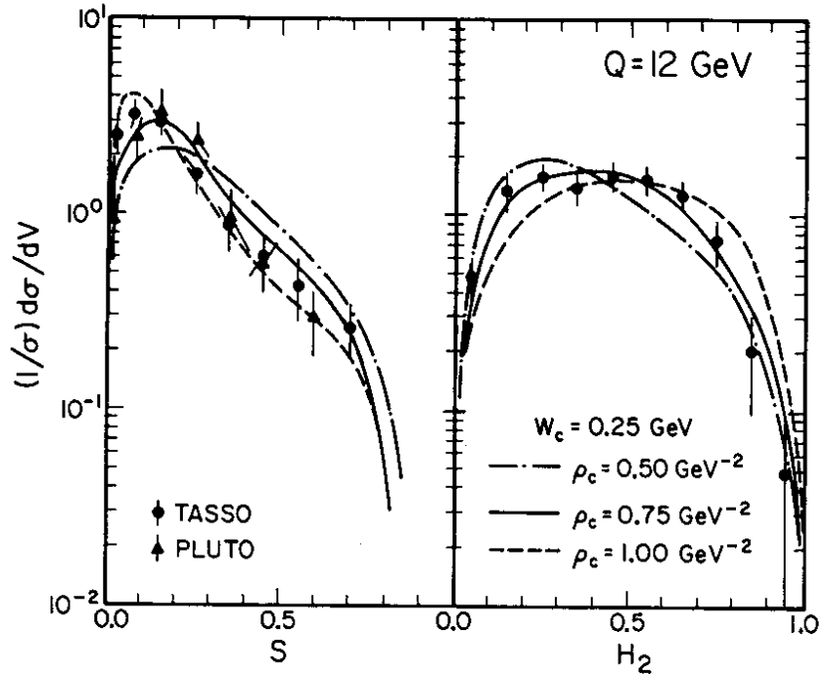

Fig. 46. String model results for shape variable distributions in e^+e^- annihilation at E_{CM} = 12 GeV. The data are from Refs. [90, 124].

the formalism only through the combination

$$\rho_c \equiv \mathrm{P}/\alpha^2 \tag{4.41}$$

The only parameters of cluster evolution in Ref. [158] are ρ_c and the cutoff W_c in

Eqs. (4.35, 4.36).

Values of ρ_c and W_c are determined in Ref. [158] from comparisons with e^+e^- annihilation data at $Q = 12$ GeV, assuming that all color evolution was "non-perturbative" (i.e., ignoring, for now, all perturbative QCD evolution). Predictions for shape variable distributions are found to be particularly sensitive to values of ρ_c and W_c, as shown in Fig. (46). The values

$$\rho_c = 0.75 \text{ GeV}^{-2} \tag{4.42}$$

$$W_c = 0.25 \text{ GeV} \tag{4.43}$$

are used in subsequent discussions. (These values, however, are not unique, as noted in Ref. [158].)

The overall structure of the non-perturbative QCD-Cluster model is extremely simple. Yet this simple model is very successful in describing a number of features of e^+e^- annihilation data.

Predictions for the scaled momentum distributions of charged hadrons at several CM energies are compared with data [122,163,181,182] in Fig. (47), where

$$z_p = 2|\vec{p}\,|/Q \tag{4.44}$$

The magnitudes and shapes of these distributions are described quite well by the model, including the Q-dependence ("scaling violations"). This suggests that fits to observed scaling violations in $s d\sigma/dz_p$ using purely perturbative QCD formulae cannot provide uncontroversial tests of QCD perturbation theory. (This point of view is also stressed in Ref. [183].)

We should note that the good agreement in Fig. (47) over all CM energies depends on the use of the accurate parameterization of low mass hadronization in Ref. [178]. If the more naïve (and less accurate) 2-body ansatz of Refs. [154-157] were used instead, the predicted distributions would generally be too low at small z_p and too high at large z_p.

Transverse momenta distributions of charged hadrons (p_T with respect to the sphericity axis) are compared with TASSO data [91,108] in Fig. (48). The non-perturbative string model cannot, of course, reproduce the "perturbative tail" in the ~30 GeV TASSO results for $p_T^2 \gtrsim 3$ GeV^2--this requires wide-angle gluon bremsstrahlung. There are, however, two important trends of the data in Fig. (48) which are easily reproduced by the model:

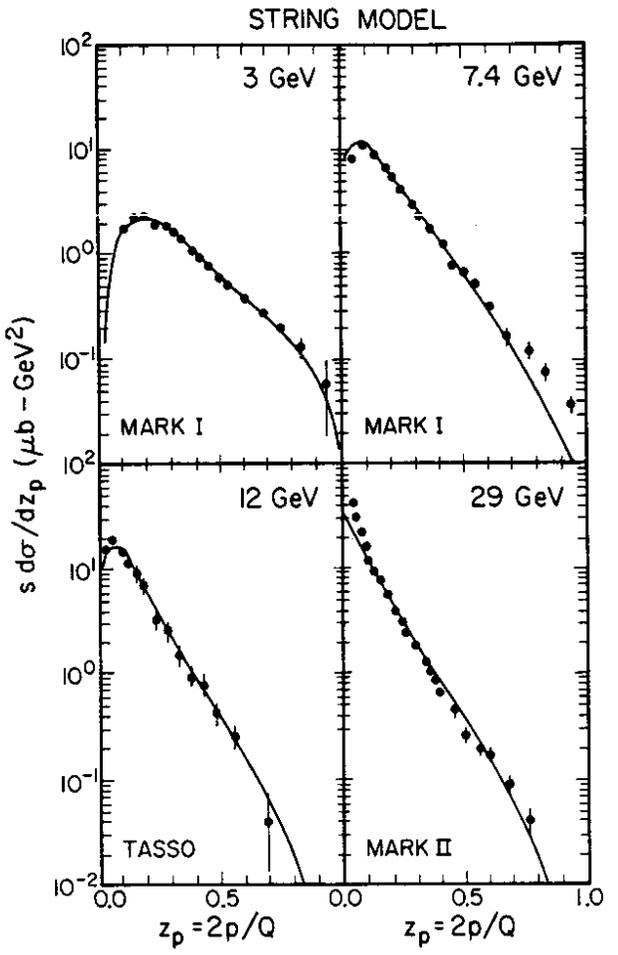

Fig. 47. String model results for the scaled momentum distributions of charged hadrons at several CM energies. The data are from Refs. [122, 163, 180, 181].

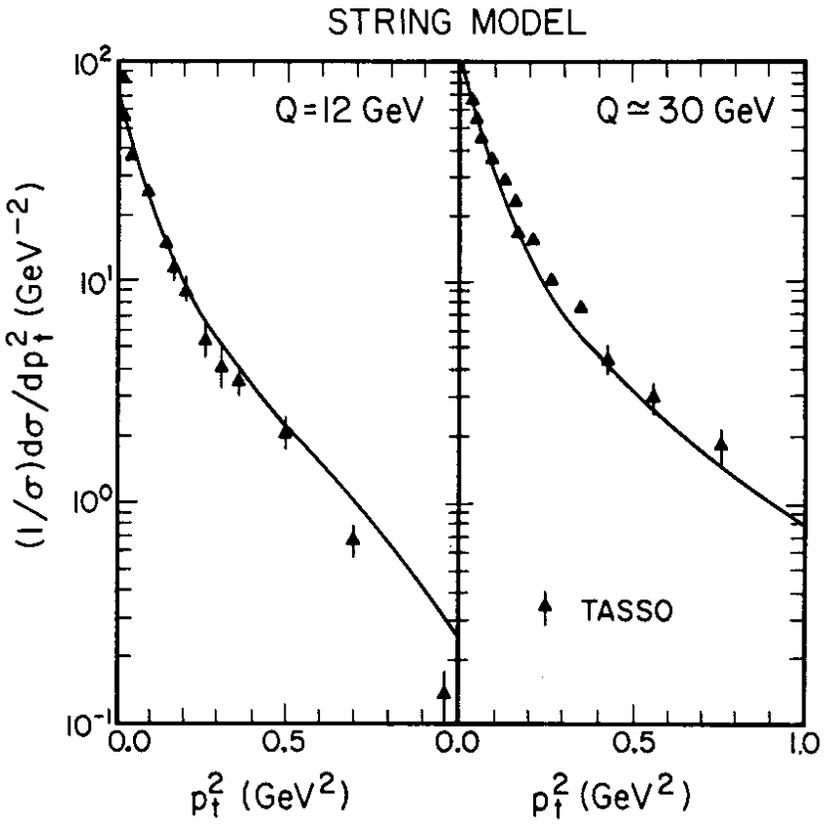

Fig. 48. Transverse momentum distributions of charged hadrons according to the string model of Ref. [158]. The TASSO data are from Refs. [91, 108].

1) Strongly cut off distributions in $d\sigma/dp_t^2$.

2) A mild broadening in $d\sigma/dp_t^2$ (larger $\langle p_t^2 \rangle$) between Q = 12 GeV and Q = 30 GeV.

The first feature is built into the FF and LUND models, by assumption, and the second feature is essentially not anticipated in these models. In the QCD-Cluster string model, however, both effects are simply understood on simple, almost kinematic grounds.

The key point in understanding Fig. (48) is the observation that string-breaking occurs very rapidly in the model, once it is allowed. For the parameter values in Eqs. (4.42, 4.43), the first (and typically only) cluster break occurs for

$$\langle ct \rangle \simeq 1.2\ fm \tag{4.45}$$

at Q = 12 GeV. Estimating $\alpha \simeq 0.2$ GeV^{-2} for the string tension, this means that the original quark and antiquark have not been slowed appreciably:

$$\langle p(q) \rangle = p_0 - \alpha \langle t \rangle \tag{4.46}$$

$$\simeq E_{CM}/2 - 1\ \text{GeV} \tag{4.47}$$

Kinematics then imply that the daughter clusters produced in this break cannot be very massive.

The rapid breaking of the excited $q\bar{q}$ string into two low-mass, high-momentum substrings leads directly to a limited-p_T spectrum, as in Fig. (48). The p_t^2 distributions of the (boosted) subclusters simply reflect the observed high multiplicities of low-mass cluster hadronization, as parameterized in Ref. [178].

Ignoring the dependence of the boundary equations in Eqs. (4.35, 4.36) on the initial cluster mass, the form of Eq. (4.40) implies that Eq. (4.45) is roughly independent of the initial cluster's mass. This implies that the masses of the 2 daughter clusters produced in the initial string break increase with increasing E_{CM}. This simple growth in subcluster mass is the qualitative explanation for the growth in $\langle p_t^2 \rangle$ observed in Fig. (48).

An increase of $\langle p_t^2 \rangle$ for E_{CM} increasing between 12 GeV and 30 GeV is a very plausible kinematic result of rapid, non-perturbative color screening. We should remark, however, that the precise form of $\langle p_t^2(E_{CM}) \rangle$ in the non-perturbative QCD-Cluster model is rather sensitive to the cutoff scheme used to separate string model color evolution from the soft cluster hadronization phase of the

model.

4.6 Adding Bremsstrahlung and an Assessment

A combined model including both hard perturbative QCD radiation and non-perturbative string model color evolution is presented in Ref. [158]. Perturbative QCD radiation is incorporated using the Fox-Wolfram parton shower formalism, but with a very hard cutoff on resolvable perturbative radiation

$$\Lambda = 0.3 \text{ GeV} \tag{4.48}$$

$$t_c = 25 \text{ GeV}^2 \tag{4.49}$$

An event is assumed to begin with hard perturbative radiation, as described by these parameter values. Large mass strings produced in the shower are subsequently evolved using the string model formalism of Section 4.5.

With the parameters in Eqs. (4.48, 4.49), there is significant perturbative radiation at $Q = 12$ GeV, and the values of the string evolution parameters ρ_c, W_c need to be changed. It is found in Ref. [158] that the values

$$\rho_c = 0.75 \text{ GeV}^{-2} \tag{4.50}$$

$$W_c = 0.5 \text{ GeV} \tag{4.51}$$

are adequate for the combined model, with shower evolution as described above.

Fig. (49) compares the simple string model (SM) and string model + bremsstrahlung (SM+B) predictions for sphericity with data [90,124] from TASSO and PLUTO. At low energies, the predictions are quite similar, while at high energy, the perturbative radiation included in SM+B is clearly required in order to reproduce the observed rate of production of planar events with large S.

Fig. (50) shows results for the (effective) rapidity y_π of charged hadrons (computed with respect to the sphericity axis)

$$y_\pi \equiv \tfrac{1}{2} \left| \ln \left\{ \frac{E_\pi(p) + p_z}{E_\pi(p) - p_z} \right\} \right| \tag{4.52}$$

where $E_\pi(p)$ is computed assuming that all detected charged hadrons are pions,

$$E_\pi(p) \equiv [p^2 + m_\pi^2]^{\frac{1}{2}} \tag{4.53}$$

The agreement with the data [108] is good. We note the development of a mild rapidity dip for $y_\pi \sim 0$. In SM+B, this is a simple kinematic consequence of the

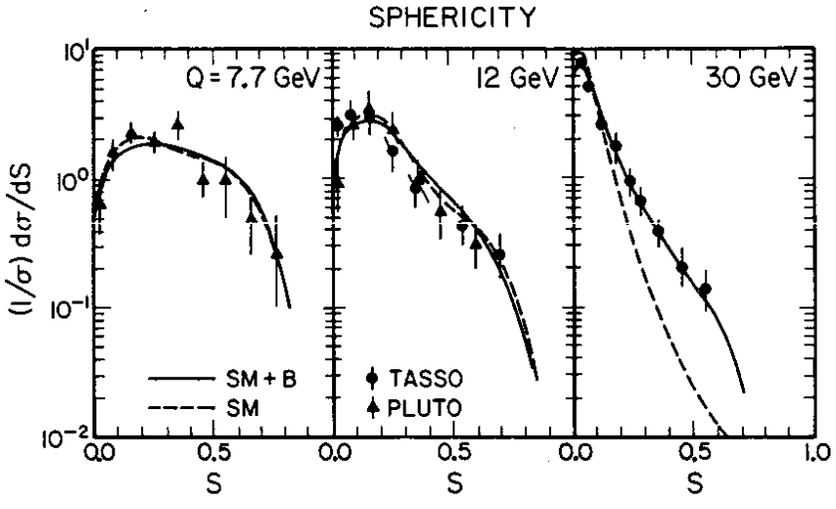

Fig. 49. Sphericity distributions at various e^+e^- CM energies for string model color evolution, both with and without initial perturbative QCD bremsstrahlung. The data are from Refs. [90, 124].

decays of a relatively small number of massive clusters [$\langle N_{cl} \rangle \simeq 3$–4 at 30 GeV in SM+B]. In the Webber model (which also reproduces $d\sigma/dy_\pi$ at 30 GeV), the number of elementary strings is large, and the rapidity dip is viewed as evidence for the soft gluon interference effects discussed in Section 4.3.

Ref. [158] compares a number of SM+B predictions with PETRA data. We show here one last result: the inclusive energy distributions for kaons and baryons at $E_{CM} \gtrsim 30$ GeV. We note that the agreement between data [117,184,185] and predictions is generally better in the SM+B case in Fig. (51) than had been found in the FW model (see Fig. (34)). This is due to the improved description of soft cluster decays developed in Ref. [158].

The SM+B predictions for baryon production rates are systematically low. The reason for this is easily understood. The simple string breaking formalism of Section 4.5 must be generalized to allow some level of baryon cluster formation during the color screening process. This is a fairly straightforward task presently under investigation.

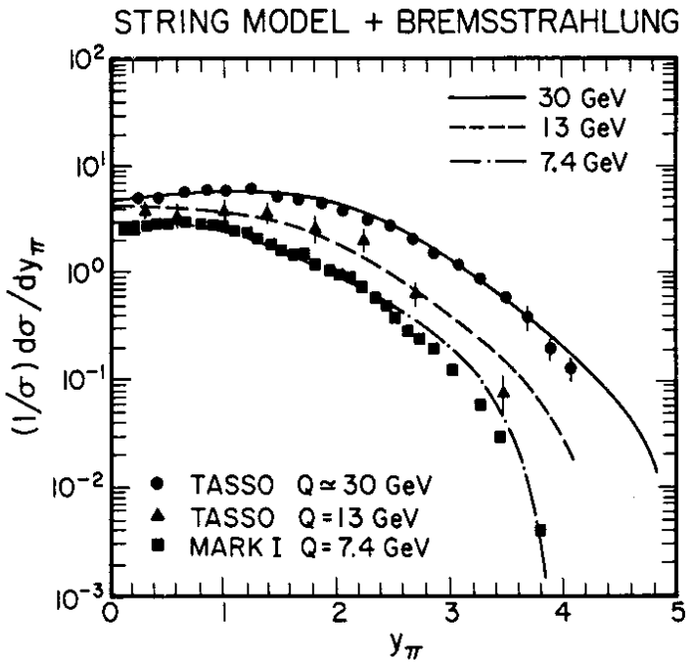

Fig. 50. SM+B Results for the rapidities of charged hadrons at several CM energies. The data are taken from Ref. [108].

A "final form" for the combined QCD-Cluster model containing very hard perturbative QCD, soft (string model) cluster evolution and very soft, parameterized cluster decay is not yet developed. As discussed in Ref. [158], the initial results of the combined model are very promising, and several "general conclusions" are suggested:

1) The role of dynamical QCD models in the analysis of e^+e^- annihilation can be limited to the description of gross features of color screening and color evolution as the initial state eventually becomes a system of low mass, colorless clusters.

2) The (unknown) physics responsible for the formation of observed hadrons can be consistently factored out of the calculation, using the simple parameterization of soft hadronization from Ref. [178]. This factorization is done in terms of colorless clusters (which can

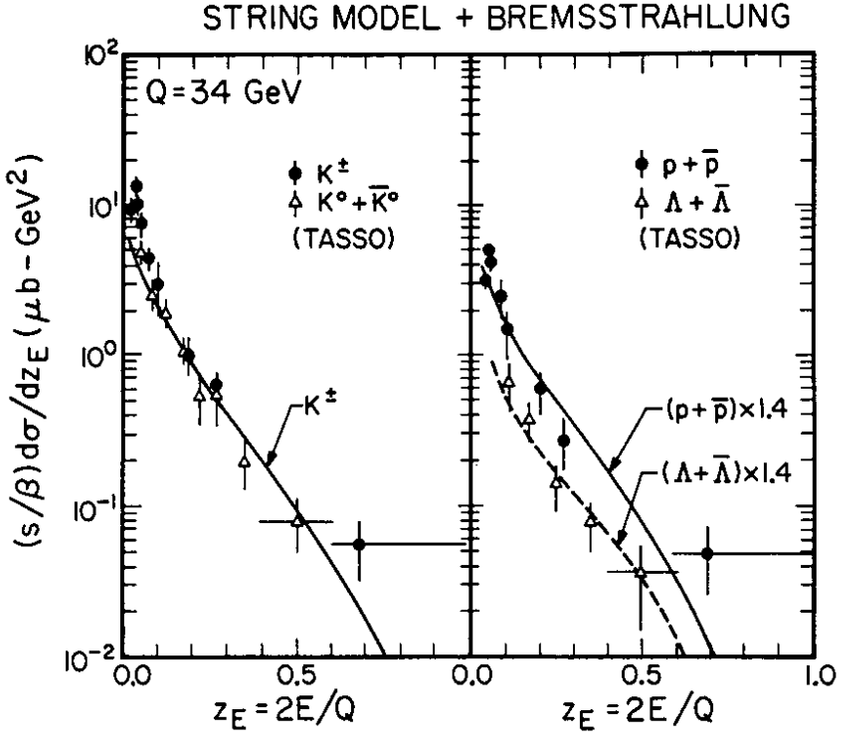

Fig. 51. Scaled energy distributions for kaons and baryons in the SM+B model of [148]. The data are from Refs. [117, 184, 188].

hadronize independently), not in terms of individual colored quarks and gluons.

3) Detailed hadronization schemes which connect perturbative quanta directly to final state hadrons (e.g., FF or LUND) are unnecessary--if not potentially misleading.

4) Soft color evolution in QCD can be described by simple non-perturbative models (e.g., the 1+1-dimensional string used in Section 4.5).

5) The picture of rapid color screening followed by independent, soft cluster decay provides a simple, physical basis for the FF parameterization--with the additional result that some mild energy dependence in the FF parameters is likely.

6) The QCD-Cluster formalism is generally successful over the entire energy range presently measured in e^+e^- annihilation.

Point #6 suggests an important general requirement for all QCD-Cluster models: The model must provide a good description of e^+e^- annihilation at all measured energies. This is important for several reasons. (1) The energy dependence of the model provides an important test on the specific formalism used to describe color evolution. (2) A cluster intermediate state at, say, Q = 30 GeV can contain subclusters of any mass below 30 GeV. Thus, inaccuracies in the model at low energy feed through to all higher energies. (3) Without good agreement at all observed energies, extrapolations to SLC/LEP energies are less reliable.

It is not clear that a small-t_c QCD-Cluster Model using only perturbative QCD and 2-body cluster decays can ever satisfy this energy independence requirement. For example, the low-energy charm data shown previously in Fig. (42) seem to require a more complex, "non-perturbative" hadronization mechanism.

The "unanswered question" in the QCD-Cluster formalism concerns the manner in which underlying models for hard color evolution (perturbative QCD), soft color evolution (string model) and very soft (parameterized) cluster decay are separated by (hard) phenomenological cutoff. The invariant mass cutoff approach used in Ref. [158] is generally successful, but there are a few small--but significant--failures. It is suggested in Ref. [158] that a space-time cutoff approach may well provide a more reasonable, consistent way of formulating the hard↔soft↔very soft separation.

It is not surprising that the improvements needed in the QCD-Cluster formalism involve "distinguishing" perturbative and non-perturbative color evolution. As stressed in Section 1, we do not yet know how perturbative and non-perturbative QCD fit together in the whole theory. The QCD-Cluster formalism provides a very clean framework for studying this question, using a wide range of data in this study.

Acknowledgements

I would like to thank the organizers of the Kupari-Dubrovnik school, particularly M. Nikolic and V. Gerc. It is a pleasure to acknowledge various conversations with M. Ciafaloni, D. Drijard, G. C. Fox, C. Gomberg, G. Ingelman, Z. Kunszt, R. Orava, D. H. Saxon, D. Schlatter, M. Shatz, P. Söding, H. Stone and B. R. Webber. This manuscript was written while visiting the theory division at CERN.

References

1. G. Arnison *et al.* (UA1), CERN preprints CERN-EP/83-118, CERN-EP/83-119, submitted to *Phys. Lett. B.*
2. P. Bagnaia *et al.* (UA2), *Z. Phys.* **C20** (1983) 117.
3. M. Banner *et al.* (UA2), *Phys. Lett.* **122B** (1983) 476; *Phys. Lett.* **112B** (1982) 260.
4. H. D. Politzer, *Phys. Reports* **14C** (1974) 129.
5. W. Marciano and H. Pagels, *Phys. Reports* **36C** (1978) 137.
6. A. H. Mueller, *Phys. Reports* **73** (1981) 237.
7. A. J. Buras, *Rev. Mod. Phys.* **52** (1980) 199.
8. E. Reya, *Phys. Reports* **69** (1981) 195.
9. G. Altarelli, *Phys. Reports* **81** (1982) 1.
10. J. F. Owens, FSU-HEP-81091, in *Orbis Scientiae* (1979) 347.
11. J. B. Kogut, *Rev. Mod. Phys.* **55** (1983) 775.
12. P. Hasenfratz, Lectures presented at the 19th *Int. School on Elementary Particle Physics*, Kupari-Dubrovnik, Yugoslavia, 1983.
13. R. P. Feynman, *Phys. Rev. Lett.* **23** (1969) 1415.
14. R. P. Feynman, Photon Hadron Interactions, Benjamin, New York, 1972.
15. J. D. Bjorken, *Phys. Rev.* **179** (1969) 1547.
16. J. D. Bjorken and E. A. Paschos, *Phys. Rev.* **185** (1969) 1975; *Phys. Rev.* **D1** (1970) 3151.
17. F. E. Close, An Introduction to Quarks and Partons, Academic Press, New York, 1979.

18. H. D. Politzer in Perturbative Quantum Chromodynamics, ed. M. Jacob, North-Holland, New York, 1983.

19. R. D. Field and R. P. Feynman, *Phys. Rev.* **D15** (1977) 2590; *Nucl. Phys.* **B138** (1978) 1.

20. E. M. Ilgenfritz, J. Kripfganz and A. Schiller, *Acta Phys. Polonica* **B9** (1978) 881.

21. S. Ritter and J. Ranft, *Acta Phys. Polonica* **B11** (1980) 259.

22. S. Ritter, *Z. Phys.* **C16** (1982) 27.

23. P. Hoyer *et al.*, *Nucl. Phys.* **B161** (1979) 349.

24. A. Ali, E. Pietarinen, G. Kramer and J. Willrodt, *Phys. Lett.* **93B** (1980) 155.

25. A. Ali, E. Pietarinen and J. Willrodt, DESY Report T-01 (1980), unpublished.

26. P. Mazzanti and R. Odorico, *Phys. Lett.* **95B** (1980) 133; *Z. Phys.* **C7** (1980) 61.

27. G. Hanson *et al.* (Mark I), *Phys. Rev.* **D26** (1982) 991.

28. W. Bacino *et al.* (DELCO), *Phys. Rev. Lett.* **41** (1978) 13.

29. A. DeRujula, J. Ellis, E. G. Floratos and M. K. Gaillard, *Nucl. Phys.* **B138** (1978) 387.

30. H. D. Politzer, *Nucl. Phys.* **B129** (1977) 309.

31. S. Libby and G. Sterman, *Phys. Lett.* **78B** (1978) 618.

32. R. K. Ellis, H. Georgi, M. Machacek, H. D. Politzer and G. Ross, *Phys. Lett.* **78B** (1978) 281; *Nucl. Phys.* **B152** (1979) 285.

33. D. Amati, R. Petronzio and G. Veneziano, *Nucl. Phys.* **B140** (1978) 54; *Nucl. Phys.* **B146** (1978) 29.

34. G. Altarelli and G. Parisi, *Nucl. Phys.* **B126** (1977) 298.

35. T. Gottschalk, E. Monsay and D. Sivers, *Phys. Rev.* **D21** (1980) 1799.

36. G. C. Fox and S. Wolfram, *Nucl. Phys.* **B149** (1979) 413.

37. E. DeRafael, Lectures on Quantum Electrodynamics, Universidad Autonoma de Barcelona, 1977.

38. N. N. Bogolubov and D. V. Shirkov, Introduction to the Theory of Quantized Fields, Interscience, New York, 1959.

39. L. Lewin, Dilogarithms and Associated Functions, MacDonald, London, 1958.

40. H. J. Duam, H. Meyer and J. Burger, *Z. Phys.* **C8** (1981) 167.

41. J. Dorfan, *Z. Phys.* **C7** (1981) 349.

42. E. S. Abers and B. W. Lee, *Phys. Reports* **9** (1973) 1, for example.

43. H. D. Politzer, *Phys. Rev. Lett.* **30** (1973) 1346.

44. D. Gross and F. Wilczek, *Phys. Rev. Lett.* **30** (1973) 1343.

45. B. Lautrup, Neils Bohr Inst. preprint NBI-HE-76-14 (1977), Lectures presented at the 12th *Int. School of Elementary Particle Physics*, Basko Polje, Yugoslavia, 1976.

46. L. D. Fadeev and V. N. Popov, *Phys. Lett.* **25B** (1967) 29.

47. L. N. Lipatov, *Soviet J. Nucl. Phys.* **20** (1975) 94.

48. E. C. G. Stueckelberg and A. Peterman, *Helv. Phys. Acta* **26** (1953) 449.

49. M. Gell-Mann and F. Low, *Phys. Rev.* **95** (1954) 1300.

50. A. Peterman, *Phys. Reports* **53** (1979) 157.

51. G. C. Fox and S. Wolfram, *Nucl. Phys.* **B168** (1980) 285.

52. G. Altarelli, G. Parisi and R. Petronzio, *Phys. Lett.* **63B** (1976) 183.

53. M. Glück and E. Reya, *Phys. Rev.* **D16** (1977) 3242.

54. A. J. Buras, *Nucl. Phys.* **B125** (1977) 125.

55. I. Hinchliffe and C. H. Llewellyn-Smith, *Nucl. Phys.* **B128** (1977) 93.

56. V. A. Novikov, M. A. Shifman, A. I. Vainstein and V. I. Zaharov, *Ann. Phys.* **105** (1977) 276.

57. J. F. Owens, *Phys. Lett.* **76B** (1978) 85.

58. T. Uematsu, *Phys. Lett.* **79B** (1978) 97.

59. H. Abramowicz *et al.* (CDHS), *Z. Phys.* **C17** (1983) 283.

60. H. Georgi and H. D. Politzer, *Phys. Rev.* **D9** (1974) 416.

61. D. J. Gross and F. Wilczek, *Phys. Rev.* **D8** (1973) 3633; *Phys. Rev.* **D9** (1974) 980.

62. J. H. Mulvey (ABCLOS), in *Proceedings of the XIX International Conf. on High Energy Physics*, Tokyo, 1978, eds. S. Homma, M. Kawaguchi and H. Miyazawa.

63. P. R. Norton (EMC), in *Proceedings of the XX International Conf. on High Energy Physics*, Madison, 1980, eds. L. Durand and L. G. Pondrom.

64. G. C. Fox, *Proceedings of the 1981 SLAC Summer School*, ed. A. Mosher (1981) 181.

65. T. D. Gottschalk, *Nucl. Phys.* **B227** (1983) 413.

66. M. P. Shatz, Caltech preprint CALT-68-1012 (1983).

67. R. Odorico, *Nucl. Phys.* **B172** (1980) 157.

68. A. Bassetto, M. Ciafaloni and G. Marchesini, *Phys. Lett.* **83B** (1979) 207; *Phys. Lett.* **86B** (1979) 366; *Nucl. Phys.* **B163** (1980) 477.

69. G. C. Fox and S. Wolfram, "A Gallimaufry of e^+e^- Annihilation Event Shapes", Caltech preprint CALT-68-723 (1979), unpublished.

70. G. Marchesini and B. R. Webber, CERN preprint CERN-TH-3525 (1983).

71. A. H. Mueller, *Phys. Lett.* **104B** (1981) 161.

72. A. Bassetto, M. Ciafaloni, G. Marchesini and A. H. Mueller, *Nucl. Phys.* **B207** (1982) 189.

73. Yu. L. Dokshitzer, V. S. Fadin and V. A. Khoze, *Phys. Lett.* **115B** (1982) 242.

74. A. Bassetto, M. Ciafaloni and G. Marchesini, *Phys. Reports*, in preparation.

75. R. D. Field, G. C. Fox and R. L. Kelly, *Phys. Lett.* **119B** (1982) 439.

76. C. DeMarzo *et al.* (NA5), *Phys. Lett.* **112B** (1982) 173.

77. P. A. Polakos (NA5), Invited talk presented at the *XIII International Symposium on Multiparticle Dynamics*, Volendam, The Netherlands, 1982.

78. H. D. Wahl (UA1), Lectures presented at the 19th *Int. School on Elementary Particle Physics*, Kupari-Dubrovnik, Yugoslavia, 1983.

79. M. Banner (UA2), Lectures presented at the 19th *Int. School on Elementary Particle Physics*, Kupari-Dubrovnik, Yugoslavia, 1983.

80. J. D. Bjorken and S. J. Brodsky, *Phys. Rev.* **D1** (1970) 1416.

81. G. C. Fox and S. Wolfram, *Phys. Rev. Lett.* **41** (1978) 1581.

82. E. Farhi, *Phys. Rev. Lett.* **39** (1977) 1587.

83. G. Sterman and S. Weinberg, *Phys. Rev. Lett.* **39** (1977) 1436.

84. C. L. Basham, L. S. Brown, S. D. Ellis and S. T. Love, *Phys. Rev.* **D17** (1978) 2298.

85. F. W. Bopp, *Z. Phys.* **C3** (1979) 171.

86. S. Brandt and H. Dahmen, *Z. Phys.* **C1** (1979) 61.

87. G. C. Fox and S. Wolfram, *Z. Phys.* **C4** (1980) 237; *Phys. Lett.* **82B** (1979) 134.

88. L. Clavelli, *Phys. Lett.* **85B** (1979) 111.

89. T. Chandramohan and L. Clavelli, *Phys. Lett.* **94B** (1980) 409.

90. C. H. Berger *et al.* (PLUTO), *Z. Phys.* **C12** (1982) 297.

91. P. Söding and G. Wolf, *Ann. Rev. Nucl. Sci.* **31** (1981) 231.

92. M. Bace, *Phys. Lett.* **78B** (1978) 132.

93. W. Celmaster and D. Sivers, *Phys. Rev.* **D23** (1981) 227, and references therein.

94. M. Dine and J. Sapirstein, *Phys. Rev. Lett.* **43** (1979) 668.

95. K. G. Chetyrkin, A. L. Kataev and F. V. Tkachev, *Phys. Lett.* **85B** (1979) 227.

96. W. Celmaster and R. Gonsalves, *Phys. Rev. Lett.* **42** (1979) 1435.

97. A. J. Buras, E. G. Floratos, D. A. Ross and C. T. Sachrajda, *Nucl. Phys.* **B131** (1977) 308.

98. P. M. Stevenson, *Phys. Rev.* **D22** (1980) 693; CERN preprint CERN-TH-3358 (1982).

99. R. K. Ellis, D. A. Ross and A. E. Terrano, *Phys. Rev. Lett.* **45** (1980) 1226; *Nucl. Phys.* **B178** (1981) 421.

100. K. Fabricius, I. Schmitt, G. Schierholz and G. Kramer, *Phys. Lett.* **97B** (1981) 431; *Z. Phys.* **C11** (1982) 315.

101. J. A. M. Vermaseren, K. J. F. Gaemers and S. J. Oldham, *Nucl. Phys.* **B178** (1981) 301.

102. T. D. Gottschalk, *Phys. Lett.* **109B** (1982) 331.

103. Z. Kunszt, *Phys. Lett.* **99B** (1981) 429; *Phys. Lett.* **D107B** (1981) 123.

104. F. Gutbrod, G. Kramer and G. Schierholz, DESY preprint DESY-83-044 (1983).

105. R. Brandelik *et al.* (TASSO), *Phys. Lett.* **89B** (1980) 418.

106. J. P. Berge *et al.* (FIMS), *Nucl. Phys.* **B203** (1982) 1.

107. T. P. McPharlin *et al.*, *Phys. Lett.* **90B** (1980) 479.

108. R. Brandelik *et al.* (TASSO), *Phys. Lett.* **86B** (1979) 243.

109. M. Barth *et al.*, *Nucl. Phys.* **B192** (1981) 289.

110. R. L. Kelly *et al.* (Particle Data Group), *Rev. Mod. Phys.* **52** (1980) No. 2, Part II.

111. H. Meyer, *Proceedings of the Conference on Perturbative QCD*, Florida State University (March 1981), AIP Conf. Proc. No. 74 (Particles and Fields Subseries, No. 24), eds. D. W. Duke and J. F. Owens.

112. Ch. Berger *et al.* (PLUTO), *Z. Phys.* **C8** (1981) 101; *Phys. Lett.* **97B** (1980) 459; *Phys. Lett.* **82B** (1979) 449.

113. J. D. Bjorken, *Phys. Rev.* **D17** (1978) 171.

114. M. Suzuki, *Phys. Lett.* **71B** (1977) 139.

115. H. Abramowicz *et al.* (CDHS), *Z. Phys.* **C15** (1982) 19.

116. B. J. Edwards and T. D. Gottschalk, *Nucl. Phys.* **B186** (1981) 309.

117. R. Odorico and V. Roberto, *Nucl. Phys.* **B136** (1978) 333.

118. S. J. Brodsky, C. Peterson and N. Sakai, *Phys. Rev.* **D23** (1981) 2745.

119. S. J. Brodsky and G. Farrar, *Phys. Rev. Lett.* **31** (1973) 1153; *Phys. Rev.* **D11** (1975) 1309.

120. D. Sivers, *Ann. Rev. Nucl. Part. Sci.* **32** (1982) 149.

121. W. Bartel *et al.* (JADE), *Phys. Lett.* **104B** (1981) 325.

122. R. Brandelik *et al.* (TASSO), *Phys. Lett.* **94B** (1980) 444; *Phys. Lett.* **105B** (1981) 75.

123. G. Wolf, Talk given at the *XIV International Symposium on Multiparticle Dynamics*, Granlibakken, Lake Tahoe, USA (1981), DESY preprint DESY-83-096.

124. R. Brandelik *et al.* (TASSO), *Phys. Lett.* **94B** (1980) 437.

125. J. Ellis and I. Karliner, *Nucl. Phys.* **B148** (1979) 141.

126. R. Brandelik *et al.* (TASSO), *Phys. Lett.* **97B** (1980) 453.

127. P. Söding, Talk presented at the *Particles and Fields Conference: Testing the Standard Model*, Santa Cruz (1981), DESY preprint DESY-81-070.

128. J. D. Bjorken, Talk presented at the 2nd *Int. Conf. on Physics in Collision, High Energy ee / ep / pp Interactions* (1982) Stockholm, preprint FERMILAB-Conf-82/42-THY and references therein.

129. B. Andersson, G. Gustafson and C. Peterson, *Phys. Lett.* **69B** (1977) 221, erratum **72B** (1978) 503; *Phys. Lett.* **71B** (1977) 337; *Nucl. Phys.* **B135** (1978) 273.

130. B. Andersson, G. Gustafson and C. Peterson, *Z. Phys.* **C1** (1979) 105; *Phys. Scr.* **19** (1979) 184.

131. B. Andersson and G. Gustafson, *Z. Phys.* **C3** (1980) 223.

132. B. Andersson, G. Gustafson and G. Nillson, *Phys. Lett.* **83B** (1979) 379.

133. B. Andersson, G. Gustafson and G. Ingelman, *Phys. Lett.* **85B** (1979) 417.

134. B. Andersson, G. Gustafson and B. Soderberg, LUND preprints LU-TP-82-1 (1982), LU-TP-83-1 (1983), LU-TP-83-2 (1983).

135. B. Andersson, G. Gustafson and T. Sjöstrand, *Z. Phys.* **C6** (1980) 235; *Phys. Lett.* **94B** (1980) 211.

136. B. Andersson, G. Gustafson and T. Sjöstrand, LUND preprint LU-TP-81-4 (1981).

137. B. Andersson, G. Gustafson and T. Sjöstrand, *Nucl. Phys.* **B197** (1982) 45.

138. B. Andersson, G. Gustafson, G. Ingelman and T. Sjöstrand, *Nucl. Phys.* **B206** (1982) 239; *Z. Phys.* **C9** (1981) 233; *Z. Phys.* **C13** (1982) 361.

139. B. Andersson, G. Gustafson, G. Ingelman and T. Sjöstrand, *Phys. Reports* **97** (1983) 31.

140. T. Sjöstrand, *Comp. Phys. Comm.* **27** (1982) 243; *Comp. Phys. Comm.* **28** (1983) 229.

141. G. Ingelman and T. Sjöstrand, LUND preprint LU-TP-80-12 (1980).

142. A. Casher, J. Kogut and L. Susskind, *Phys. Rev.* **D10** (1974) 732.

143. A. Casher, H. Neuberger and S. Nussinov, *Phys. Rev.* **D20** (1979) 179.

144. X. Artru and G. Mennessier, *Nucl. Phys.* **B70** (1971) 93.

145. X. Artru, *Phys. Reports* **97** (1983) 147.

146. J. Schwinger, *Phys. Rev.* **82** (1951) 664.

147. G. S. Abrams *et al.* (Mark II), *Phys. Rev. Lett.* **44** (1980) 10.

148. H. J. Behrend *et al.* (CELLO), *Nucl. Phys.* **B218** (1983) 269.

149. G. Rudolf (TASSO), presentation at the *EPS Int. Conf. on High Energy Physics* (1983) Brighton.

150. D. P. Barber *et al.* (Mark J), *Phys. Rev. Lett.* **50** (1983) 2051.

151. A. Ali and F. Barreiro, *Phys. Lett.* **118B** (1982) 155.

152. W. Bartel *et al.* (JADE), *Phys. Lett.* **123B** (1983) 460.

153. W. Bartel *et al.* (JADE), DESY preprints DESY-83-079 (1983), DESY-83-080 (1983).

154. R. D. Field and S. Wolfram, *Nucl. Phys.* **B213** (1983) 65.

155. R. D. Field, *Proceedings of the Conference on Perturbative QCD*, Florida State University (March 1981), AIP Conf. Proc. No. 74 (Particles and Fields Subseries No. 24), eds. D. W. Duke and J. F. Owens.

156. T. D. Gottschalk, *Nucl. Phys.* **B214** (1983) 201.

157. B. R. Webber, Talk at XVIII Rencontre de Moriond (1983), CERN preprint CERN-TH-3569 (1983).

158. T. D. Gottschalk, Caltech preprint CALT-68-1052 (1983), to be published in *Nucl. Phys.* **B**.

159. B. R. Webber, CERN prepint CERN-TH-3713 (1983).

160. R. D. Field, Florida preprint UFTP-83-16 (1983).

161. J. Dorfan (Mark II), *Proceedings of the 1981 SLAC Summer School*, ed. A. Mosher (1981) 569.

162. C. Bacci *et al.* ($\gamma\gamma 2$), *Phys. Lett.* **86B** (1979) 234.

163. J. L. Siegrist *et al.* (Mark I), *Phys. Rev.* **D26** (1982) 969.

164. R. Brandelik *et al.* (DASP), *Nucl. Phys.* **B148** (1979) 189.

165. Ch. Berger *et al.* (PLUTO), *Phys. Lett.* **81B** (1979) 410; *Phys. Lett.* **78B** (1978) 176.

166. R. Brandelik *et al.* (TASSO), *Phys. Lett.* **89B** (1980) 418.

167. W. Bartel *et al.* (JADE), *Phys. Lett.* **88B** (1979) 171.

168. C. Bebek *et al.* (CLEO), *Phys. Rev. Lett.* **49** (1982) 610.

169. W. B. Atwood *et al.* (DELCO), Talk given at *XXI Int. Conf. on High Energy Physics*, Paris (1982).

170. J. M. Yelton *et al.* (Mark II), *Phys. Rev. Lett.* **49** (1982) 430.

171. R. Brandelik *et al.* (TASSO), *Phys. Lett.* **113B** (1982) 198.

172. M. Althoff *et al.* (TASSO), *Z. Phys.* **C17** (1983) 5.

173. R. Brandelik *et al.* (TASSO), *Phys. Lett.* **108B** (1982) 71.

174. H. J. Behrend *et al.* (CELLO), *Z. Phys.* **C14** (1982) 189.

175. C. Baltay *et al.*, *Phys. Rev.* **145** (1966) 1103.

176. M. W. Coles *et al.* (Mark II), *Phys. Rev.* **D26** (1982) 2190.

177. P. A. Rapidis *et al.* (Mark I), *Phys. Lett.* **84B** (1979) 507.

178. T. D. Gottschalk, Caltech preprint CALT-68-1030 (1983), to be published in *Nucl. Phys.* B.

179. H. J. Muirhead, *Proceedings of the Fifth European Symposium on Nucleon-Antinucleon Interactions* (1980) 147.

180. P. K. Malhotra and R. Orava, *Z. Phys.* **C17** (1983) 85.

181. R. Brandelik *et al.* (TASSO), *Phys. Lett.* **114B** (1982) 65.

182. J. F. Patrick *et al.* (Mark II), *Phys. Rev. Lett.* **49** (1982) 1232.

183. C. Peterson, D. Schlatter, I. Schmitt and P. Zerwas, *Phys. Rev.* **D27** (1983) 105.

184. S. L. Wu, *Proceedings of the 1983 SLAC Summer School*, DESY preprint DESY-83-007 (1983).

185. R. Brandelik *et al.* (TASSO), *Phys. Lett.* **94B** (1980) 91; *Phys. Lett.* **105B** (1981) 75.